Polar Lights Optimizer: Algorithm and Applications in Image Segmentation and Feature Selection

Chong Yuan [1], Dong Zhao [1,*], Ali Asghar Heidari [2], Lei Liu [3], Yi Chen [4], Huiling Chen [4,*]

[1] College of Computer Science and Technology, Changchun Normal University, Changchun, Jilin 130032, China
(yc18338414794@163.com, zd-hy@163.com)

[2] School of Surveying and Geospatial Engineering, College of Engineering, University of Tehran, Tehran, Iran
(aliasghar68@gmail.com)

[3] College of Computer Science, Sichuan University, Chengdu, Sichuan 610065, China
(liulei.cx@gmail.com)

[4] Key Laboratory of Intelligent Informatics for Safety & Emergency of Zhejiang Province, Wenzhou University, Wenzhou 325035, China
(kenyoncy2016@gmail.com, chenhuiling.jlu@gmail.com)

*Corresponding Author: Dong Zhao, Huiling Chen
E-mail: zd-hy@163.com (Dong Zhao), chenhuiling.jlu@gmail.com (Huiling Chen)

Abstract

This study introduces Polar Lights Optimization (PLO), a metaheuristic algorithm inspired by the aurora phenomenon or polar lights. The aurora is a unique natural spectacle that occurs when energetic particles from the solar wind converge at the Earth's poles, influenced by the geomagnetic field and the Earth's atmosphere. By analyzing the motion of high-energy particles and delving into the underlying principles of physics, we propose a unique model for mimicking particle motion. This model integrates both gyration motion and aurora oval walk, with the former facilitating local exploitation while the latter enabling global exploration. By synergistically combining these two strategies, PLO achieves a better balance between local exploitation and global exploration. Additionally, a particle collision strategy is introduced to enhance the efficiency of escaping local optima. To evaluate the performance of PLO, a qualitative analysis experiment is designed to assess its ability to explore the problem space and search for solutions. PLO is compared with nine classic algorithms and eight high-performance algorithms using 30 benchmark functions from IEEE CEC2014. Furthermore, we compare and analyze PLO with the current state-of-the-art methods in the field, utilizing 12 benchmark functions from IEEE CEC2022. Subsequently, PLO is successfully applied to multi-threshold image segmentation and feature selection. Specifically, a PLO-based multi-threshold segmentation model and a binary PLO-based feature selection method are developed. The performance of PLO is also evaluated using 10 images from the Invasive Ductal Carcinoma (IDC) medical dataset, while the overall adaptability and accuracy of the feature selection model are tested using 8 medical datasets. These results affirm the emergence of PLO as an effective optimization tool ready for solving real-world problems, including those in the medical field. The source codes of PLO are available in

https://aliasgharheidari.com/PLO.html and other websites.

Keywords: Metaheuristic algorithms; Polar Lights Optimization; Medical applications; Multi-threshold image segmentation; Feature selection

Nomenclature			
PLO	Polar Lights Optimization	$R, r_1, r_2, r_3, r_4 r_5$	A random number with values between $[0,1]$.
MAs	Metaheuristic algorithms	K	The collision probability
N	The population size	m	Mass of the particle
D	The problem's dimension	v	Velocity vector of the particle
$X(N,D)$	The PLO population	q	Charge of the particle
$X_{i,j}$	The energetic particles	B	Geomagnetic field intensity
UB, LB	Upper and lower bounds of the solution space	X_{avg}	The center-of-mass position of the energetic particle population
$best$	The current optimal solution computed by the algorithm	W_1, W_2	The weights of the gyration strategy and the auroral ellipse strategy
Ao	Variation of the auroral oval walk	t, T	Current and maximum number of iterations
α	Damping factor	X_{best}	The optimal solution searched by the meta-heuristic algorithm

1. Introduction

In the fields of science and engineering, addressing optimization problems is crucial for enhancing efficiency and optimizing resource utilization [1]. These problems typically involve the task of finding the optimal solution under given conditions and encompass various domains such as logistics, production planning, and financial investments. Researchers have proposed deterministic and stochastic methods to tackle current challenges. While deterministic methods such as dynamic programming and branch and bound can ensure optimal solutions, they require convex feasible domains, continuous differentiable objective functions, or additional constraints. Moreover, their computational costs often increase sharply with the problem's scale, limiting their applicability to large-scale problems. In contrast, the emergence of heuristic algorithms and metaheuristic algorithms in stochastic methods has provided a more feasible approach for solving new problems [2].

Heuristic algorithms (HAs) are methods that utilize specific heuristic rules, experience, or intuition to generate solutions [3]. They can find solutions within a reasonable time frame and exhibit scalability in dealing with complex problems [4]. Therefore, when exhaustive search becomes impractical in certain situations, HAs can provide satisfactory approximate solutions [5]. Metaheuristic algorithms (MAs) represent a more advanced form of HAs, possessing solution strategies independent of the optimization problem and constituting a general algorithmic framework applicable to a wider range of problem types [6, 7]. Over the past two decades, MAs have been applied across various scientific domains to address optimization challenges [8, 9]. Notably, when dealing with real-world problems characterized by non-convexity, nonlinearity, non-smoothness, or dynamics [10], MAs exhibit higher efficiency and popularity than traditional

mathematical methods due to their simplicity and independence from problem-specific gradient information [11]. The stochastic nature of MAs enables them to search candidate solutions across the entire space, effectively avoiding local optima [12, 13]. As described in the literature [14], these algorithmic characteristics make them particularly suitable for practical challenges where derivative information is unclear. Even in limited environments or with constrained computational resources, MAs can generate excellent solutions to optimization problems regardless of this fact that they are single objective, multi objective or many objective [15]. Different MAs originate from distinct research perspectives, leading to variations in concept and performance.

MAs draw inspiration from real-world phenomena and replicate the potential operational rules found in physical or biological group dynamics to discover improved heuristic solutions. Currently, there is no rigid classification for MAs in the existing research. In a recent review paper [16], MAs may be classified into three branches: physics-based, swarm-based, and evolution-based methods. Physics-based methods derive inspiration from physical phenomena observed in reality and devise a set of rules to simulate the underlying principles. By modeling the interaction of various forces, such as electromagnetic, inertial, and gravitational forces, these methods enable exploring the solution space. Examples include the well-known simulated annealing (SA) [17], the earlier proposed black hole optimization (BHO) [18], equilibrium optimizer (EO) [19], multi-verse optimizer (MVO) [20], the galaxy-based search algorithm (GbSA) [21], sonar-inspired optimization (SIO) [22], RIME algorithm (RIME) [23], gravitational search algorithm (GSA) [24], water cycle algorithm (WCA) [25], central force optimization (CFO) [26], and electromagnetic field optimization (EFO) [27], etc.

Swarm-based algorithms are a class of methods designed to explore the interactions between individuals in a group and their behavior in relation to the environment. Examples include the well-known particle swarm optimization (PSO) [28], artificial bee colony (ABC) [29], hunger games search (HGS) [30], slime mold algorithm (SMA) [31], Harris Hawk optimizer (HHO) [32], parrot optimizer (PO) [33], cuckoo search (CS) [34], or ant colony optimization (ACO) [35], hunger games search (HGS) [36], Runge Kutta optimization (RUN) [37], weighted mean of vectors (INFO) [38], colony predation algorithm (CPA) [39], grey wolf optimizer (GWO) [40], liver cancer algorithm (LCA) [41] and grasshopper optimization algorithm (GOA) [42], etc.

Meanwhile, most evolution-based algorithms are inspired by natural and biological evolution, such as crossover, reproduction and mutation. Examples include the well-known genetic algorithm (GA) [43], the genetic programming (GP) [44], and the differential evolution algorithm (DE) [45]. Evolution-based methods can search for optimal solutions globally through these operations. Their robustness usually allows them to deal with noise and uncertainty in the solution space [46]. Almost all such algorithms start from the perspective of natural selection theory and create unique models. However, the variability of ideas between different algorithms arises from studying different species and their distinct biological habits for evolving and producing new offspring. Examples include fruit fly optimization (FOA) [47], bio-geography-based optimizer (BBO) [48], black widow optimization algorithm (BWOA) [49], evolutionary strategy (ES) [50], etc.

As stated by the "No Free Lunch Theorem" (NFL) [51], these methods cannot guarantee superiority across all challenges. Researchers seek various avenues to enhance and improve existing algorithms, striving to overcome the limitations algorithms face when confronted with various engineering problems [52]. These strategies encompass implementing optimization modules, refining algorithm structures, and leveraging parallel computing or distributed systems. Over time, with ongoing technological advancements, these strategies may become increasingly complex, potentially reducing the space for performance improvement.

Moreover, at times, further improvements encounter diminishing returns, where each enhancement yields progressively smaller performance gains or fails to meet expected standards. Developing new algorithms can alleviate such stagnation and provide fresh sources of inspiration for enhancing existing ones. Many existing optimization algorithms exhibit their own strengths and limitations [53], offering valuable insights and aiding in the development of more resilient optimization algorithms. Furthermore, one of the current research motivations is continually seeking improvements and innovations to address evolving and emerging problems [54]. By continuously introducing new ideas, methods, and technologies, researchers can propel advancements in the field of optimization algorithms, offering a diverse array of solutions to real-world problems.

Within the domain of MAs, scholars engage in a scholarly pursuit that involves reviewing academic literature and conducting interdisciplinary research to assimilate the insights of their predecessors, accumulate empirical knowledge, and glean inspiration. Behind these flashes of light, inspiration has always been present in people's view. Above the Earth's polar regions, a mesmerizing and extraordinary phenomenon occurs – the aurora. Behind it lies a complex interplay of energetic particles in the solar wind, influenced by Earth's magnetic field, colliding with the atmosphere, resulting in a series of intricate movements. Drawing inspiration from the Aurora phenomenon, a metaheuristic algorithm called Polar Lights Optimization (PLO) is proposed in this paper. In PLO, two novel models are formed by simulating the flight trajectories of energetic particles and their motion processes. The flight of energetic particles toward the Earth is modeled in PLO, which contains three main forms of motion and is used to propose three optimization strategies, including:

1) A gyration motion method is introduced to replicate the situation where energetic particles are deflected poleward by Earth's magnetic field and subsequently collide with atmospheric molecules on their way to Earth's poles. This method is proposed based on physics laws, helping to find optimal solutions locally and improving convergence accuracy.

2) An auroral oval walk is proposed by modeling the phenomenon where energetic particles gradually converge above the poles and form a luminous elliptical ring. Energetic particles move freely within the oval ring, colliding with other particles and chaotically following changes in Earth's magnetic field. This strategy aims to explore the entire solution space in large steps, using the center of mass of the energetic particles as a guide to ensure the convergence direction of the entire cluster.

3) Throughout the entire flight process of high-energy particles, collisions between particles occur continuously. A particle collision strategy is proposed by simulating these chaotic and disordered collisions. This strategy enhances the algorithm's ability to escape local optima.

A series of experiments are conducted to evaluate the performance of PLO. To verify the competitiveness of PLO among popular MAs, several sets of comparison experiments are established. PLO is compared with nine classic algorithms and eight high-performance algorithms using the IEEE CEC 2014 benchmark function set. Additionally, PLO is compared with five highly referenced algorithms and four variants using the latest benchmark function set from IEEE CEC 2022. Subsequently, a series of qualitative analysis experiments are conducted to elucidate PLO's characteristics and adaptability.

After these works, this research involves two key issues: multi-threshold image segmentation and feature selection. In the case of multi-threshold image segmentation, we take advantage of PLO to address intricate challenges in image segmentation. By integrating PLO with a Multi-Threshold Image Segmentation (MTIS) system, we achieve higher accuracy in calculating the optimal threshold set. In the experiment, we conduct a series of segmentation experiments using ten image samples from the medical dataset "Invasive Ductal Carcinoma" (IDC) [55]. And a multi-group comprehensive comparative study is designed to compare PLO

with seven other algorithms as benchmarks at different threshold levels, evaluating the results of image segmentation using various methods of threshold set computation. In terms of feature selection, this paper develops a binary version of PLO to address challenging feature selection issues. This paper devises a PLO-based wraparound feature selection method, enabling the selection of pertinent features and evaluating the proposed PLO's performance using eight medical datasets, demonstrating the algorithm's advantages in real-world optimization problems.

These results establish PLO as a potent optimization tool to address a diverse array of practical problems. This paper contributes the following:

(1) Drawing inspiration from the fascinating phenomenon of the aurora borealis, a novel algorithm polar lights optimizer is proposed.

(2) In this study, the effectiveness of PLO is examined using the classical IEEE CEC2014 and the latest IEEE CEC2022 unconstrained benchmark function sets. In-depth comparisons are made with the simulation results of various well-known algorithms.

(3) A set of qualitative analysis experiments are designed to analyze the optimization solution process of PLO.

(4) PLO is integrated with the MTIS system to provide a superior threshold set for breast cancer images segmentation.

(5) Developed a wraparound feature selection model based on binary version (bPLO). The performance of the proposed method is evaluated using medical datasets, demonstrating proficiency in real optimization problems.

The remainder of the paper consists of the following sections: Section 2 delves into the intricate mechanism underlying aurora formation while simultaneously elucidating the insights gleaned from it. Section 3 expounds on the modeling aspects of the PLO, shedding light on its conceptualization and implementation. Section 4 compares the PLO with existing algorithms, emphasizing its novelty. Section 5 shows the experiments set up to test the performance of the PLO, meticulously analyzing the obtained results. Section 6 discusses the application of the PLO to the MTIS and FS problems. Finally, Section 7 encapsulates the entirety of the work in this paper, outlining the prospects and avenues for further research.

2. Inspiration from the polar lights, or aurora borealis

The aurora is a beautiful natural phenomenon of electrical impulses occurring at altitudes between 80 and 500 kilometers above the horizon. The Earth's magnetic field forms a strong magnetic shield from the South Pole to the North Pole, manifesting itself in a pattern of curved magnetic lines of force. As a result, energetic particles are funneled toward the poles in a spiral motion, colliding with the many molecules of atmospheric gas over the poles. These collisions produce luminescence, as shown in Figure 1. Auroras form as a result of the interaction between solar activity, the Earth's magnetic field, and the atmosphere[56].

(a) (b)

Figure 1. An aurora borealis light curtain high in the sky[1]

Initially, the main driving force behind the formation of auroras is solar activity. On the surface of the Sun, there exists a high-temperature plasma containing charged particles commonly referred to as the solar wind. The charged particles and their complex and variable motion processes are the focus. These particles carry enormous amounts of energy from the Sun into the vastness of cosmic space. In addition, the Earth possesses a powerful magnetic field that arises from the rotation of its core and the motion of its outer core. This magnetic shield wraps around the Earth, forming a protective layer known as the magnetosphere. When charged particles from the solar wind enter the Earth's magnetosphere, they interact with the magnetic field. Changes in the trajectory of charged particles are due to the Earth's magnetic field. Specifically, it will encounter the Lorentz force and be deflected in a specific direction, thus entering an orbit consisting of the geomagnetic field. As shown in Figure 2, this orbit will guide the charged particle close to the Earth's polar regions, the North and South Poles. At this stage, the charged particles have two velocity components: parallel to the magnetic field and perpendicular to it. As a result, they are in gyratory motion while traveling along the magnetic field lines. This marks the beginning of the first major phase, in which the trajectories of the energetic particles undergo their first change. During this phase, the charged particles will gradually encounter the atmosphere over the polar regions and collide with gas molecules in the atmosphere. Then, the energy initially possessed by the charged particles will gradually be transferred to the air molecules, causing them to ionize and subsequently glow. Due to the loss of energy, the trajectory radius of the charged particles will be significantly affected and reduced, which again leads to a change in their trajectory.

[1] Pictures obtained from https://pixabay.com/ as copy right free images

(a) https://pixabay.com/photos/aurora-borealis-lake-snow-aurora-5599375/

(b) https://pixabay.com/photos/aurora-polar-lights-northern-lights-1190254/

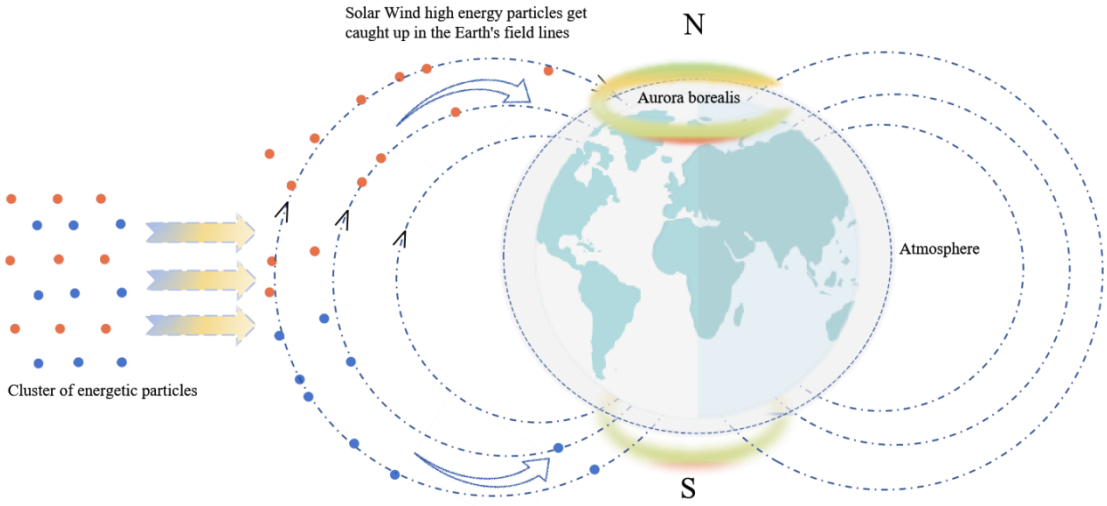

Figure 2. Solar wind energetic particles enter the earth's magnetic field lines.

As a result of the energy transfer due to the collision, the gas molecule is excited, and the electrons in the ground state jump from one energy level to another and then back to the ground state. During the energy level jump, the gas molecule releases energy and produces photons. These photons are the visible light that makes up the aurora borealis. Different gas molecules have different energy level structures and emission spectra. For example, oxygen molecules emit green and red light, and nitrogen molecules emit violet and blue light. As the collision continue, the energy contained in the energetic particles is gradually lost, leading to the transition to a significant phase. These particles encounter considerable obstacles in directly bombarding polar ice and the ground due to atmospheric obstructions. Instead, they pause briefly in the atmosphere and gather to form a luminous ring, as shown in Figure 3. This glowing ring band is usually oval around the polar axis, hence the name "auroral oval". Charged particles that are in an auroral oval undergo further collisions with gas molecules. More specifically, the energy of electrons drops relatively quickly and is absorbed by the atmosphere, while the energy of protons drops more slowly. After protons collide with gas molecules, some of them will be absorbed by the atmosphere, while the other part will deviate from the ring band region in the atmosphere and bounce along a different path. The periods of magnetic quiescence and magnetic perturbation in the Earth's magnetic field affect the auroral oval, causing irregular changes that manifest as irregular expansion and contraction. Thus, in the second major phase, the trajectory of the particle undergoes a third change. After three trajectory changes, the journey of the particles towards the Earth will end.

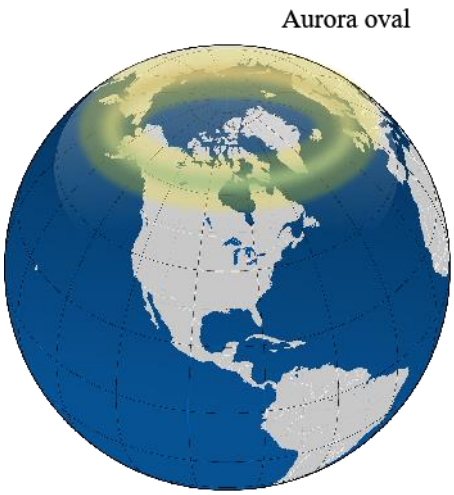

Figure 3. Aurora oval in the Earth's Arctic

In summary, the formation of auroras is determined by the interaction between charged particles in the solar wind and the Earth's magnetic field. This interaction causes the charged particles to enter the Earth's atmosphere and contact with gas molecules, thereby exciting them and releasing energy in the form of photons, ultimately forming visible bands of colored light. In this study, we designed a new model to simulate this complex process. The model includes an in-depth study of the principles of aurora formation, precise tracking of the particle trajectories, division of the entire process into two distinct phases, and three changes to the trajectory. Based on this elaborate model, three strategies are proposed to lead to Polar Lights Optimization (PLO).

3. Methodology

This section gives the inspiration for PLO, i.e., an optimization strategy based on the motion process of energetic charged particles guided by a magnetic field. The mathematical model is expounded upon, enabling comprehension of PLO's structure through the presentation of pseudo-code, a flowchart, and the computation of the algorithm's time complexity.

3.1 Mathematical model of the PLO

Inspired by the phenomenon of aurora borealis, a stream of charged particles (solar wind) moves in the air near the north and south poles of the Earth under the influence of the magnetic field environment and displays a variety of shapes and brilliant colors in the night sky. Auroras are produced under the atmosphere, magnetic field, and high-energy charged particles. The behavior of auroras is attributed to various dynamic processes of interaction between charged particle streams and magnetic fields [57]. In this study, the gyration motion is proposed through the motion process of energetic charged particles spiraling forward around magnetic lines of inductance; then, the aurora oval walk is proposed by synthesizing the energies, velocities, and trajectories of charged particles, as well as the compositions and conditions in the atmosphere, where auroras present an elliptical luminous ring belt in the sky. Finally, the particle collision strategy is proposed through the phenomenon of energetic charged particles colliding with one another continuously on their flights.

3.1.1 Initialization phase

In PLO, the iterative process will start with an initial population that is generated based on pseudo-random numbers. As described in Eq. (1), the entire population is represented in the form of a matrix with N rows and D columns in size, where N denotes the size of the candidate solutions contained in the population and D denotes the scalable dimension of the solution space.

$$X(N,D) = LB + R \times (UB - LB) = \begin{bmatrix} X(1,1) & X(1,2) & \cdots & X(1,D) \\ X(2,1) & X(2,2) & \cdots & X(2,D) \\ \vdots & \vdots & \ddots & \vdots \\ X(N,1) & X(N,2) & \cdots & X(N,D) \end{bmatrix} \quad (1)$$

where UB and LB denote the boundaries of the solution space, and R denotes a random number sequence that takes values in $[0,1]$. In PLO, the travel of a swarm of energetic charged particles flying towards the Earth around the magnetic susceptor towards the polar center is simulated with a search agent in the solution space.

3.1.2 Gyration motion

This section will delineate the method for searching for optimal solutions in PLO, namely the gyration motion, inspired by the extensive journeys of high-energy particles toward the Earth. Roughly 150 million kilometers from Earth, the Sun continuously emits electrons and protons towards our planet, which is entirely enveloped by its magnetic field, extending outward from the Earth by approximately 50,000 to 65,000 kilometers [58]. As these particles approach Earth, they encounter resistance from the Earth's magnetic field and radiate in various directions under its influence. During this process, charged particles approaching Earth interact with its magnetic field, experiencing rotational motion along magnetic field lines, a phenomenon describable by the Lorentz force. Mathematically, assuming a charge (q) and velocity (v) for the charged particle within Earth's magnetic field (B), the Lorentz force F_L can be expressed as Eq. (2):

$$F_L = qvB \quad (2)$$

The F_L causes a centripetal force to be exerted on a charged particle, resulting in its gyratory motion along the magnetic lines of force in a magnetic field. Also, the equation of a charged particle can be described by the Lorentz force and Newton's second law:

$$F_L = m\frac{dv}{dt} \quad (3)$$

where m is the mass of a charged particle. This equation describes the variation of the velocity of the charged particle with time so that its trajectory in the magnetic field can be determined. By joining the above two equations (Eq. (2) and Eq. (3)), a first-order ordinary differential equation can be obtained, as shown in Eq. (4):

$$m\frac{dv}{dt} = qvB \quad (4)$$

This differential equation describes the change in velocity of the charged particle over time. Solving this differential equation yields the law governing the variation of the particle's velocity with time, providing insight into its motion within the Earth's magnetic field, as depicted below.

Rearrange the two sides and integrate them simultaneously, with the interval of integration from the initial velocity v_0 to v and the time from 0 to t:

$$\frac{dv}{v} = \frac{qB}{m}dt \tag{5}$$

$$\int_{v_0}^{v} \frac{1}{v}dv = \int_{0}^{t} \frac{qB}{m}dt \tag{6}$$

$$\ln(v) - \ln(v_0) = \frac{qBt}{m} \tag{7}$$

$$\frac{v}{v_0} = e^{\frac{qBt}{m}} \tag{8}$$

$$v(t) = v_0 e^{\frac{qBt}{m}} \tag{9}$$

In an ideal scenario, the aforementioned equation adequately describes the motion of charged particles within Earth's magnetic field, as illustrated in Figure 4. However, these high-energy particles encounter resistance from air molecules in the atmosphere, resulting in the non-smooth circling motion. This non-smooth circling motion is due to the damping effect of the atmosphere. As charged particles enter the atmosphere, collisions with atmospheric molecules diminish their kinetic energy, causing the radius of their circular motion to decrease.

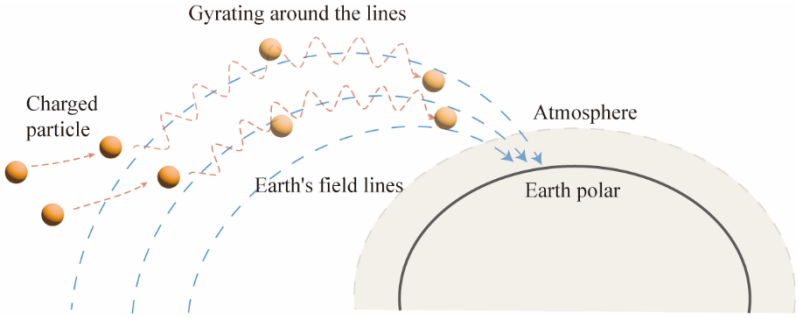

Figure 4. Charged particles gyrate around the magnetic line.

After accounting for the damping effect of the atmosphere on charged particles, we can incorporate this damping phenomenon into the equation governing the variation of the particle's velocity with time. In this equation, we introduce a damping factor α, representing the rate of decay of the particle's velocity. Thus, the equation (Eq. (4)) describing the variation of the charged particle's velocity with time can be modified accordingly, as in Eq. (10).

$$m\frac{dv}{dt} = qvB - \alpha v \tag{10}$$

The modification results in a nonhomogeneous first-order linear differential equation, Eq. (10). By employing the method of constant variation, assuming a solution $v = Ce^{\lambda t}$, where C and λ are undetermined coefficients. Substituting this into the equation, we obtain:

$$m\lambda Ce^{\lambda t} = qBCe^{\lambda t} - aCe^{\lambda t} \tag{11}$$

Solving yields $\lambda = \frac{qB-\alpha}{m}$, so the final solution to the equation Eq. (12) is:

$$v(t) = Ce^{\frac{qB-a}{m}t} \tag{12}$$

where C is the constant of integration, in this equation the charge q carried by the charged particle, the mass m and the strength of the earth's magnetic field B do not change. For simplicity, in this strategy, C, q, and B take the value of 1, and m is 100. The damping factor α is a random value taking the value of $[1,1.5]$, and the fitness evaluate process of the algorithm is utilized within the strategy to simulate the time

(t) course of Eq. (12).

In this section, the gyration motion within PLO introduces an equation describing the variation of charged particle velocity over time. This equation combines the Lorentz force law and Newton's second law. Moreover, considering the damping effect exerted by the atmosphere on the charged particles, a damping factor α is introduced into the equation, enhancing its precision.

When charged particles undergo gyration motion, they exhibit the following characteristics:

(1) Prior to coming into contact with magnetic field lines, charged particles follow their initial trajectory. Only when they enter the influence range of the Earth's magnetic field do they gradually alter their path, spiraling around the magnetic field lines.

(2) During the gyration motion, particles experience damping effects generated by the atmosphere, causing a reduction in their energy and consequent decrease in velocity.

(3) The damping effects of the atmosphere become increasingly pronounced as the particles travel further.

(4) Despite the occurrence of damping effects, the ultimate destination of particle flight remains unchanged (the Earth's poles).

This strategy enhances the algorithm's capability for local exploitation, enabling it to finely exploit local regions and explore optimal solutions within those regions.

3.1.3 Aurora oval walk

This section describes the auroral oval walk in PLO, a method that helps to search the solution space efficiently. The idea of this strategy originated from the extensive study of auroras by astronomical observers. They concluded that auroras tend to form along an elliptical band called an auroral oval. The size of the auroral oval depends on the north-south component of the interplanetary magnetic field, and its boundaries vary with geomagnetic activity. The Earth's complex atmosphere further contributes to the movement of various energetic particles in this phenomenon.

The intricate fluctuation of the auroral oval walk will significantly impact the global search. It is the unpredictable chaos that fulfills the need of the PLO for a fast global search of the solution space. It is worth noting that Levy Flight (LF) is often used in MAs to enhance global exploration because it is essentially a random non-Gaussian Walk. Its step values are dispersed based on the Levy stable distribution. The LF can be expressed in Eq. (13) as follows:

$$Levy(d) \sim |d|^{-1-\beta}, 0 < \beta \leq 2 \tag{13}$$

where β denotes an important LF index of adjustment stability and d is the step size.

In the auroral oval walk, the energetic particles simulated with LF are affected by geomagnetic activity as well as the atmosphere and exhibit contraction of the auroral oval boundary in the polar direction and expansion in the equatorial direction. The specific change process is shown in Eq. (14):

$$Ao = Levy(d) \times \left(X_{avg}(j) - X(i,j)\right) + LB + r_1 \times (UB - LB)/2 \tag{14}$$

$$X_{avg} = \frac{1}{N} \times \sum_{i=1}^{N} X(i) \tag{15}$$

where X_{avg} is the center-of-mass position of the energetic particle population, calculated by Eq. (15). $X(i,j)$ is the current position of the energetic particles, while $X_{avg}(j) - X(i,j)$ represents the tendency of the particles to move. Ao is a complex variation of the auroral oval simulated by the dispersed distribution of the LFs, which drive energetic particles between the poles and the equator. The motion of

each particle is briefly simulated as shown in Figure 5.

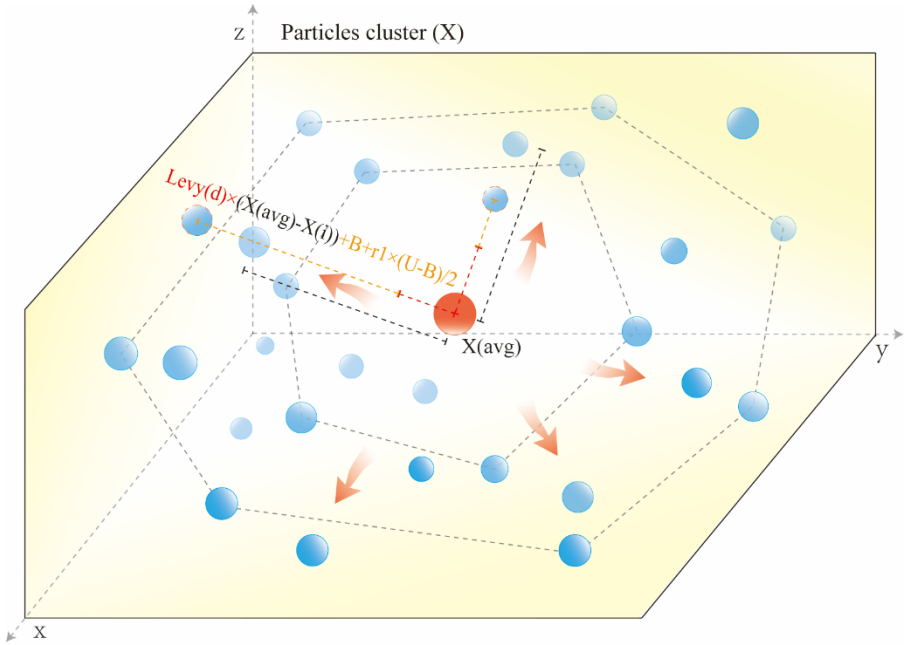

Figure 5. The aurora oval walk

This strategy enhances PLO's global exploration capabilities, allowing it to quickly navigate the entire solution space and search for valuable regions.

In the PLO, the search process follows a unique pattern. It comprises two main motion patterns: gyration motion and aurora oval walk, each representing distinct search strategies and behavioral characteristics. Together, they constitute the trajectory of particles flying from the start (the Sun) to the end (the Earth's poles).

Firstly, the gyration motion manifests as particles spiraling along the Earth's magnetic field lines, exhibiting slow movement along fixed trajectories. This motion pattern emphasizes local exploitation and fine adjustments, aiming to explore local solution spaces more deeply to find local optima or optimize the local structure of the current solution. This aligns with the local search phase in MA, where subtle adjustments and small steps are taken to enhance the quality of solutions, bringing them closer to the optimal solution.

Secondly, the aurora oval walk involves rapid motion around candidate points for the best solution or local optima. This pattern emphasizes global exploration characteristics, with particles exploring the solution space with larger steps to discover more valuable regions. This corresponds to the global exploration phase in MA, where the solution space is searched with larger step lengths to find global optima or better solutions.

Therefore, this paper combines these two strategies in PLO, and the proposed new computational model is represented by Equation (16).

$$X_{new}(i,j) = X(i,j) + r_2 \times (W_1 \times v(t) + W_2 \times Ao) \tag{16}$$

where $X_{new}(i,j)$ is the position of the energetic particle after completing the update, and r_2 represents the interference brought by factors such as the uncontrollable environment for the particle and is a value taking the value of $[0,1]$. To maximize the efficiency of local exploitation and global exploitation during the process, two adaptive weights W_1 and W_2 are introduced that change with each iteration of the algorithm. as calculated in Eq. (17) and Eq. (18) are obtained:

$$W_1 = \frac{2}{(1 + e^{-2(t/T)^4})} - 1 \tag{17}$$

$$W_2 = e^{-(2t/T)^3} \tag{18}$$

where W_1 and W_2 control the weights of the gyration motion and the auroral oval walk in Eq. (16), as shown in (a) in Figure 6, the weight of $v(t)$ will increase with W_1; as shown in (b) in Figure 6, the weight of Ao, W_2, gradually decreases. As the algorithm iterates, global search and local exploitation rely on the changing weights to achieve a balance and explore the optimal solution.

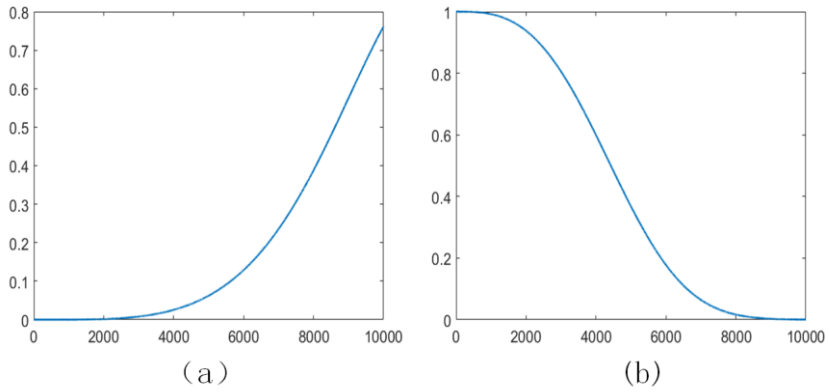

Figure 6. Trajectories of change in W_1 and W_2

In summary, the particle motion in the PLO encompasses both global exploration and local exploitation. Comprehensive optimization of the solution space is achieved by combining the gyration motion and aurora oval walk motion patterns. This design aims to strike a balance between global search and local optimization, intending to effectively find the optimal solution or solutions close to optimality within the solution space.

3.1.4 Particle collision

Robust global and strong local strategies are not the sole pivotal constituents of a refined algorithm. Additionally, a more potent capability to evade convergence into local optima or break free from them is imperative. Consequently, this section introduces a particle collision strategy to boost the capacity to jump out of a stuck situation.

In the solar wind, charged particles such as electrons and protons travel from the sun to the earth at high speeds and collide with each other as they hit the atmosphere. When they enter the Earth's magnetic field and are guided by magnetic lines of force, they move along the lines near the Earth's polar regions. During this process, energetic particles that have changed speed and direction collide violently with each other. These collisions can lead to the transfer of energy and the conversion of energy forms, further enhancing the process of aurora formation. Collusions can lead to changes in the speed and direction of the particles and scatter them in different areas. In addition, they can stimulate the excitation and ionization of more particles, thus enhancing the brightness and complexity of the aurora [59]. Thus, particle collisions play a crucial role in the formation of auroras.

Inspired by this, a particle collision strategy is proposed. The chaotic collision between particles allows PLO to leave the local optimal. In this strategy, if we focus on the current moving particle, it may chaotically collide with any particle in the particle swarm to create a new position along the way, as shown in Figure 7. If a particle is the focus of attention, it may randomly drift out of the established flight trajectory and collide with any of its surrounding particles. When the particle it is about to collide with is used as a reference, the collision may occur at any angle, just like the uncertain outcome of a novice billiards game. Also, minor collisions can occur when energetic particles fly from the solar to the earth. However, as these particles enter

the atmosphere and converge within the auroral oval, collisions occur more frequently, resulting in the ever-changing shape of the aurora. The mathematical model is shown in Eq. (19):

$$X_{new}(i,j) = X(i,j) + \sin(r_3 \times \pi) \times (X(i,j) - X(a,j)), r_4 < K \; and \; r_5 < 0.05 \quad (19)$$

$$K = \sqrt{(t/T)} \quad (20)$$

where $X(a,j)$ represents any particle in the particle cluster. Collisions between particles become more frequent as the algorithm proceeds and are therefore controlled by the collision probability K, calculated by Eq. (20). r_3 and r_4 are random values, taking values in $[0,1]$.

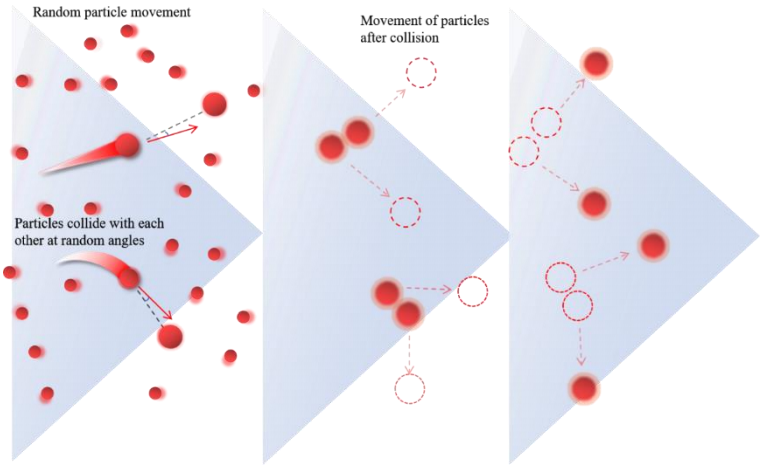

Figure 7. Chaotic collisions between particles.

3.2 The proposed PLO

In essence, this paper draws inspiration from the aurora, a captivating physical phenomenon, and melds it with the principles of physics to devise PLO. Search agents are likened to high-energy particles emanating from solar radiation towards the Earth, all subject to the influences of magnetic fields and atmospheric conditions as they journey towards the Earth's poles. Nevertheless, owing to various uncontrollable factors, the trajectory of each particle remains unpredictable, yet converging toward the vicinity of the polar regions constitutes the ultimate destination of their journey.

In PLO, initially charged, the geomagnetic force influences particles and moves them towards the poles, continuously colliding with gas molecules in the atmosphere and gradually impeding their gyration motion. Subsequently, these particles gather near the upper atmosphere of the poles, forming an elliptical-shaped region known as the auroral oval. Due to the irregular deformation of the auroral oval, this elliptical ring-shaped region becomes unstable, contracting towards the poles during magnetic quiescence periods and expanding towards the equator during disturbance periods.

Inspired by these phenomena, we based our proposal on the Lorentz force theorem and Newton's second law to propose a modified modeling equation for the variation of charged particle velocity over time, incorporating a damping factor. Furthermore, we propose an auroral oval walk strategy based on the auroral oval phenomenon. Then, by combining the gyration motion and aurora oval walk motion patterns, we construct comprehensive optimization progress to assist PLO in global exploration and local exploitation. Finally, we introduced the particle collision strategy to facilitate interactions among particles, enabling the PLO to effectively escape from local optima states.

As shown in Algorithm 1, the PLO's pseudo-code can better help to understand the process. In Figure

8, flowcharts will clearly show the structure.

Algorithm 1 PLO's pseudo-code

Parameters initializing: $FEs = 0, MaxFEs,\ t = 0$

Initialize high-energy particle cluster X.

Calculate the fitness value $f(X)$.

Sort X according to $f(X)$.

Update the current optimal solution X_{best}.

While $FEs < MaxFEs$

Calculate the velocity $v(t)$ for each particle, according to Eq. (12).

Calculate aurora oval walk Ao for each particle, according to Eq. (14).

Calculate weights W_1 and W_2 according to Eq. (17) and Eq. (18).

For each energetic particle **do**

Updating particles X_{new} using Eq. (16).

If $r_4 < K$ and $r_5 < 0.05$

Particle collision strategy: update particle X_{new} using Eq. (19).

End If

Calculate the fitness $f(X_{new})$.

$FEs = FEs + 1$.

End For

If $f(X_{new}) < f(X)$

Iterating over X using the greedy selection mechanism.

End If

Sort X according to $f(X)$.

Update the optimal solution X_{best}.

$t = t + 1$.

End While

Return the X_{best}.

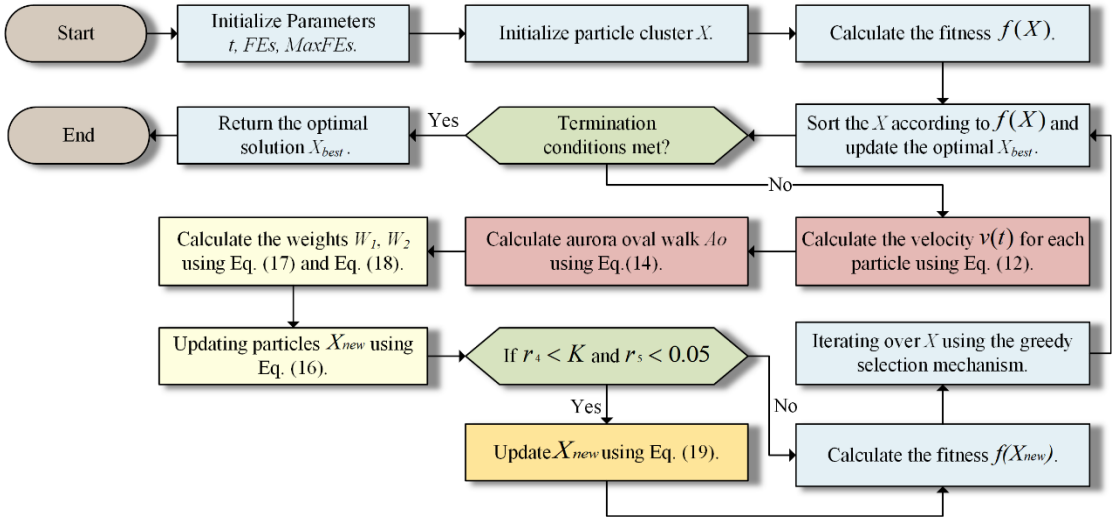

Figure 8. The flowchart of PLO

The algorithmic time complexity for calculating PLO will be concerned with the maximum number of evaluations (ME) set for the problem, the size of the population (n), and the dimension size of the problem

(d). Meanwhile, the complexity of PLO mainly includes the gyration motion strategy, auroral oval walk strategy, particle collision strategy, and fitness value calculation. First, due to the unique mechanism design of the PLO, the gyration motion and the auroral oval strategy are organically combined, so the time complexity of the two strategies together is $O(n \times d)$. Then, the complexity of the particle collision strategy is $O(n \times d)$. Finally, the fitness value computation requires $O(n \times logn)$ computation time. Therefore, the complexity of the PLO is $O(PLO) = O(2 \times (n^2 \times d) \times logn \times ME)$.

5. Performance evaluation experiments and analysis

The preceding section elucidated the theoretical model of PLO and its feasibility in implementation. This section will examine the performance of PLO. Firstly, several sets of comparative experiments are devised to substantiate the advantages of PLO over existing algorithms, including comparisons between PLO and similar peers and between PLO as well as high-performance enhanced algorithms. Subsequently, the optimization process of PLO will be explored, analyzing its advantages in seeking optimality and its search characteristics.

5.1 Experimental settings

In the field of scientific research, maintaining the fairness and appropriateness of experiments is crucial to judging the effectiveness of new methods. In this experiment, to ensure the fairness of the trial, we establish a set of 30 search agents in the initial population for all participating algorithms, and the termination condition is set to 300,000 times for the fitness evaluation. In addition, 30 separate runs of each algorithm are performed to mitigate the effects of randomness and prevent any one run from skewing the understanding of the algorithm's true performance.

Then this paper utilizing benchmark functions from the classical IEEE CEC2014 and the latest IEEE CEC2022. These two benchmark datasets are universally recognized datasets for evaluating the performance of different optimization methods against established criteria.

In the results evaluation, the Wilcoxon Signed-Rank Test (WSRT) [61] is utilized to assess different algorithms, comparing and ranking. WSRT examines whether the differences between PLO and other algorithms' test results are significant, with a p-value less than 0.05 indicating a significant difference and a value greater than or equal to 0.05 suggesting high similarity. Moreover, differences and comparative superiority are denoted using "+/-/=" symbols for counting statistics. Additionally, the Friedman Test (FT) [62] is employed to compute the average results of algorithms across all functions, facilitating an intuitive presentation of the comparative outcomes through rankings.

5.2 Performance analysis of the PLO

In this section, the advantages and characteristics of the algorithm are experimentally verified. Initially, the performance advantages of the algorithm are experimentally validated by comparing PLO with its counterparts. Furthermore, it is juxtaposed with current state-of-the-art algorithms to validate our contribution and obtain a comprehensive understanding of the landscape in the current field. Subsequently,

qualitative analysis experiments are conducted to examine the PLO's optimization process and convergence behavior fully.

5.2.1 Comparison with classical algorithms

This subsection compares PLO with 9 classical algorithms utilizing 30 function problems from IEEE CEC2014. Table 5 lists all the algorithms and parameter settings. In this section, the average value (AVG) and standard deviation (STD) of each algorithm after 30 independent runs are listed in Table 6.

Table 5. Algorithms and parameter settings.

Algorithms	Parameter(s)
Particle swarm optimizer (PSO) [63]	$c_1 = 2;\ c_2 = 2;\ V_{max} = 6$
Gravitational search algorithm (GSA) [24]	$Rnorm = 2$
Harris Hawk optimizer (HHO) [32]	$k = 0$
Moth-flame optimization algorithm (MFO) [64]	$b = 1$
Ant colony optimization for continuous domains (ACOR) [35]	$k = 10; q = 0.5;\ ibslo = 1$
Multi-verse optimizer (MVO) [20]	$W_{max} = 1; W_{min} = 0.2$
Whale optimization algorithm (WOA) [65]	$a_1 = [2,0]; a_2 = [-2,-1]; b = 1$
Sine cosine algorithm (SCA) [66]	$a = 2$
Jaya optimization algorithm (JAYA) [67]	~
Polar lights optimization (PLO)	$m = 100;\ a = [1,1.5]$

Table 6. Comparison results of the PLO and 9 classical algorithms

Function	F1		F2		F3	
Algorithm	AVG	STD	AVG	STD	AVG	STD
PLO	2.11804E+06	8.78432E+05	**1.78164E+04**	**8.92904E+03**	7.31835E+03	3.13733E+03
PSO	8.64579E+06	2.34388E+06	1.48018E+08	1.81499E+07	9.62486E+02	1.00254E+02
GSA	1.40443E+06	4.25286E+05	2.11526E+07	2.35424E+06	7.13329E+03	2.85544E+03
HHO	6.03793E+06	2.74404E+06	9.24189E+06	2.00882E+06	2.42856E+03	7.22091E+02
MFO	1.00050E+08	9.61917E+07	1.32557E+10	8.91896E+09	1.02706E+05	6.27487E+04
ACOR	4.11557E+06	4.95229E+06	6.01421E+07	2.36075E+08	1.03365E+04	1.24159E+04
MVO	7.51352E+07	7.05984E+07	1.30532E+10	9.75808E+09	8.88128E+04	4.61328E+04
WOA	3.11295E+07	1.23148E+07	3.91285E+06	5.75133E+06	3.14270E+04	2.60307E+04
SCA	2.29334E+08	5.89800E+07	1.66283E+10	3.54635E+09	3.62478E+04	6.38897E+03
JAYA	5.14444E+07	2.21353E+07	5.18576E+09	8.23713E+08	3.31822E+04	7.04046E+03
	F4		F5		F6	
	AVG	STD	AVG	STD	AVG	STD
PLO	**4.71807E+02**	**2.08699E+01**	5.20531E+02	3.90076E-01	6.10458E+02	2.29444E+00
PSO	4.75148E+02	3.28127E+01	5.20950E+02	4.26706E-02	6.21474E+02	3.65945E+00
GSA	4.82612E+02	5.99102E+01	5.20941E+02	5.45715E-02	6.08846E+02	1.86002E+00
HHO	5.42867E+02	5.29459E+01	5.20116E+02	1.31619E-01	6.28859E+02	4.16745E+00
MFO	1.78948E+03	1.55333E+03	5.20324E+02	1.84935E-01	6.24206E+02	2.89791E+00
ACOR	4.92806E+02	1.32385E+02	5.20924E+02	4.84442E-02	6.12291E+02	3.00215E+00
MVO	1.24332E+03	9.53484E+02	5.20312E+02	1.71188E-01	6.23950E+02	4.24446E+00
WOA	5.88925E+02	6.35832E+01	5.20371E+02	1.91303E-01	6.34901E+02	3.79290E+00

SCA	1.46786E+03	2.71963E+02	5.20934E+02	6.37100E-02	6.33266E+02	2.68864E+00
JAYA	1.08915E+03	1.14626E+02	5.20953E+02	4.88477E-02	6.30972E+02	2.50236E+00
	F7		F8		F9	
	AVG	STD	AVG	STD	AVG	STD
PLO	**7.00025E+02**	**1.33663E-02**	**8.25417E+02**	**6.18392E+00**	**9.54546E+02**	1.13514E+01
PSO	7.02276E+02	1.61008E-01	9.71633E+02	2.42663E+01	1.10218E+03	3.05657E+01
GSA	7.01198E+02	2.36638E-02	8.38505E+02	7.03766E+00	9.61488E+02	9.45307E+00
HHO	7.01085E+02	1.72633E-02	8.82317E+02	1.04023E+01	1.08410E+03	2.25363E+01
MFO	7.99782E+02	5.18679E+01	9.44094E+02	3.82491E+01	1.10882E+03	5.34486E+01
ACOR	7.02957E+02	1.22532E+01	8.59972E+02	1.89139E+01	1.01221E+03	5.28648E+01
MVO	8.03441E+02	6.64632E+01	9.53443E+02	3.81886E+01	1.11294E+03	4.00506E+01
WOA	7.01035E+02	4.89553E-02	9.78445E+02	4.10009E+01	1.12637E+03	6.08373E+01
SCA	8.47201E+02	2.35220E+01	1.03627E+03	1.74137E+01	1.17377E+03	1.67324E+01
JAYA	7.11309E+02	2.19798E+00	1.00719E+03	1.97062E+01	1.14148E+03	1.52357E+01
	F10		F11		F12	
	AVG	STD	AVG	STD	AVG	STD
PLO	**1.77226E+03**	3.20354E+02	3.92413E+03	5.77381E+02	1.20043E+03	2.15168E-01
PSO	5.10613E+03	5.43633E+02	5.80319E+03	4.59626E+02	1.20239E+03	2.21750E-01
GSA	2.33474E+03	2.03035E+02	2.92700E+03	2.92743E+02	1.20091E+03	1.26204E-01
HHO	2.23361E+03	6.18729E+02	5.04692E+03	6.76686E+02	1.20153E+03	4.59830E-01
MFO	4.67011E+03	8.93027E+02	5.08593E+03	7.91569E+02	1.20042E+03	1.63674E-01
ACOR	3.21143E+03	6.14184E+02	4.21318E+03	1.87682E+03	1.20250E+03	2.89895E-01
MVO	4.41163E+03	9.41803E+02	5.31152E+03	6.92313E+02	1.20042E+03	2.54887E-01
WOA	4.98395E+03	9.06766E+02	6.03757E+03	8.93239E+02	1.20177E+03	4.56727E-01
SCA	7.01130E+03	3.89290E+02	8.10652E+03	3.00569E+02	1.20251E+03	3.33964E-01
JAYA	7.18260E+03	4.12594E+02	8.02355E+03	2.36123E+02	1.20252E+03	2.42585E-01
	F13		F14		F15	
	AVG	STD	AVG	STD	AVG	STD
PLO	1.30031E+03	6.25260E-02	**1.40023E+03**	**3.70858E-02**	**1.50545E+03**	1.43031E+00
PSO	1.30038E+03	8.09065E-02	1.40029E+03	1.18701E-01	1.51720E+03	1.08168E+00
GSA	1.30017E+03	2.04549E-02	1.40035E+03	3.79031E-02	1.51305E+03	7.61710E-01
HHO	1.30051E+03	1.16594E-01	1.40028E+03	1.20478E-01	1.53918E+03	8.19681E+00
MFO	1.30183E+03	1.27103E+00	1.43275E+03	2.95546E+01	1.06919E+05	2.04480E+05
ACOR	1.30050E+03	1.17547E-01	1.40082E+03	2.48416E-01	5.89052E+03	2.35774E+04
MVO	1.30191E+03	1.14176E+00	1.43409E+03	2.85496E+01	2.43655E+05	3.72453E+05
WOA	1.30053E+03	1.18320E-01	1.40027E+03	1.05468E-01	1.57656E+03	3.31120E+01
SCA	1.30300E+03	3.33023E-01	1.44181E+03	5.56476E+00	4.16208E+03	2.49122E+03
JAYA	1.30142E+03	3.59309E-01	1.40317E+03	2.89896E+00	1.53035E+03	3.94161E+00
	F16		F17		F18	
	AVG	STD	AVG	STD	AVG	STD
PLO	**1.61115E+03**	4.62027E-01	**1.47378E+05**	**7.43903E+04**	**7.15315E+03**	**4.89747E+03**
PSO	1.61209E+03	4.82499E-01	3.51099E+05	1.59469E+05	2.21697E+06	7.51169E+05
GSA	1.61302E+03	3.35425E-01	2.83351E+05	2.37599E+05	7.53440E+04	2.50678E+04
HHO	1.61230E+03	3.67731E-01	1.05122E+06	6.52895E+05	6.19645E+04	2.68552E+04

MFO	1.61284E+03	6.99251E-01	4.07702E+06	8.16001E+06	7.57072E+07	2.25269E+08
ACOR	1.61159E+03	4.16877E-01	2.17233E+05	4.41195E+05	1.05396E+04	8.55612E+03
MVO	1.61262E+03	6.15450E-01	2.74360E+06	3.41646E+06	2.19665E+07	8.44954E+07
WOA	1.61273E+03	3.57414E-01	4.30749E+06	3.15882E+06	2.59047E+04	6.92390E+04
SCA	1.61273E+03	2.91449E-01	6.02334E+06	3.18895E+06	1.72113E+08	8.86854E+07
JAYA	1.61275E+03	1.68697E-01	2.83678E+06	1.35349E+06	4.02139E+07	1.65813E+07
	F19		F20		F21	
	AVG	STD	AVG	STD	AVG	STD
PLO	**1.90611E+03**	**1.04663E+00**	4.79181E+03	2.02594E+03	**3.08905E+04**	**2.66474E+04**
PSO	1.91646E+03	2.40026E+00	2.35263E+03	9.46868E+01	1.14677E+05	6.93073E+04
GSA	1.90746E+03	1.20844E+00	3.18685E+04	1.23045E+04	1.10166E+05	7.10347E+04
HHO	1.92599E+03	2.95438E+01	6.68935E+03	2.54166E+03	3.14890E+05	2.22243E+05
MFO	1.95749E+03	4.76411E+01	6.93570E+04	4.06528E+04	2.11333E+06	5.16761E+06
ACOR	1.92106E+03	2.49926E+01	6.45998E+03	8.80111E+03	7.41971E+04	6.55863E+04
MVO	1.96148E+03	4.61751E+01	5.84776E+04	3.12738E+04	9.47910E+05	1.72539E+06
WOA	1.94323E+03	3.06546E+01	3.16471E+04	2.88149E+04	1.71420E+06	2.17102E+06
SCA	1.99435E+03	2.29917E+01	1.77713E+04	3.93616E+03	1.32344E+06	6.89273E+05
JAYA	1.92459E+03	2.60580E+00	5.20392E+03	1.93952E+03	6.19585E+05	2.33167E+05
	F22		F23		F24	
	AVG	STD	AVG	STD	AVG	STD
PLO	**2.34627E+03**	**6.97860E+01**	2.61524E+03	2.02579E-04	2.62420E+03	8.13742E-01
PSO	2.90447E+03	1.91434E+02	2.61600E+03	4.91742E-01	2.62750E+03	4.85209E+00
GSA	3.06824E+03	2.67096E+02	2.61510E+03	5.77287E+00	2.60833E+03	4.78149E-01
HHO	3.04304E+03	2.35024E+02	2.50000E+03	0	2.60000E+03	9.90250E-05
MFO	3.05714E+03	2.39478E+02	2.67797E+03	6.11112E+01	2.67557E+03	3.83805E+01
ACOR	2.57688E+03	2.35756E+02	2.61779E+03	7.95074E+00	2.64276E+03	7.14782E+00
MVO	2.98332E+03	2.77576E+02	2.66783E+03	3.59803E+01	2.67524E+03	2.45758E+01
WOA	3.02959E+03	2.09526E+02	2.63216E+03	1.05383E+01	2.60622E+03	3.78078E+00
SCA	2.96537E+03	1.46290E+02	2.66890E+03	1.20485E+01	2.60006E+03	5.68196E-02
JAYA	2.81769E+03	1.52449E+02	2.64140E+03	5.60837E+00	2.62220E+03	2.22317E+01
	F25		F26		F27	
	AVG	STD	AVG	STD	AVG	STD
PLO	2.70430E+03	6.04237E-01	**2.70030E+03**	**6.08050E-02**	3.18228E+03	5.59585E+01
PSO	2.71276E+03	6.94754E+00	2.77710E+03	4.30640E+01	3.44520E+03	2.92059E+02
GSA	2.70192E+03	1.25516E-01	2.77433E+03	4.27648E+01	3.23268E+03	2.15286E+02
HHO	2.70000E+03	0	2.77014E+03	4.63917E+01	2.90000E+03	0
MFO	2.71515E+03	8.27838E+00	2.70228E+03	1.29613E+00	3.56876E+03	2.73005E+02
ACOR	2.70780E+03	4.78638E+00	2.72456E+03	7.28413E+01	3.43275E+03	9.70817E+01
MVO	2.71657E+03	9.29336E+00	2.70166E+03	1.03711E+00	3.58862E+03	2.55700E+02
WOA	2.71843E+03	1.82197E+01	2.70045E+03	1.16569E-01	3.80732E+03	3.16691E+02
SCA	2.72705E+03	8.97416E+00	2.70241E+03	6.79014E-01	3.42547E+03	3.12349E+02
JAYA	2.71847E+03	4.86995E+00	2.70076E+03	1.02989E-01	3.42040E+03	2.26617E+02
	F28		F29		F30	
	AVG	STD	AVG	STD	AVG	STD

PLO	3.63967E+03	3.36084E+01	5.62948E+03	8.02789E+02	**5.02396E+03**	**4.02173E+02**
PSO	6.92616E+03	1.16049E+03	7.82418E+04	1.36791E+05	1.49820E+04	6.11889E+03
GSA	4.75518E+03	4.94556E+02	3.59419E+07	5.59353E+07	7.88794E+03	1.04783E+03
HHO	3.00000E+03	0	3.10000E+03	0	5.29478E+03	5.41021E+03
MFO	3.97290E+03	2.30698E+02	2.32032E+06	3.48385E+06	5.77526E+04	5.65330E+04
ACOR	3.87478E+03	1.95295E+02	2.97905E+06	4.33568E+06	9.83242E+03	7.81635E+03
MVO	3.87714E+03	1.44785E+02	2.71869E+06	3.86312E+06	4.62740E+04	3.89747E+04
WOA	4.95012E+03	4.72671E+02	7.05295E+06	4.37111E+06	8.24271E+04	5.40183E+04
SCA	4.84274E+03	3.37062E+02	1.11467E+07	6.52644E+06	2.47814E+05	6.98566E+04
JAYA	4.80474E+03	4.98293E+02	7.08109E+06	3.74381E+06	1.81546E+04	4.12412E+03

Table 7. WSRT results and FT rankings for PLO and classical algorithmic competitions.

Algorithm	Mean	Rank	+/-/=
PLO	**1.87**	**1**	~
PSO	5.07	5	26/2/2
GSA	4.13	3	20/7/3
HHO	3.67	2	21/8/1
MFO	7.40	9	28/1/1
ACOR	4.40	4	22/0/8
MVO	6.83	7	28/1/1
WOA	6.30	6	27/2/1
SCA	8.43	10	29/1/0
JAYA	6.90	8	28/0/2

In Table 6, PLO has the best AVG and STD in most functions, indicating that it finds a better optimal solution among many competitors and is more stable. Subsequently, in Table 7, the FT rankings of all the participating algorithms are based on their combined performance in the 30 functions. In the column of the "Mean" of the combined rankings of all functions, the PLO has an average of 1.87, indicating that it ranks relatively high in all individual functions and is finally ranked in 1st place. In addition, the "+/-/=" column metrics also indicate that PLO's results on most functions are superior to those of its competitors. Thus, the comprehensive results show that PLO have better search capability, which is mainly attributed to the unique exploration and exploitation capabilities that PLO possess to better search for optimal solutions.

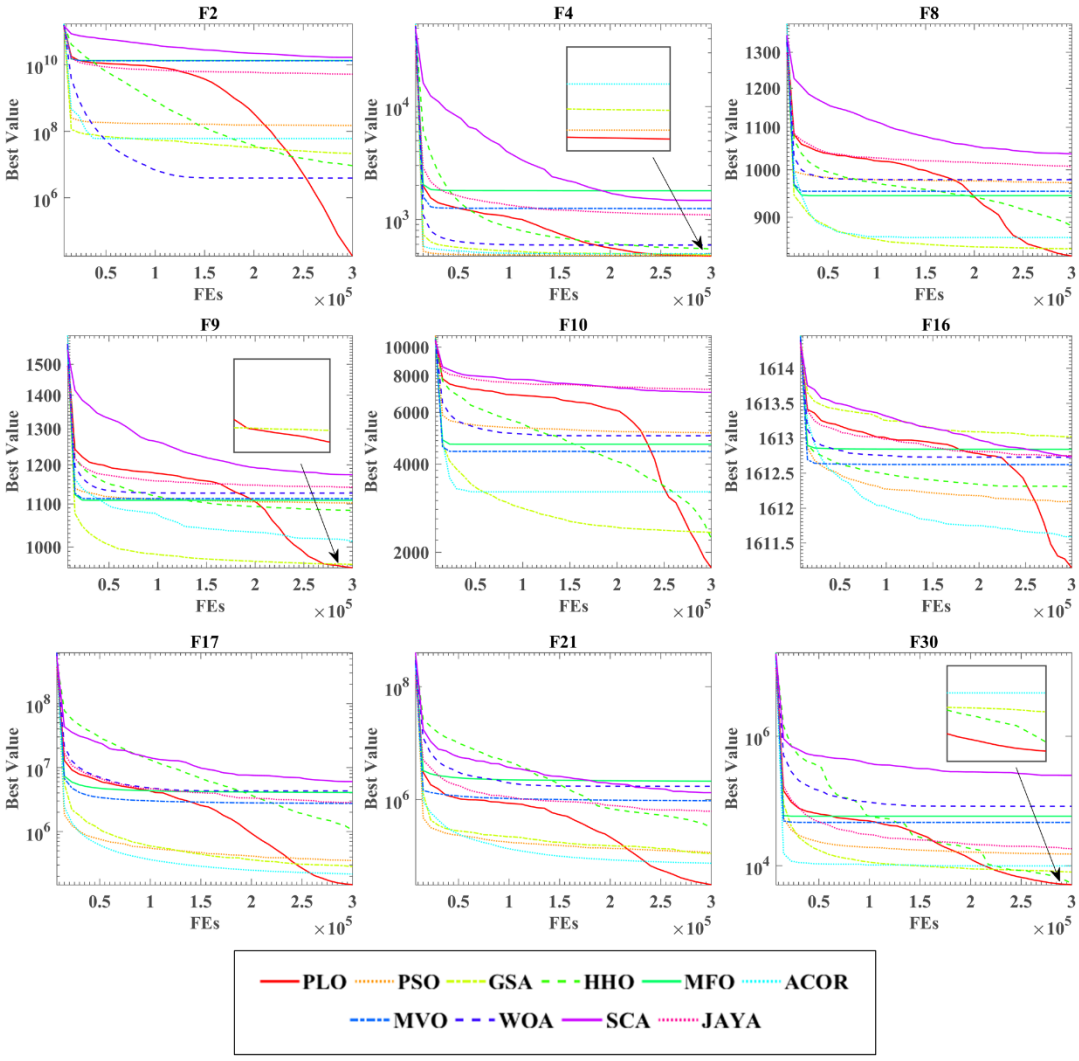

Figure 9. Convergence curves of the PLO with classical peers

Subsequently, to further comprehend the PLO's specific performance when competing with other algorithms, we generate curves illustrating the optimization processes of the competitors based on numerical values from experiments. In Figure 9, "Best Value" represents the optimal fitness value discovered by each algorithm during the iteration process. According to the PLO's curve, its major advantage, compared to other algorithms, lies in its sustained exploitation capability. The population update strategy, composed of gyration motion and aurora oval walk, balances global exploration with local exploitation. Some algorithms like PSO, GSA, and ACOR enter the convergence phase early on, indicating that their search agents might swiftly explore promising regions. However, these regions might be in the vicinity of local optima, causing the algorithms to converge to them. The distinctiveness of PLO from other algorithms lies in its steady trend of exploring the solution space early in the search process, constraining the step size in the initial stages and gradually exploring the global optimum as the search progresses based on accumulated experiences. Moreover, the particle collision strategy effectively addresses situations where the algorithm gets trapped in local areas. Therefore, in classical test sets, PLO, incorporating the three strategies, demonstrates a competitive advantage in achieving the optimal solution compared to other algorithms.

5.2.2 Comparison with improved algorithms

The competitiveness of PLO is initially demonstrated by comparing it with 9 classical algorithms utilizing 30 function problems from IEEE CEC2014. In addition, continuous research efforts have spawned many enhanced versions of the original algorithm, greatly improving its performance. As a result, these improved versions have become strong competitors. This section compares PLO with eight existing, enhanced algorithms to further demonstrate its superiority. Table 8 lists all the algorithms and parameter settings. The listed improved algorithms are all based on the original to improve the defects and increase performance. Therefore, it is worthwhile to compare PLO with 8 improved algorithms. The average value (AVG) and standard deviation (STD) of each algorithm after 30 independent runs are listed in Table 9.

Table 8. Algorithms and parameter settings.

Algorithms	Parameter(s)
A-C parametric WOA (ACWOA) [68]	$a_1 = [2,0];$ $a_2 = [-2,-1]; b = 1$
Double adaptive random spare reinforced whale optimization algorithm (RDWOA) [69]	$s = 0; a_1 = [2,0];$ $a_2 = [-2,-1]; b = 1$
Enhanced whale optimization algorithm (EWOA)[70]	$W_{max} = 0.7; W_{min} = 0.2$
Multi-population outpost mechanism enhanced Fruit fly optimizer (MOFOA) [71]	$M = 3$
Modified sine cosine algorithm (MSCA) [72]	$a = 2; \mathrm{JR} = 0.1$
The hybridization of HHO and DE(HHODE) [73]	$k = 0$
Novel random walk grey wolf optimizer (RWGWO)[74]	$a = [2\ 0]$
Boosted grey wolf optimizer (OBLGWO) [75]	$a = [2\ 0]$
Polar Lights Optimization (PLO)	$m = 100;\ a = [1,1.5]$

Table 9. Comparison results of the PLO and 8 enhanced algorithms

Function	F1		F2		F3	
Algorithm	AVG	STD	AVG	STD	AVG	STD
PLO	**2.58888E+06**	**1.37254E+06**	1.60022E+04	**7.16515E+03**	6.47824E+03	2.69953E+03
RDWOA	9.00898E+06	5.28923E+06	2.00340E+07	2.70048E+07	6.47326E+03	4.18534E+03
EWOA	4.06264E+06	3.21964E+06	1.24524E+04	1.11080E+04	5.66810E+03	3.53498E+03
MOFOA	1.23247E+09	6.79276E+07	7.63319E+10	2.60493E+09	7.86242E+04	5.75286E+03
MSCA	6.47601E+07	4.30416E+07	6.73724E+09	4.22215E+09	2.61552E+04	7.28091E+03
ACWOA	1.32478E+08	5.98124E+07	7.62074E+09	3.77871E+09	4.70727E+04	1.07912E+04
OBLGWO	1.87897E+07	9.62180E+06	1.26458E+07	8.04195E+06	9.31821E+03	3.30118E+03
RWGWO	4.66299E+06	2.31297E+06	4.31865E+04	2.16373E+04	6.92678E+02	3.62708E+02
HHODE	1.14056E+07	5.50907E+06	1.29535E+07	2.77570E+06	2.92326E+03	1.86966E+03
	F4		F5		F6	
	AVG	STD	AVG	STD	AVG	STD
PLO	**4.74061E+02**	**2.27437E+01**	5.20561E+02	3.37363E-01	6.09731E+02	2.24606E+00
RDWOA	5.45928E+02	4.29797E+01	5.20166E+02	1.80030E-01	6.24312E+02	3.07851E+00
EWOA	5.19614E+02	3.75406E+01	5.20106E+02	9.47625E-02	6.22602E+02	4.16211E+00
MOFOA	1.00269E+04	9.52576E+02	5.21041E+02	4.84214E-02	6.40862E+02	8.85176E-01
MSCA	8.17669E+02	1.43110E+02	5.20620E+02	1.33670E-01	6.21197E+02	3.14095E+00

ACWOA	1.21599E+03	2.86265E+02	5.20800E+02	2.18868E-01	6.33798E+02	2.60545E+00
OBLGWO	5.50197E+02	4.05828E+01	5.20951E+02	5.83239E-02	6.18597E+02	3.53868E+00
RWGWO	5.04711E+02	2.48334E+01	5.20455E+02	7.89524E-02	6.06751E+02	3.72543E+00
HHODE	5.36043E+02	3.31342E+01	5.20379E+02	1.25569E-01	6.18815E+02	2.50021E+00
	F7		F8		F9	
	AVG	STD	AVG	STD	AVG	STD
PLO	**7.00020E+02**	**7.35680E-03**	**8.24937E+02**	**6.69565E+00**	9.60520E+02	1.21681E+01
RDWOA	7.00870E+02	3.26513E-01	8.47610E+02	1.23758E+01	1.07602E+03	4.29832E+01
EWOA	7.00056E+02	7.64890E-02	8.37036E+02	1.13575E+01	1.06597E+03	3.54986E+01
MOFOA	1.40203E+03	4.63059E+01	1.17376E+03	1.39548E+01	1.26014E+03	6.12727E+00
MSCA	7.48131E+02	2.72574E+01	9.41051E+02	2.46217E+01	1.05383E+03	2.50578E+01
ACWOA	7.39354E+02	1.98148E+01	9.94044E+02	2.56494E+01	1.12966E+03	1.82469E+01
OBLGWO	7.01175E+02	1.05930E-01	9.28162E+02	3.67700E+01	1.05457E+03	3.80579E+01
RWGWO	7.00206E+02	1.70290E-01	8.37837E+02	6.95506E+00	9.57362E+02	1.30094E+01
HHODE	7.01112E+02	2.60225E-02	8.85842E+02	1.94788E+01	1.03321E+03	3.37957E+01
	F10		F11		F12	
	AVG	STD	AVG	STD	AVG	STD
PLO	1.90314E+03	3.28041E+02	3.78625E+03	5.07754E+02	1.20060E+03	2.76753E-01
RDWOA	1.64316E+03	2.83566E+02	4.64524E+03	5.97713E+02	1.20052E+03	2.62386E-01
EWOA	1.71205E+03	3.19032E+02	4.85535E+03	5.55956E+02	1.20037E+03	1.44304E-01
MOFOA	9.20768E+03	4.36682E+02	9.02506E+03	2.12850E+02	1.20308E+03	2.94277E-01
MSCA	4.37563E+03	5.52377E+02	4.93374E+03	9.02916E+02	1.20072E+03	3.53224E-01
ACWOA	4.84635E+03	8.21653E+02	6.08422E+03	9.10747E+02	1.20170E+03	5.37723E-01
OBLGWO	4.08182E+03	7.31952E+02	5.26152E+03	1.05074E+03	1.20243E+03	4.03388E-01
RWGWO	2.00752E+03	2.84101E+02	3.62333E+03	3.59447E+02	1.20047E+03	1.43993E-01
HHODE	2.37637E+03	5.86895E+02	4.53435E+03	1.01942E+03	1.20129E+03	5.11721E-01
	F13		F14		F15	
	AVG	STD	AVG	STD	AVG	STD
PLO	1.30029E+03	6.28405E-02	**1.40022E+03**	**3.58625E-02**	**1.50513E+03**	**1.36021E+00**
RDWOA	1.30042E+03	9.29129E-02	1.40024E+03	4.25697E-02	1.52242E+03	6.92987E+00
EWOA	1.30053E+03	1.07148E-01	1.40032E+03	1.49723E-01	1.52019E+03	6.06033E+00
MOFOA	1.30807E+03	2.91344E-01	1.63648E+03	1.12729E+01	2.29187E+05	2.99937E+04
MSCA	1.30087E+03	6.17514E-01	1.41527E+03	1.00715E+01	2.35065E+03	1.41699E+03
ACWOA	1.30153E+03	9.42553E-01	1.41405E+03	7.83670E+00	1.77465E+03	3.53956E+02
OBLGWO	1.30052E+03	9.75390E-02	1.40036E+03	1.32506E-01	1.51632E+03	5.50589E+00
RWGWO	1.30027E+03	5.91778E-02	1.40034E+03	1.60472E-01	1.50672E+03	2.02223E+00
HHODE	1.30047E+03	1.31728E-01	1.40030E+03	1.15910E-01	1.52273E+03	1.07047E+01
	F16		F17		F18	
	AVG	STD	AVG	STD	AVG	STD
PLO	1.61138E+03	4.18109E-01	**1.37689E+05**	**1.07592E+05**	7.41686E+03	6.07695E+03
RDWOA	1.61149E+03	6.17319E-01	1.14829E+06	1.00200E+06	5.37050E+03	4.95124E+03
EWOA	1.61164E+03	4.84462E-01	8.92898E+05	6.60515E+05	6.76060E+03	6.28557E+03
MOFOA	1.61345E+03	2.39033E-01	9.03589E+07	2.24826E+07	5.90779E+09	7.72096E+08
MSCA	1.61167E+03	5.10167E-01	1.49651E+06	1.52651E+06	2.84004E+07	4.72097E+07

ACWOA	1.61213E+03	3.93641E-01	1.71702E+07	1.35279E+07	4.86749E+07	4.31102E+07
OBLGWO	1.61207E+03	5.05751E-01	1.36272E+06	1.03422E+06	2.91097E+04	2.99895E+04
RWGWO	1.61030E+03	7.59522E-01	4.02997E+05	2.88595E+05	4.78847E+03	3.38017E+03
HHODE	1.61179E+03	4.49416E-01	1.28840E+06	9.12481E+05	5.89776E+03	5.27030E+03
	F19		F20		F21	
	AVG	STD	AVG	STD	AVG	STD
PLO	**1.90597E+03**	**8.84139E-01**	3.90475E+03	1.63956E+03	**2.93044E+04**	**1.51433E+04**
RDWOA	1.93048E+03	3.43452E+01	6.42805E+03	2.52514E+03	4.24150E+05	3.11509E+05
EWOA	1.93148E+03	4.07490E+01	4.17354E+03	2.53285E+03	5.17404E+05	4.17397E+05
MOFOA	2.23580E+03	1.17537E+01	1.74898E+05	8.31455E+04	3.55478E+07	1.08773E+07
MSCA	1.94735E+03	2.22443E+01	1.16050E+04	4.12061E+03	4.01535E+05	3.51706E+05
ACWOA	2.00938E+03	3.23774E+01	3.59644E+04	1.23469E+04	5.82263E+06	4.39701E+06
OBLGWO	1.91246E+03	2.52098E+00	5.86769E+03	2.31491E+03	4.94282E+05	3.62913E+05
RWGWO	1.90941E+03	1.37851E+00	2.25106E+03	6.99597E+01	1.75143E+05	1.79297E+05
HHODE	1.92036E+03	1.96240E+01	5.66388E+03	2.60203E+03	3.21142E+05	3.15404E+05
	F22		F23		F24	
	AVG	STD	AVG	STD	AVG	STD
PLO	**2.32289E+03**	**5.30930E+01**	2.61524E+03	9.19024E-05	2.62348E+03	1.74628E+00
RDWOA	2.69868E+03	1.64819E+02	2.51179E+03	3.59691E+01	2.60000E+03	1.52847E-04
EWOA	2.72148E+03	1.77466E+02	2.61541E+03	4.56766E-01	2.60616E+03	1.17224E+01
MOFOA	1.88998E+04	1.03262E+04	2.50000E+03	0	2.60000E+03	0
MSCA	2.60815E+03	1.44123E+02	2.63788E+03	8.94771E+00	2.60000E+03	5.92355E-04
ACWOA	3.06437E+03	2.50681E+02	2.53413E+03	7.78892E+01	2.60000E+03	9.90233E-06
OBLGWO	2.72758E+03	2.11202E+02	2.61774E+03	1.19805E+00	2.60099E+03	5.44973E+00
RWGWO	2.46499E+03	1.27906E+02	2.61526E+03	6.22712E-03	2.60001E+03	2.78022E-03
HHODE	2.66106E+03	1.43916E+02	2.50000E+03	0	2.60000E+03	2.99477E-04
	F25		F26		F27	
	AVG	STD	AVG	STD	AVG	STD
PLO	2.70441E+03	7.50508E-01	**2.70032E+03**	**7.27466E-02**	3.18389E+03	3.85842E+01
RDWOA	2.70000E+03	0	2.70106E+03	2.63843E+00	2.95318E+03	2.06260E+02
EWOA	2.71345E+03	4.81043E+00	2.71049E+03	3.04128E+01	3.64167E+03	1.48862E+02
MOFOA	2.70000E+03	0	2.78592E+03	3.20490E+01	2.90000E+03	0
MSCA	2.71412E+03	3.56094E+00	2.70083E+03	2.62975E-01	3.16435E+03	1.19885E+02
ACWOA	2.70000E+03	0	2.75039E+03	5.04639E+01	3.59702E+03	3.75158E+02
OBLGWO	2.70000E+03	0	2.70055E+03	1.22076E-01	3.07799E+03	3.38456E+02
RWGWO	2.70515E+03	1.14305E+00	2.74782E+03	5.97202E+01	3.17592E+03	8.53553E+01
HHODE	2.70000E+03	0	2.70049E+03	1.35214E-01	2.90000E+03	0
	F28		F29		F30	
	AVG	STD	AVG	STD	AVG	STD
PLO	3.63750E+03	2.96402E+01	5.67137E+03	7.83014E+02	5.03128E+03	5.14600E+02
RDWOA	3.07709E+03	2.93445E+02	2.60507E+06	4.04255E+06	1.09039E+04	5.18296E+03
EWOA	4.44018E+03	4.03578E+02	4.65796E+06	4.43013E+06	1.12920E+04	6.72554E+03
MOFOA	3.00000E+03	0	3.10000E+03	0	3.20000E+03	0
MSCA	3.92934E+03	1.24918E+02	1.13782E+06	3.07439E+06	5.15822E+04	2.67005E+04

ACWOA	4.09153E+03	1.20821E+03	2.02662E+07	1.66326E+07	4.88251E+05	3.06028E+05
OBLGWO	3.62837E+03	5.97363E+02	3.75535E+06	4.34368E+06	2.19586E+04	1.46415E+04
RWGWO	3.70573E+03	9.98039E+01	5.78212E+05	2.16710E+06	7.20355E+03	1.26970E+03
HHODE	3.00000E+03	0	1.09505E+06	3.36433E+06	1.65759E+04	2.06178E+04

Table 10. WSRT results and FT rankings for PLO and enhanced algorithm competitions

Algorithm	Mean	Rank	+/-/=
PLO	**2.77**	**1**	**~**
RDWOA	3.97	4	17/7/6
EWOA	4.70	5	21/4/5
MOFOA	7.13	8	23/7/0
MSCA	6.37	7	26/2/2
ACWOA	7.33	9	27/3/0
OBLGWO	5.53	6	26/2/2
RWGWO	3.03	2	17/7/6
HHODE	3.73	3	21/7/2

As depicted in Table 9, PLO exhibits dominance in comparison to enhanced algorithms. This demonstrates that PLO possesses the stable ability to search for superior solutions when faced with competition from these algorithms. Furthermore, Table 10 presents the results of a comparative analysis between PLO and the eight improved algorithms using WSRT and FT. By examining the "Mean" columns and the "+/-/=" columns, it becomes apparent that these enhanced algorithms possess enhanced search ability compared to the original algorithm. Nevertheless, PLO continues to secure the first rank, indicated by a "Mean" of 2.77, thereby substantiating its performance superiority over these enhancers.

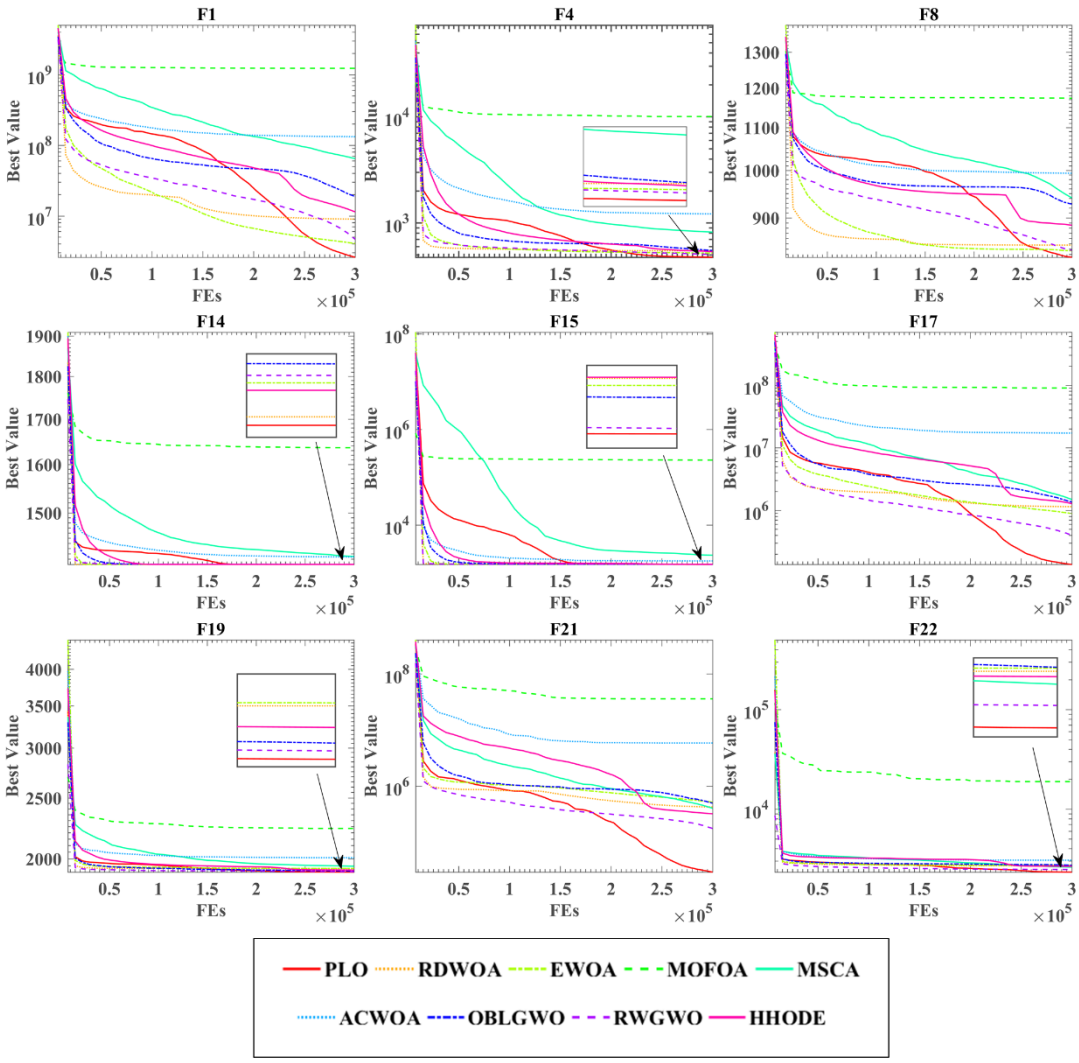

Figure 10. Convergence curves of PLO and enhancers

Figure 10 demonstrates that the enhanced algorithms exhibit a refined convergence process. Compared to the original algorithm, these enhanced algorithms effectively enhance convergence accuracy through improved exploration and exploitation capabilities. The graph shows that PLO continues to maintain its advantage, with gyration motion aiding in local exploitation and aurora oval walk facilitating step-wise refinement in global exploration, ultimately achieving higher accuracy in attaining the optimal solution. Hence, PLO successfully surpasses the enhanced algorithms, demonstrating its remarkable performance.

5.2.3 Comparison and analysis based on the latest IEEE CEC2022

In the previous subsection, the success of PLO's comparison experiments in IEEE CEC2014 shows that PLO is highly adaptable and optimizable to the classical set of benchmark functions. The IEEE CEC2022 benchmark function set makes improvements in accuracy, comprehensiveness, and diversity and is more accurate and challenging compared to the former; the performance of different optimization algorithms can be better evaluated and compared. Therefore, this study compares PLO with nine algorithms utilizing 12 functions from IEEE CEC2022, including five classical algorithms as well as four improved algorithms, and Table 11 lists the competitors and their parameter settings. In this experiment, the difference from the previous subsections is that the setting is 20 dimensions (the default value) due to the dimensionality

limitation of the test function, along with 200,000 fitness evaluations (FEs) of each algorithm.

Table 11. Algorithms and parameter settings.

Algorithms	Parameters
Gravitational search algorithm (GSA) [24]	$Rnorm = 2$
Harris Hawk optimizer (HHO) [32]	$k = 0$
The hybridization of HHO and DE(HHODE) [73]	$k = 0$
Particle swarm optimizer (PSO) [63]	$c_1 = 2;\ c_2 = 2;\ V_{max} = 6$
Whale optimization algorithm (WOA) [65]	$a_1 = [2,0]; a_2 = [-2,-1]; b = 1$
Double adaptive random spare reinforced whale optimization algorithm (RDWOA) [69]	$s = 0; a_1 = [2,0];$ $a_2 = [-2,-1]; b = 1$
Enhanced whale optimization algorithm (EWOA) [70]	$W_{max} = 0.7; W_{min} = 0.2$
Moth-flame optimization algorithm (MFO) [64]	$b = 1$
Comprehensive learning Jaya algorithm(CLJAYA) [76]	~
Polar Lights Optimization (PLO)	$m = 100, a = [1,1.5]$

Table 12. Comparison results of PLO and peers in IEEE CEC2022

Function	F1		F2		F3	
Algorithm	AVG	STD	AVG	STD	AVG	STD
PLO	2.8025E+03	8.7755E+02	**4.2984E+02**	1.7513E+01	**6.0003E+02**	**5.2462E-03**
PSO	3.7239E+02	1.3269E+01	4.3497E+02	2.6235E+01	6.4321E+02	1.3361E+01
GSA	2.8341E+04	5.9535E+03	4.5713E+02	1.4349E+01	6.0150E+02	6.4317E-01
HHO	3.0876E+02	3.0949E+00	4.5177E+02	2.1142E+01	6.4922E+02	8.1762E+00
MFO	3.2221E+04	2.5442E+04	5.2829E+02	1.0937E+02	6.2331E+02	1.0432E+01
WOA	3.6525E+03	3.2479E+03	4.9471E+02	4.2330E+01	6.6359E+02	1.3470E+01
RDWOA	1.4302E+03	1.1354E+03	4.6529E+02	2.8458E+01	6.0166E+02	1.6313E+00
HHODE	3.8104E+02	6.2600E+01	4.6228E+02	1.1842E+01	6.1576E+02	7.1073E+00
EWOA	3.3751E+02	2.5027E+01	4.5891E+02	1.2724E+01	6.1070E+02	8.7615E+00
CLJAYA	3.0000E+02	1.1725E-09	4.3787E+02	1.9851E+01	6.0025E+02	5.2729E-01
	F4		F5		F6	
	AVG	STD	AVG	STD	AVG	STD
PLO	**8.3831E+02**	1.0980E+01	9.0845E+02	6.8652E+00	9.3410E+03	6.9851E+03
PSO	8.9395E+02	1.9548E+01	1.6146E+03	9.0429E+02	1.3449E+06	3.3342E+05
GSA	8.5772E+02	9.7625E+00	9.0249E+02	3.7211E-01	1.7420E+05	5.7650E+04
HHO	8.8326E+02	1.7302E+01	2.4894E+03	2.3097E+02	5.8520E+04	3.2964E+04
MFO	9.0427E+02	2.4685E+01	2.9222E+03	9.2013E+02	1.0604E+07	1.5511E+07
WOA	9.1443E+02	3.4836E+01	3.5780E+03	1.3935E+03	1.4146E+04	2.3211E+04
RDWOA	9.1546E+02	3.5017E+01	2.4617E+03	5.6110E+02	8.5933E+03	6.8561E+03
HHODE	8.6155E+02	2.2986E+01	1.5985E+03	4.0551E+02	4.2818E+03	3.3157E+03
EWOA	8.8640E+02	3.2501E+01	2.0384E+03	5.8491E+02	7.9893E+03	6.4194E+03
CLJAYA	8.7942E+02	1.6901E+01	9.0675E+02	9.0369E+00	8.7790E+03	7.3969E+03
	F7		F8		F9	
	AVG	STD	AVG	STD	AVG	STD
PLO	**2.0317E+03**	**6.9219E+00**	**2.2251E+03**	**1.3537E+00**	2.4808E+03	3.2679E-03
PSO	2.1336E+03	5.3138E+01	2.3183E+03	8.7876E+01	2.4658E+03	1.1410E-01
GSA	2.2386E+03	9.3274E+01	2.3289E+03	6.9004E+01	2.4864E+03	5.4579E-01

HHO	2.1538E+03	4.2211E+01	2.2474E+03	3.3092E+01	2.4838E+03	1.7135E+00
MFO	2.1169E+03	3.3698E+01	2.2617E+03	5.3296E+01	2.4990E+03	1.8949E+01
WOA	2.1915E+03	6.3906E+01	2.2509E+03	3.0478E+01	2.4967E+03	1.8223E+01
RDWOA	2.0824E+03	5.0892E+01	2.2292E+03	2.2118E+01	2.4811E+03	6.9223E-01
HHODE	2.0834E+03	2.9810E+01	2.2297E+03	8.5891E+00	2.4844E+03	3.6474E+00
EWOA	2.0866E+03	4.3626E+01	2.2308E+03	2.6025E+01	2.4809E+03	1.2385E-01
CLJAYA	2.0429E+03	2.3608E+01	2.2319E+03	4.3762E+00	2.4808E+03	1.2610E-12
	F10		F11		F12	
	AVG	STD	AVG	STD	AVG	STD
PLO	**2.5004E+03**	**6.8985E-02**	**2.6001E+03**	**2.2371E-02**	2.8598E+03	**1.2322E+00**
PSO	4.2156E+03	1.0723E+03	2.7008E+03	1.5950E+02	2.8541E+03	1.6468E+01
GSA	2.8448E+03	3.8265E+02	2.8309E+03	1.5133E+02	2.8794E+03	1.6767E+01
HHO	3.0675E+03	5.4938E+02	2.7853E+03	1.3997E+02	2.8872E+03	3.2423E+01
MFO	3.7391E+03	1.0153E+03	2.8188E+03	1.5086E+02	2.8648E+03	4.4151E+00
WOA	4.5073E+03	1.0058E+03	2.7831E+03	1.4491E+02	2.8815E+03	2.9317E+01
RDWOA	2.6008E+03	1.1062E+02	2.8853E+03	2.0788E+02	2.8689E+03	1.0270E+01
HHODE	2.5299E+03	8.0654E+01	2.6631E+03	7.2919E+01	2.8639E+03	1.6712E+00
EWOA	2.9545E+03	3.8171E+02	2.7767E+03	1.4438E+02	2.8652E+03	3.8596E+00
CLJAYA	2.8599E+03	6.9902E+02	2.6985E+03	1.3808E+02	2.8668E+03	7.5038E+00

Table 13. WSRT results and FT rankings for PLO and competitor comparisons at IEEE CEC2022

Algorithm	Mean	Rank	+/-/=
PLO	**2.25**	**1**	~
PSO	5.50	5	8/3/1
GSA	6.42	7	11/1/0
HHO	6.58	8	11/1/0
MFO	8.17	9	12/0/0
WOA	8.50	10	10/0/2
RDWOA	5.67	6	9/1/2
HHODE	3.92	3	10/2/0
EWOA	4.75	4	9/1/2
CLJAYA	3.25	2	6/2/4

In Table 12, PLO's performance in the latest test set manages to show excellent exploration results, which shows that the algorithm can adapt to new problems while being very stable. The IEEE CEC2022 benchmark function set places higher demands on the accuracy and stability of algorithmic exploration. In Table 13, PLO stands out with its advantages and tops the list with an " Mean" value of 2.25. In addition, PLO outperforms peers in most of the functions in the "+/-/=" column. These findings demonstrate that PLO exhibits superior fitness and exploration results compared to other algorithms in the latest test set.

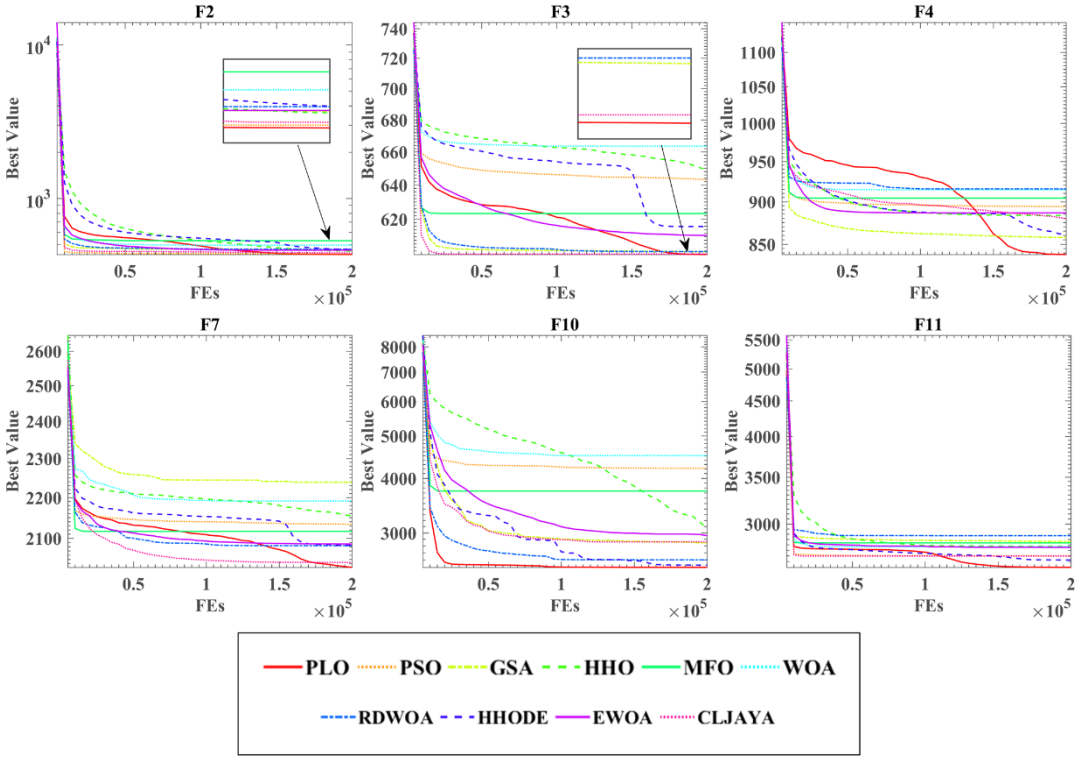

Figure 11. Convergence curves of the PLO and competitors in the IEEE CEC2022

Figure 11 showcases the exploration process of the optimal solution by PLO and its competitors using the most recent test set. PLO demonstrates a recognizable inclination to escape the confines of local optimal during the later stages of local exploitation in F4, F7, and F11, culminating in attaining the highest convergence accuracy. Conversely, PLO efficiently identifies a superior solution during the initial search phase of the algorithm in F2, F10, and F11, subsequently advancing continuously from this foundation. Consequently, PLO effectively optimizes the entire solution process in terms of both accuracy and speed, thereby substantiating its superior performance in handling intricate problems. Consequently, PLO emerges as a highly potent meta-heuristic algorithm capable of upholding remarkable levels of accuracy and efficiency when confronted with these latest challenges.

5.2.4 Comparison with state-of-the-art algorithms on the latest IEEE CEC2022

In this section, we compare and analyze our proposed PLO with the current state-of-the-art methods in the field utilizing 12 functions from IEEE CEC2022. This comparison serves two purposes: firstly, to further evaluate the effectiveness of our method and gather insights for potential improvements; secondly, by engaging in this process, we aim not only to validate our contribution but also to gain a comprehensive understanding of the landscape within which our work operates in the current field. Therefore, this study will compare the PLO with three state-of-the-art algorithms, including LSHADE [64], EBOwithCMAR [65] and RUN [27], which are currently the most widely recognized advanced methods. Table 14 lists their parameter settings. The dimensionality is set to 20 dimensions (default), and the fitness evaluations (FEs) for each algorithm are set to 200,000 iterations.

Table 14. Algorithms and parameter settings.

Algorithms	Parameter(s)
Polar Lights Optimization (PLO)	$m = 100;\ a = [1,1.5]$

LSHADE[77]	$p = 0.11, r_{arc} = 1.4, N_{min} = 4, M_{size} = 5$
EBOwithCMAR[78]	$PS1_{max} = 18D; PS1_{min} = 4;$ $PS2_{max} = 46.8D; PS2_{min} = 10;\ H = 6;$ $PS3 = 4 + (3\log(D)); \sigma = 0.3; prob_{ls} = 0.1;$ $cfe_{ls} = 0.25MaxFEs$
RUN [37]	$a = 20; b = 12$

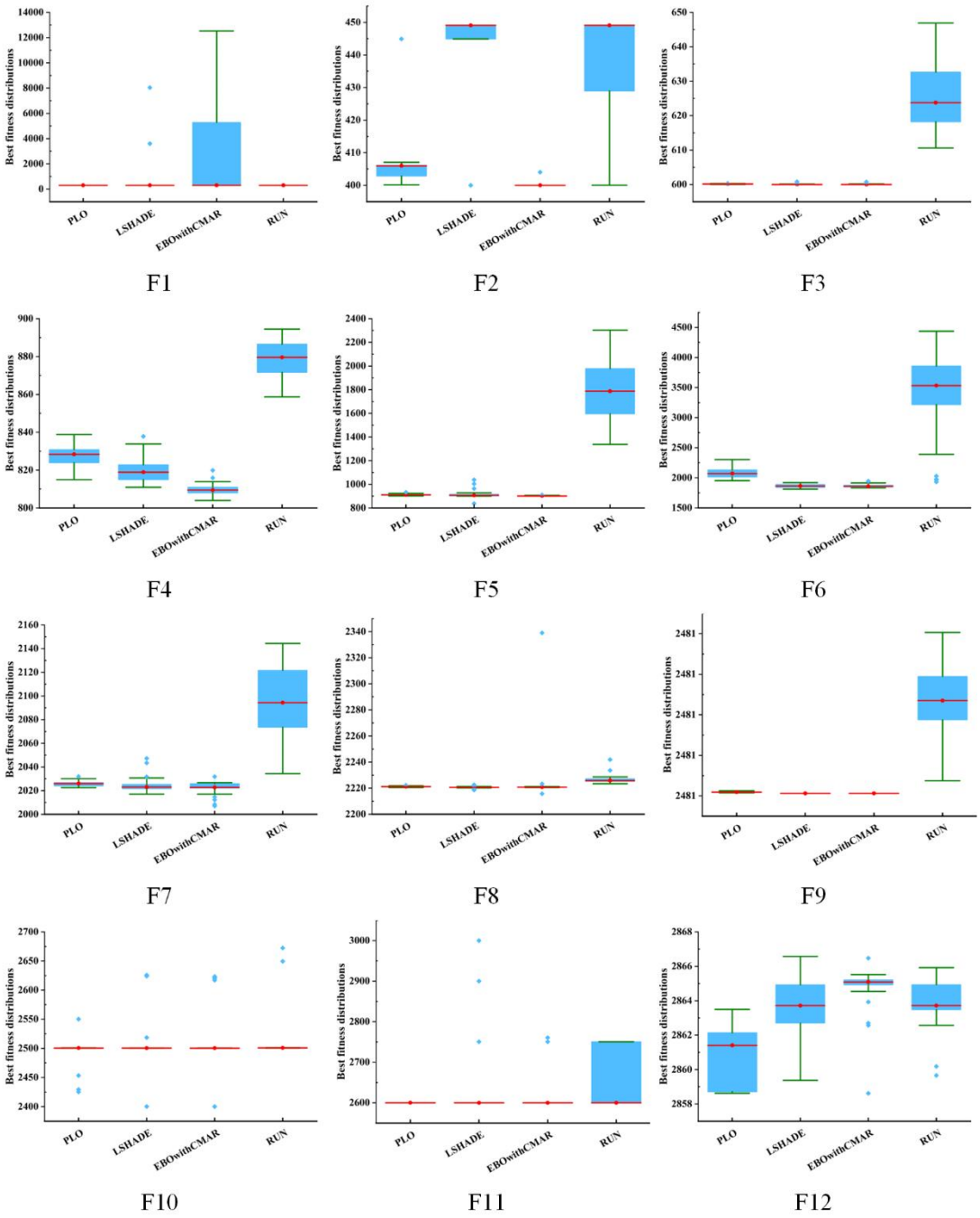

Figure 12. Boxplots of PLO and excellent algorithms.

In this section, the PLO is compared with advanced algorithms on 12 functions, and boxplots are generated from 30 independent runs to provide a visual analysis of the results. As depicted in the Figure 12, the PLO demonstrates encouraging outcomes, achieving optimal solutions or satisfactory approximations in

most functions. Furthermore, the morphology of the box plots and whisker plots indicates that the results from 30 independent runs of the PLO are distributed within a smaller range, demonstrating the stability of its solving process. Lastly, observing the presence of outliers shows that the PLO is more likely to produce consistent and reliable results compared to other methods. Table 15 presents the ranking results of this comparison, with PLO securing the first rank overall, indicating its superiority over the current state-of-the-art methods.

Table 15. WSRT results and FT rankings for PLO and competitor comparisons

Algorithm	Mean	Rank	+/-/=
PLO	**2**	**1**	~
LSHADE	2.25	2	3/5/4
EBOwithCMAR	2.25	2	3/5/4
RUN	3.5	4	9/1/2

Figure 13 illustrates the convergence process of PLO and competitors. Here, it can be observed that LSHADE and EBOwithCMAR exhibit competitive advantages by swiftly narrowing down to local regions containing the global optimum in the early stages of convergence and focusing on developing optimal solutions within them. In contrast, PLO concentrates on consolidating the convergence process by integrating the knowledge acquired thus far and progressively exploring. Consequently, PLO effectively optimizes the accuracy of the entire process, thereby demonstrating its outstanding performance in tackling complex problems.

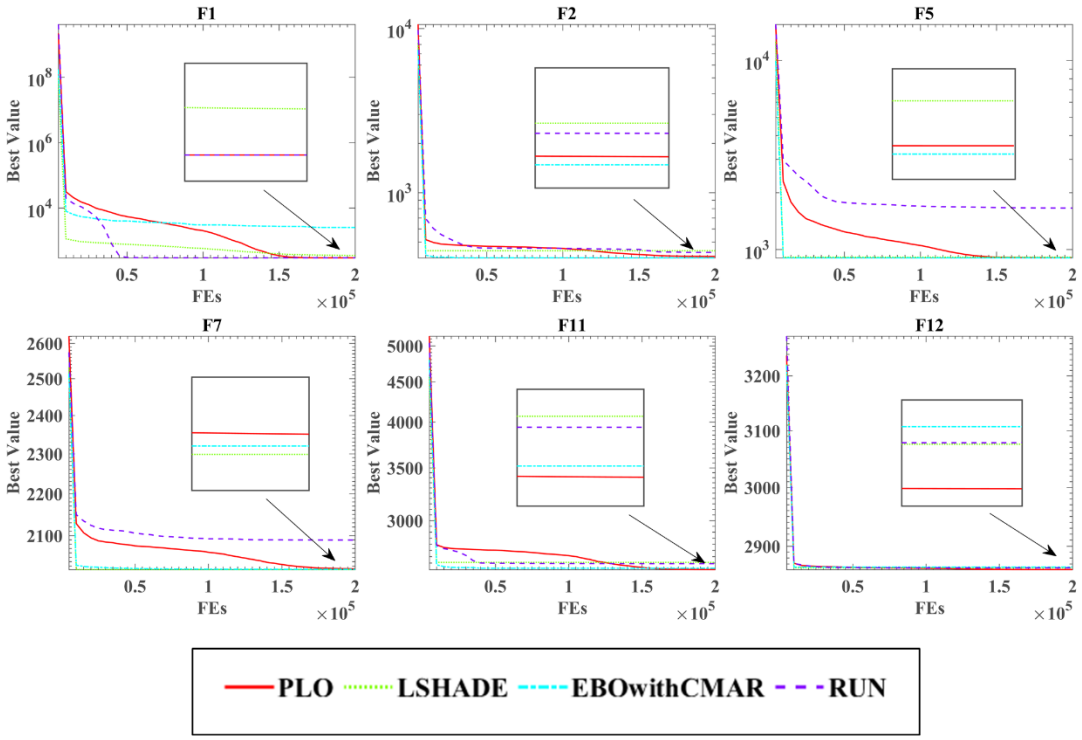

Figure 13. Convergence curves of PLO and state-of-the-art methods.

5.3 Qualitative analysis experiment

Since only models and theories are elaborated, it does not provide a clear understanding of the searching process for the most solutions to the proposed method. Therefore, this subsection presents the abstract algorithmic solution process in graphs, etc., enabling a more intuitive understanding of the

algorithm's workings and internal mechanisms. Then, the scalability of the PLO to large-scale problems is analyzed.

5.3.1 Optimization process analysis

This subsection describes an experiment that reflects the historical trajectory of an agent's position by recording the best position for each iteration. In addition, this paper investigates the updates performed on the agent and analyzes the particles inside the agent, particularly the agent's transversal dimension vector. This analysis aims to reveal the mode and extent of particle variations. In this subsection, a particle change experiment is designed to record the optimal agent for a particle's position in each round of iteration. In addition, a devised experiment on the alteration of fitness value is conducted to record the fitness value after each iteration. The experiment meticulously marked down the ultimate fitness value after every update. Finally, we set up iterative curve experiments to reflect the overall trend of PLO.

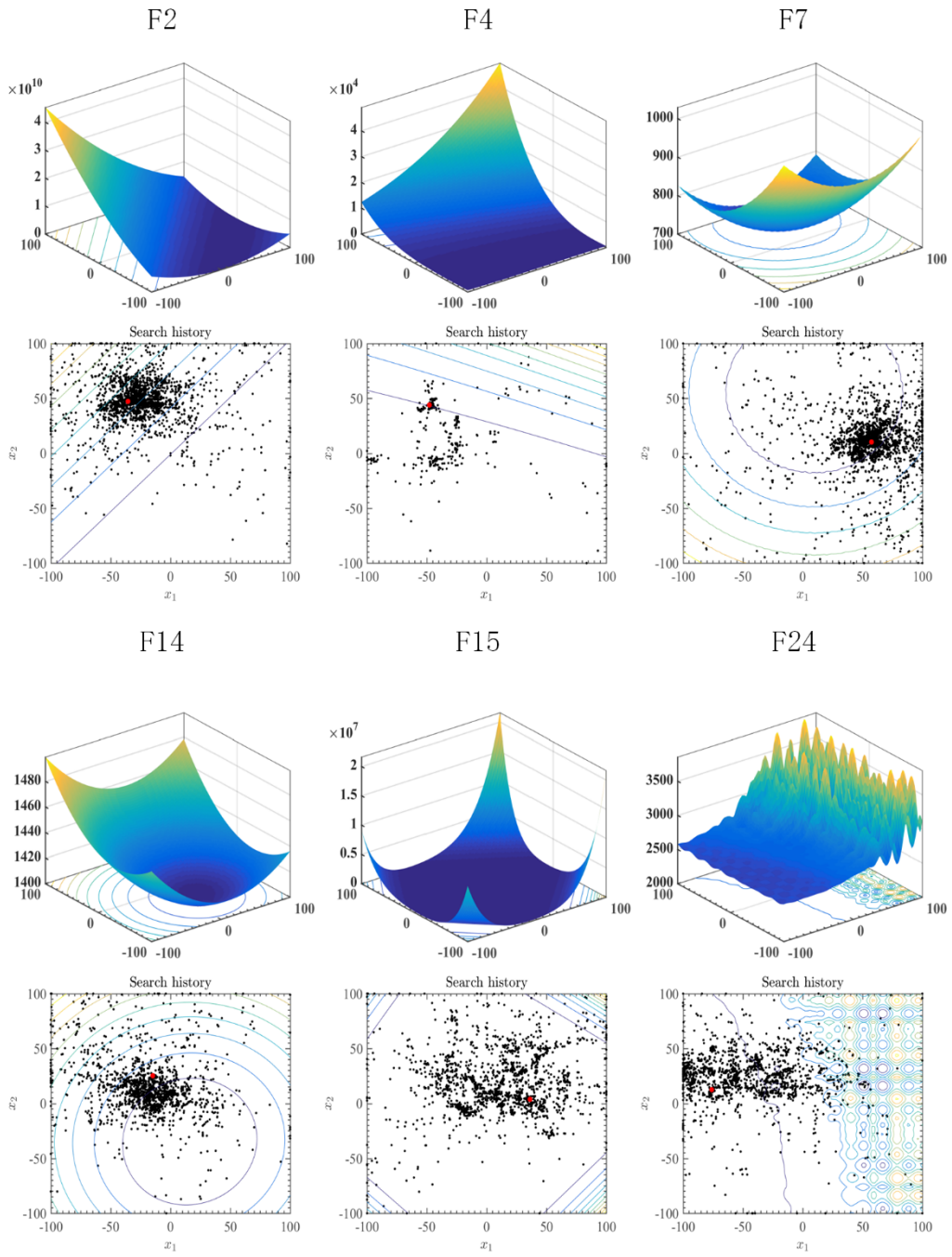

Figure 14. The 3D image of benchmark functions and PLO's solution distribution

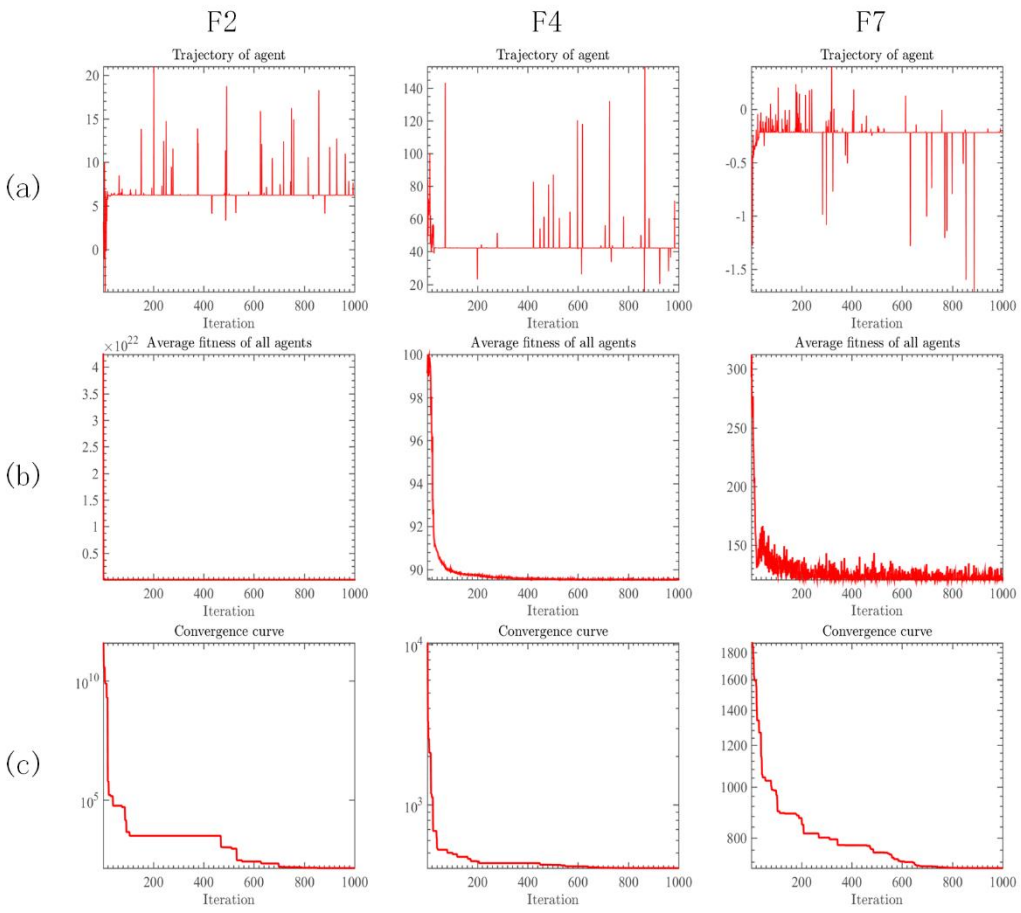
F2
F4
F7
(a)
(b)
(c)
Trajectory of agent
Average fitness of all agents
Convergence curve
Iteration

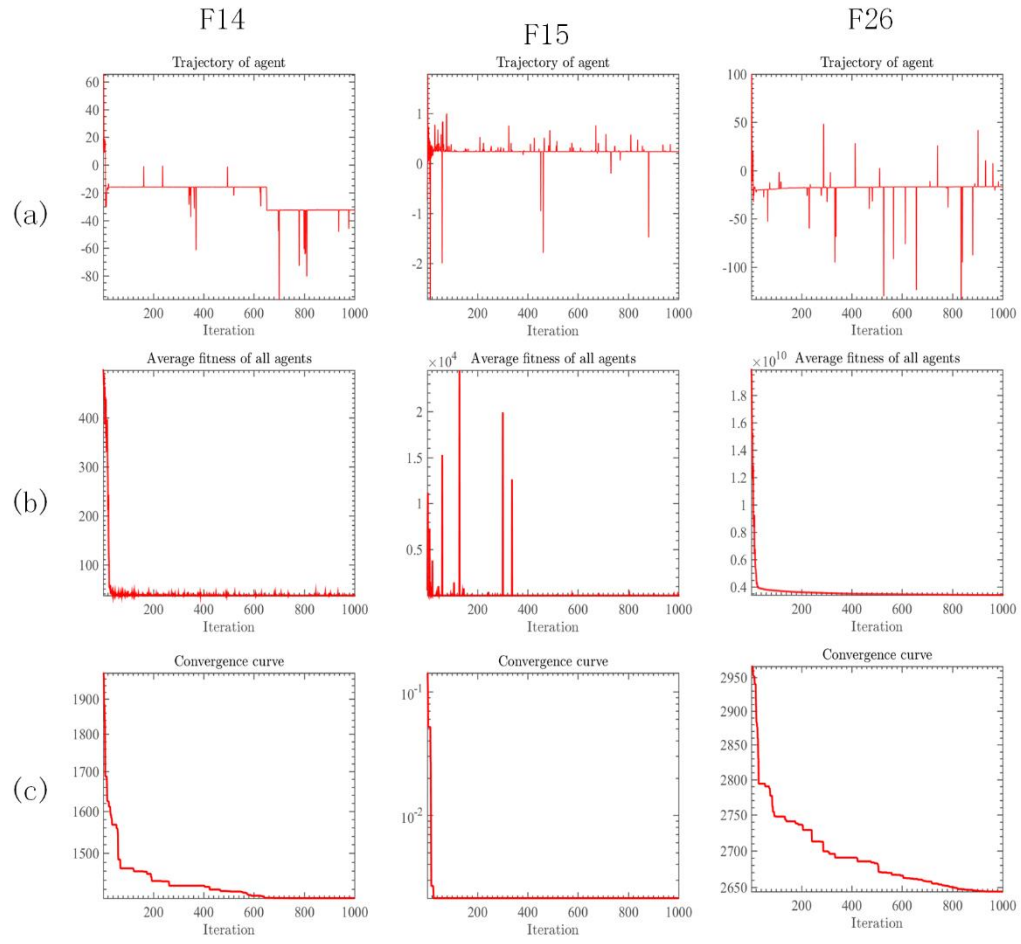
F14
F15
F26
(a)
(b)
(c)
Trajectory of agent
Average fitness of all agents
Convergence curve
Iteration

Figure 15. Qualitative analysis experiment of PLO

The results of PLO for the above experiments are shown in Figure 14 and Figure 15. In Figure 14, the three-dimensional stereo images of all the solutions of each benchmark function, which can help to better understand and observe the distribution of the solution space, are followed by the distribution of the record points of PLO's historical search for the optimal solution in the two-dimensional plane of the solution space. After observation, it is not difficult to find that a minority of historical optimal solutions are scattered within the solution space, whereas the majority of historical optimal solutions congregate around the global optimum. This suggests that PLO exhibits a stable trend of early exploration of the solution space during the search process, initializing computational strides in the initial stages, and progressively exploring toward the optimal value based on accumulated experience throughout the search process.

In Figure 15, column (a) shows the trend of a dimension component of the PLO's agent. PLO has a large search step due to the combined effect of gyration motion and auroral oval walk, allowing it to perform a global search. In later iterations, the particle collision strategy gradually plays an important role, helping the algorithm escape local optima. As the iteration proceeds, the oscillation amplitude of the agent's dimension decreases, and the algorithm gradually transitions to the exploitation stage to finely converge to the optimal solution.

The average fitness value, calculated by all agents after every iteration of PLO, is recorded in column (b). It is apparent that the search agents consistently adapt positions during the updating process, and the fitness values in each iteration align with the fluctuations of the agents, ultimately converging to one point. This observation highlights that the search pattern employed by PLO drives the agents to update their locations continuously and progressively explore until they reach the optimal solution, aligning with the algorithm's intended design.

Column (c) also shows PLO's iterative convergence curve. For MAs, the algorithm's performance is more intuitive to the researcher during the successive solving process, meaning the quality of the explored solution increases with the number of iterations until the optimal or near-optimal solution is found when the iteration stops. Throughout this process, the algorithm needs to refine its search increasingly and avoid falling into local optima. In all aspects, PLO fits the above description, effectively searching for high-quality solutions, maintaining sensitivity to local optima, and quickly escaping them.

In conclusion, the architecture of PLO demonstrates conformity with the principles underlying MAs. It possesses the ability to perform a continual search for an optimal solution with a primary focus on exploring and enhancing accuracy. Moreover, while guaranteeing convergence, PLO actively modifies its search strategy during the update process, thus eliminating the restrictions imposed by local optimality. Throughout the search for an optimal solution, PLO incorporates a weighting mechanism to better coordinate global search with local exploitation, resulting in a seamless and uninterrupted transition from extensive exploration to precise exploitation. Consequently, the quest for an optimal solution through the PLO encompasses both breadth and depth.

5.3.2 The scalability test for PLO

The stability and scalability of a method can be significantly influenced by its components and dimensions. Understanding how these factors interact is crucial, especially when augmenting its [79]. Thus, it's imperative to investigate. To do so, under identical conditions, we set the function dimensions to 50 and 100, utilizing 30 function problems from IEEE CEC2014, and conduct comparative tests between the PLO and classical algorithms.

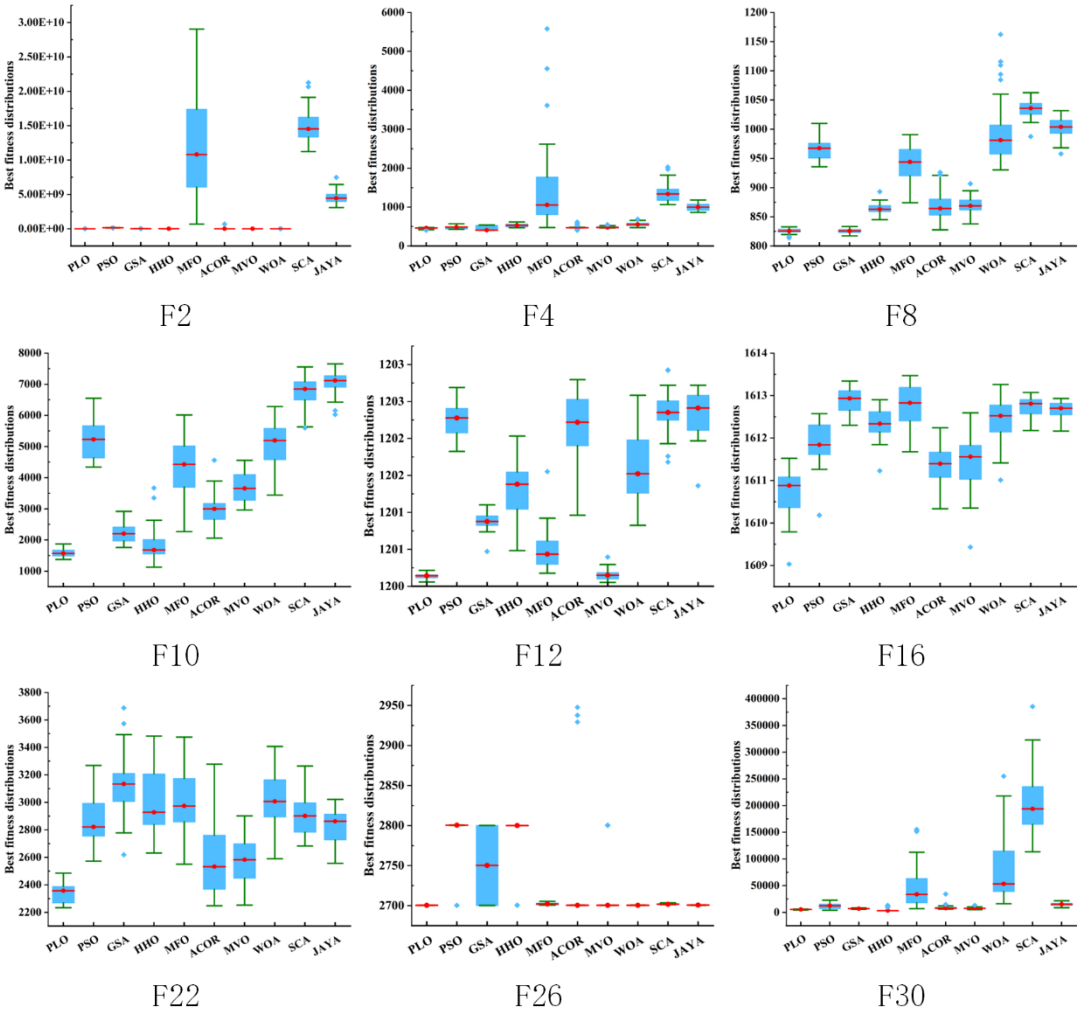

Figure 16. Scalability test results in 50 dimensions

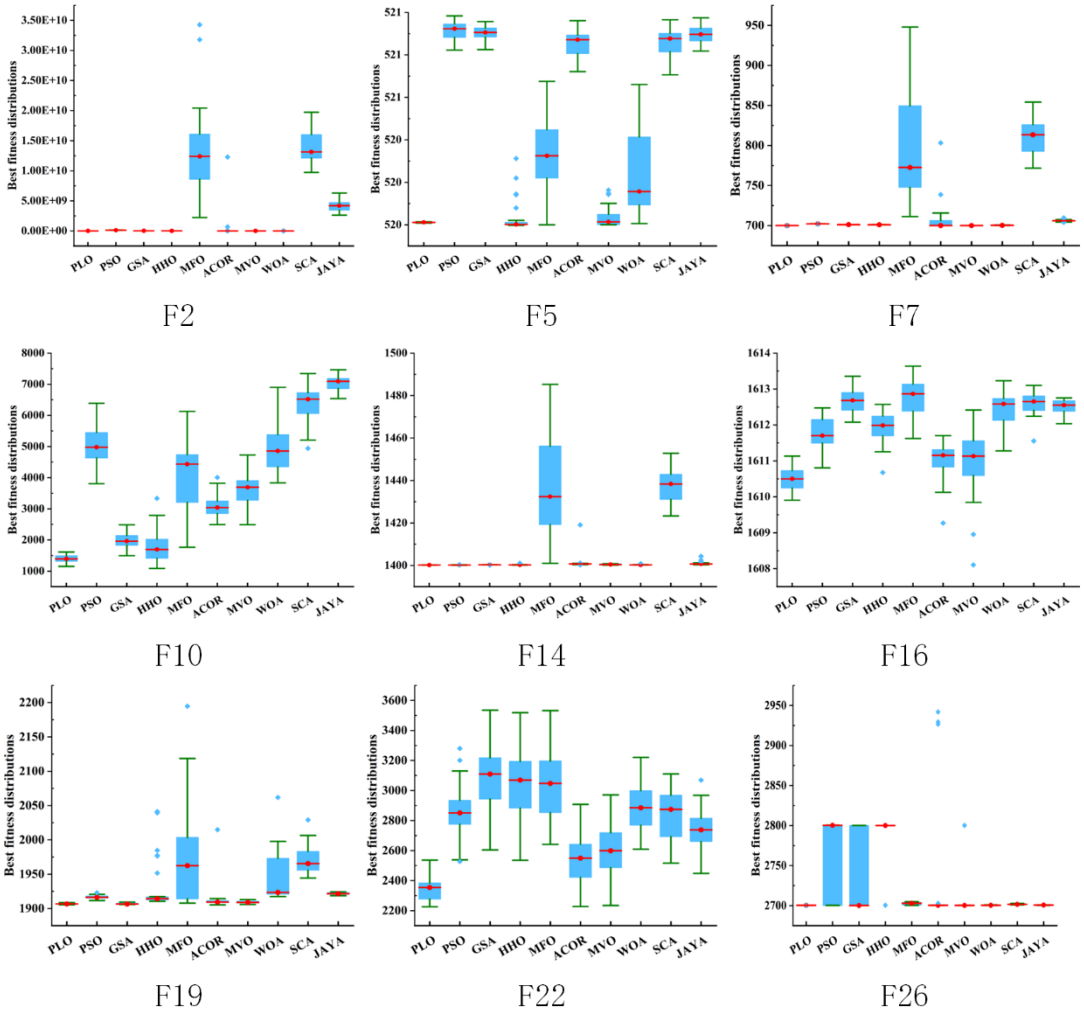

Figure 17. Scalability test results in 100 dimensions

In this section, we compare the PLO with classical algorithms across 30 functions, generating box plots from 30 independent runs to facilitate intuitive analysis of the results. The corresponding experimental results are depicted in Figure 16 and Figure 17. According to the experimental findings, the PLO continues to demonstrate promising results at 50 dimensions, and it maintains stable performance even at 100 dimensions. In other words, regardless of the complexity of the functions, the PLO exhibits a commendable ability to find optimal solutions across most functions. Furthermore, based on the results of the WSRT presented in Table 16 and Table 17, it is evident that the PLO maintains its advantage in terms of both capability and stability in finding optimal solutions compared to classical algorithms.

As per our observations, we find that PLO exhibits better performance and considerable stability across varying levels of complexity. Throughout the problem-solving process, PLO demonstrates a heightened ability to avoid local optima, aiding in the discovery of superior solutions for the given functions. In conclusion, the proposed PLO showcases enhanced problem-solving capabilities and significant advantages, making it more likely to achieve satisfactory results when extended to large-scale problem domains.

Table 16. Scalability test results at 50 dimensions.

Algorithm	Mean	Rank	+/-/=
PLO	2.17	1	~
PSO	5.60	6	22/3/5
GSA	4.33	4	16/8/6

HHO	4.13	3	21/9/0
MFO	7.87	9	30/0/0
ACOR	5.27	5	22/1/7
MVO	3.00	2	15/7/8
WOA	6.63	7	28/1/1
SCA	8.60	10	29/1/0
JAYA	7.40	8	28/1/1

Table 17. Scalability test results at 100 dimensions.

Algorithm	Mean	Rank	+/-/=
PLO	2.13	1	~
PSO	5.60	6	21/3/6
GSA	4.23	4	17/6/7
HHO	4.13	3	20/9/1
MFO	8.07	9	30/0/0
ACOR	5.30	5	24/0/6
MVO	3.20	2	18/5/7
WOA	6.70	7	29/1/0
SCA	8.53	10	29/1/0
JAYA	7.10	8	28/1/1

6. Application of the PLO: MTIS and FS

In this section, our research delves into two pivotal challenges: multi-threshold segmentation (MTIS) of breast cancer pathology images and feature selection (FS) for medical datasets.

In the domain of MTIS, the conventional approach to breast cancer analysis and diagnosis, rooted in radiology or pathology expertise, is fraught with the intricacies of interpreting pathological images of breast cancer, laden with copious amounts of intricate and often redundant information, thereby resulting in human error. The conventional radiological diagnosis is inherently constrained and heavily reliant on the subjective interpretation and experiential knowledge of medical practitioners [80]. Hence, the imperative arises to segment breast cancer pathological images, eliminating superfluous data, to lay a robust foundation for subsequent pathological analysis, comprehension, and diagnosis. However, traditional segmentation methodologies predominantly focus on grayscale information, disregarding the influence of pixel spatial context on segmentation outcomes, and fail to reconcile the optimal segmentation thresholds across image channels, rendering them incapable of effecting a more rational image segmentation [81]. This study proposes a multi-threshold segmentation method based on metaheuristic algorithms and Kapur entropy to address this challenge. This method optimizes the segmentation thresholds of breast cancer images based on pixel intensity and spatial neighborhood two-dimensional histograms, thereby enhancing the precision of lesion area segmentation.

In the realm of FS, it entails the process of choosing a subset of relevant features from a given feature set. The objective of FS is to alleviate the complexity of learning tasks by eliminating irrelevant and redundant features, thereby conserving computational and storage costs, and mitigating the risk of overfitting. However, the majority of feature extraction models based on feature fusion struggle to effectively adapt to the extraction of medical features in high-dimensional and voluminous datasets. Managing large feature

spaces presents challenges, yet the binary variant of MAs offers a solution by effectively exploring the search space to identify the optimal feature subset [82]. Consequently, this paper introduces a binary variant of PLO (bPLO) specifically tailored for feature selection, thereby optimizing Kernel Extreme Learning Machine (KELM) to enhance classification accuracy.

When faced with real-world interference factors, such as redundant noise in images or noisy, incomplete datasets, the exploration task undertaken by PLO may become notably more challenging. Data noise can lead to the algorithm failing to accurately assess the search space, thereby selecting suboptimal solutions instead of the global optimum. Additionally, data incompleteness increases uncertainty, potentially necessitating more iterations for convergence, consequently augmenting algorithm runtime and resource consumption, and affecting the final solution accuracy. In essence, real-world interference factors pose obstacles to the optimization task of PLO, putting its ability to explore the search space to the test.

This section is organized as follows: Section 6.1 will present the designed multi-threshold image segmentation method and feature selection model. Section 6.2 will show the testing of the MTIS method at different threshold levels, which includes the comparison of several similar algorithms to evaluate the efficacy of PLO. Section 6.3 demonstrates the performance of the proposed FS method. This subsection tests the PLO algorithm against some well-known algorithms on different datasets and compares the results.

6.1 Integration of related technologies with the PLO

6.1.1 Multi-threshold image segmentation

Multi-threshold image segmentation (MTIS) is an image processing technique designed to partition images into different regions, with every region delineated by several thresholds. In contrast to conventional methods, MTIS demonstrates superior efficacy in managing images containing multiple objects or showcasing non-uniform color or brightness variations. At its core, MTIS operates by assessing pixel intensity values within the image against a predefined set of thresholds, thereby allocating pixels into distinct regions based on this comparison. These methods often have lower computational complexity, making them advantageous for real-time processing and low-power devices. The simplicity and versatility of this approach render it suitable for various types of images. However, conventional threshold segmentation methods often fail to effectively leverage inherent spatial positional information within images [80, 83, 84]. In cases where objects occupy a relatively small portion of the image, this method can lead to noticeable segmentation errors, making the results susceptible to noise interference. To address this, Abutaleba [85] proposed a segmentation method based on a two-dimensional histogram. This approach integrates the original grayscale histogram with pixel local averages, resulting in a non-local mean two-dimensional (2D) histogram. This integration significantly reduces such segmentation errors, substantially enhancing segmentation quality, albeit at the cost of additional computational burden.

While the segmentation method based on a 2D histogram proves effective, it also comes with limitations. These techniques necessitate extensive threshold optimization computations, potentially incurring substantial computational costs and still possibly overlooking certain image details [86]. To address such challenges, we devise a MTIS method that integrates non-local mean filtering, 2D histograms, Kapur's entropy, and PLO.

In the designed MTIS system, there are four primary components introduced: non-local mean filtering, a denoising technique, that filters each pixel by considering the pixel values in its surrounding area, producing

a denoised image, and synthesizing a 2D histogram. Its role is to reduce image noise, ensuring subsequent segmentation steps are stable and accurate. The 2D histogram, a graphical representation illustrating the correlation between two variables, elucidates the associations among various grayscale levels present in the image, thereby assisting in identifying multiple threshold divisions. Kapur's entropy measures image information and assists in choosing optimal thresholds, maximizing the image's entropy after segmentation. In the MTIS, Kapur's entropy serves as the objective function optimized through MAs, determining the best combinations of multiple thresholds. To get a clear overview of the MTIS system, we give the flowchart as shown in Figure 18.

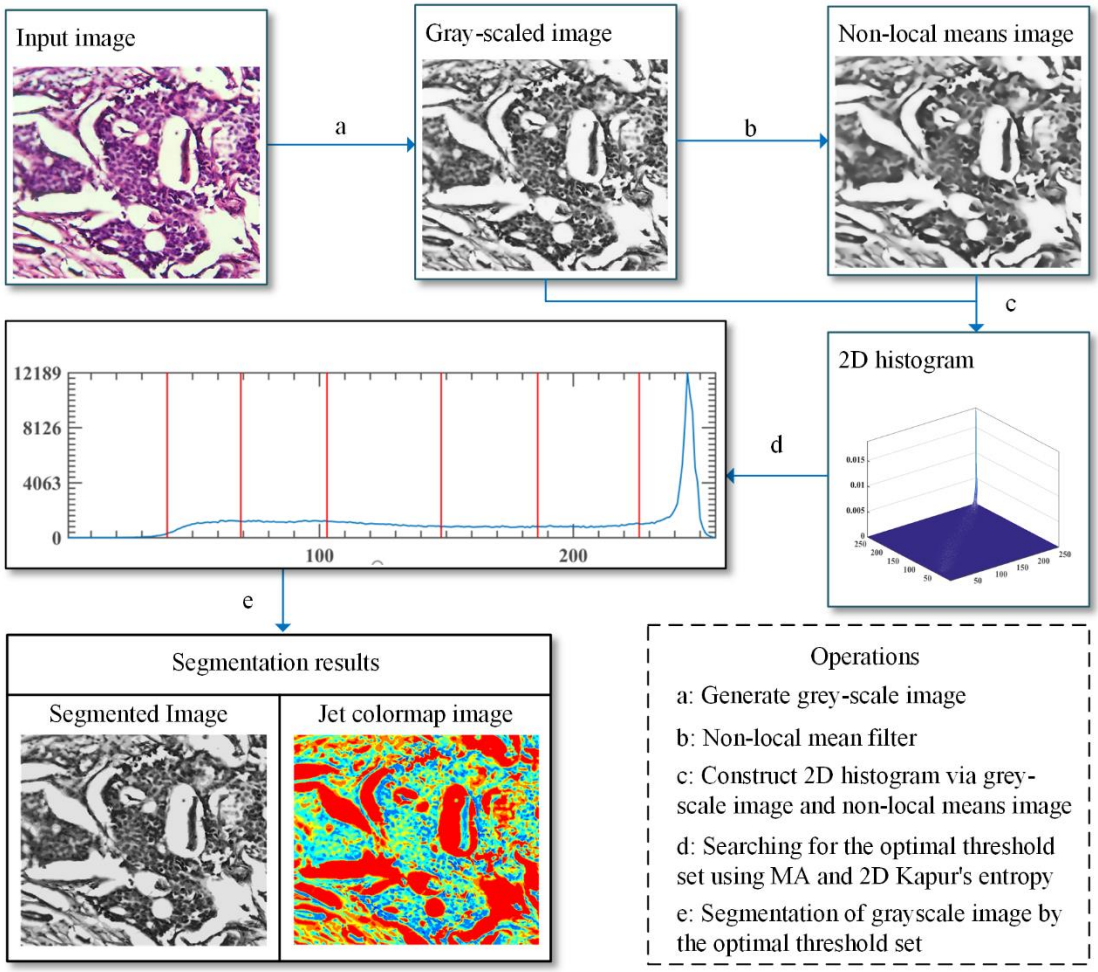

Figure 18. The flowchart of MTIS modeling

Figure 18, this method follows a specific sequence of steps: initially, the input image (sourced from the Invasive Ductal Carcinoma (IDC) dataset [55]) is transformed into grayscale, creating a grayscale image, which is then subjected to non-local mean filtering to reduce noise, ensuring subsequent processes' stability. The grayscale image and the output from non-local mean filtering are used to construct a 2D histogram. Kapur's entropy serves as the evaluation metric, which calculates the entropy for each threshold combination. The objective here is to maximize Kapur's entropy, meaning selecting threshold combinations that maximize the entropy of the segmented image, thus maximizing information content. MAs are employed to optimize the computation of Kapur's entropy. This optimization process involves searching the multi-dimensional parameter space to find the optimal threshold combination that maximizes the entropy. Finally, the identified optimal threshold set is utilized to segment the image, producing the completed segmented image.

6.1.2 Feature selection

Feature Selection (FS) represents a pivotal phase in model construction, encompassing the process of filtering and selecting pertinent features from datasets. Its primary aim is to augment model training, mitigate overfitting, and enhance generalization capabilities. FS has demonstrated advantageous outcomes across diverse medical domains, particularly within medical datasets, which frequently exhibit high dimensions. In the realm of Machine Learning (ML), three prevalent FS techniques are employed: filtering, wrapping, and embedding methods. Coping with extensive feature spaces poses challenges, yet binary variant of MA provides solutions by adeptly traversing search spaces to pinpoint optimal feature subsets. Integrating MAs into FS serves to elevate model accuracy and performance.

Within the realm of FS, methodologies encompass selecting pertinent features, assessing subsets via diverse measurement techniques, identifying various subsets, and validating features [87]. While wrapping methods yield more refined results, they entail longer completion times compared to filtering methods [88]. A harmonious blend of both methodologies strikes a balance, guaranteeing precise outcomes while curtailing filtering durations. The fitness function of MAs gauges the efficacy of each feature set, constituting a pivotal facet for FS and machine learning algorithms. Researchers concentrate on fortifying these systems, harnessing MAs to augment classification accuracy and streamline search spaces [82].

The PLO algorithm, integrated with the Kernel Extreme Learning Machine (KELM), is proposed for feature selection purposes. Leveraging the binary variant of PLO (bPLO), the algorithm extracts the optimal feature subset from the dataset, subsequently utilized for feature selection. These selected subsets serve as input parameters for KELM, culminating in deriving final classification results. However, it is crucial to reevaluate how the fitness function is set when combining bPLO with the KELM classifier. The data preprocessing procedure has two primary requirements. Firstly, the obtained feature subset should exhibit high classification accuracy; in other words, it needs to encompass features strongly correlated with the classes. Secondly, the derived feature subset should contain as few features as possible to mitigate interference caused by high dimensionality. The generated solutions need continuous evaluation during the iterative process to ensure its effectiveness. This is achieved through the fitness function of the classifier, as demonstrated in Eq. (42).

$$fit = \alpha \times error + \beta \times \frac{|R|}{|D|} \tag{42}$$

where α denotes the weight for assessing the classification error rate, and the $error$ is the error rate; β is the number of selected features, $|R|$ represents the final subset attributes number, and $|D|$ is the dataset dimension, i.e., the entire subset attributes number. In this work, the value of α is set to 0.99 and the value of β is set to 0.01 as in many previous studies.

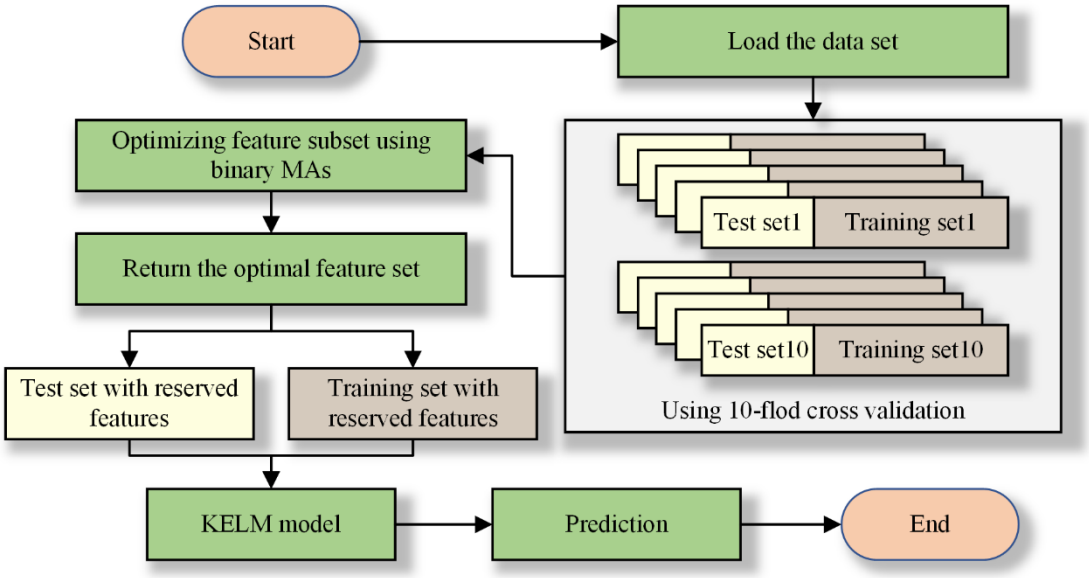

Figure 19. Flowchart of feature selection

To gain a comprehensive understanding of this process, a detailed flowchart is provided, as in Figure 19. Firstly, the dataset undergoes preprocessing, being normalized to the range of [-1,1], and samples are partitioned using a 10-fold cross-validation approach. Subsequently, bPLO is initialized, and based on the fitness function Eq. (42), the fitness of each feature subset is computed. The feature subset with the lowest fitness value is chosen as the optimal solution. These optimal feature subsets are then returned and serve as initial parameters for the KELM model, which is employed to find the ultimate classification solution. Finally, the KELM model is utilized to predict the filtered test set using the best-selected feature subsets.

6.2 Segmentation experiments on breast cancer pathology images

This section employs ten breast cancer pathology images as the target images for segmentation. These datasets provide histopathological microscope images, derived from breast tissues stained with H&E. Figure 20 displays the original images of these selected pictures along with their non-local mean 2D histograms. Our objective is to examine whether PLO's segmentation performance remained excellent when confronted with diverse images, as each image is treated as a separate issue associated with the threshold levels used for segmentation [89]. To comprehensively assess the PLO, this paper conducts two sets of experiments at both low and high threshold levels, and the segmentation results will be compared with seven other algorithms. All participants are outlined in the Table 18.

Table 18. Participants and parameter settings.

Participants	Parameters
Polar lights optimization (PLO)	$m = 100;\ \alpha = [1,1.5]$
Whale optimization algorithm (WOA) [65]	$a_1 = [2,0]; a_2 = [-2,-1]; b = 1$
JAYA algorithm (JAYA) [67]	~
Slime mould algorithm (SMA) [31]	$z = 0.03$
Multi-verse optimizer (MVO) [20]	$MaxWEP = 1;\ MinWEP = 0.2$

Multi-strategy enhanced sine cosine algorithm (MSCA) [90]	$a = 2;\ \mathrm{JR} = 0.1$
Harris Hawks optimization (HHO) [32]	$k = 0$
Enhanced grey wolf optimization (IGWO) [91]	$\beta = 10;\ \omega = 15$

In the experiment, we utilized Peak Signal-to-Noise Ratio (PSNR) [92], Structural Similarity Index (SSIM) [93], and Feature Similarity Index (FSIM) [94] as evaluation metrics. We presented the metrics' means and variances and performed statistical analysis using WSRT and FT to examine the results. Furthermore, all algorithms compared are subjected to identical experimental conditions. The evaluation is conducted over 2000 times, with image dimensions set at 512x512, a solution space size of 30, and each algorithm independently run 30 times.

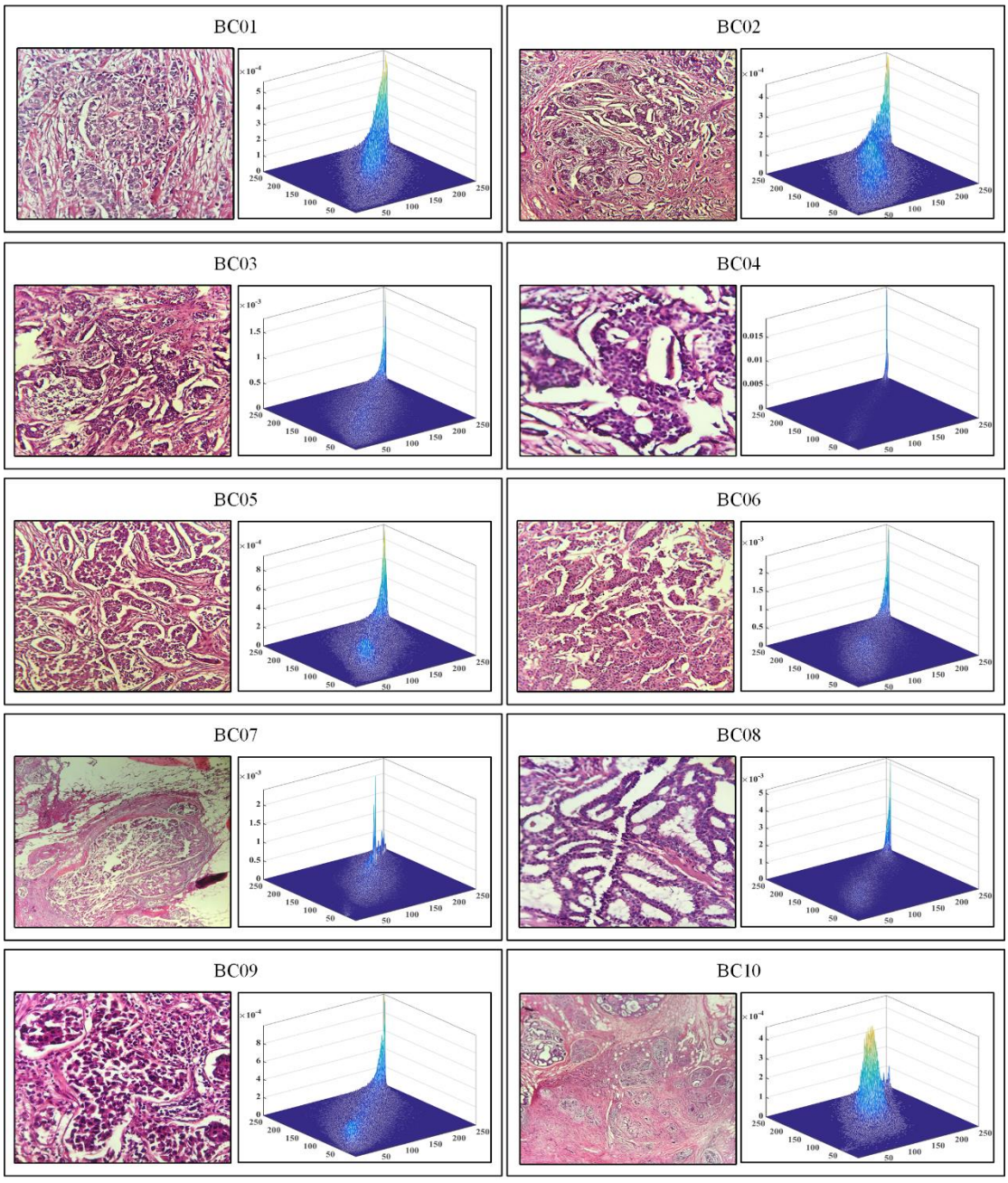

Figure 20. Segmented samples with 2D histograms

6.2.1 Experimental at low threshold levels

In this section, the low-threshold groups are categorized into 2, 4, and 6 threshold levels. PLO, along with the seven algorithms, segments the ten selected images. In Appendix Tables A.3 to A.5, we report the averages and standard deviations of the three metrics after segmentation using PLO and the other seven algorithms. PLO achieves the highest average and the smallest standard deviation in most images, indicating its superior overall performance in segmentation with consistent and stable results. Additionally, Tables 19, 20, and 21 display the statistical results of these three metrics using WSRT and FT. The statistical analysis demonstrates that the proposed PLO algorithm outperforms other algorithms in low threshold image segmentation.

Table 19. The FSIM results at 2, 4 and 6 threshold level

Thresholds	2			4			6		
	Mean	Rank	+/-/=	Mean	Rank	+/-/=	Mean	Rank	+/-/=
PLO	**1.5**	**1**	~	**1.7**	**1**	~	**1.7**	**1**	~
WOA	5.3	6	6/0/4	5.4	5	8/0/2	3.4	2	4/0/6
SMA	2.7	2	1/0/9	2.7	2	6/3/1	3.7	3	5/3/2
JAYA	4.6	4	6/0/4	3.1	3	5/1/4	5.0	6	6/1/3
MVO	4.9	5	4/1/5	4.4	4	7/0/3	4.7	5	5/0/5
MSCA	6.8	8	5/0/5	7.3	8	9/0/1	6.9	8	8/0/2
HHO	6.7	7	7/0/3	5.7	6	6/0/4	4.5	4	4/0/6
IGWO	3.5	3	2/0/8	5.7	7	9/0/1	6.1	7	8/0/2

Table 20. The PSNR results at 2, 4 and 6 threshold level

Thresholds	2			4			6		
	Mean	Rank	+/-/=	Mean	Rank	+/-/=	Mean	Rank	+/-/=
PLO	**2.4**	**1**	~	**1.8**	**1**		**1.7**	**1**	~
WOA	6.0	7	6/0/4	5.0	5	8/0/2	4.2	4	8/0/2
SMA	3.9	3	2/0/8	2.2	3	4/4/2	2.3	2	5/2/3
JAYA	4.0	4	2/0/8	2.0	2	2/2/6	2.4	3	6/3/1
MVO	3.6	2	2/0/8	4.4	4	8/0/2	4.7	5	9/0/1
MSCA	5.6	6	5/0/5	7.3	8	10/0/0	7.6	8	10/0/0
HHO	6.5	8	5/0/5	6.8	7	9/0/1	6.0	6	10/0/0
IGWO	4.0	5	3/0/7	6.5	6	10/0/0	7.1	7	10/0/0

Table 21. The SSIM results at 2, 4 and 6 threshold level

Thresholds	2			4			6		
	Mean	Rank	+/-/=	Mean	Rank	+/-/=	Mean	Rank	+/-/=
PLO	**2.5**	**1**	~	**1.7**	**1**	~	**1.8**	**1**	~
WOA	6.4	7	7/0/3	5.5	5	9/0/1	4.5	4	9/0/1
SMA	3.0	2	3/0/7	2.4	3	2/2/6	1.9	2	4/1/5
JAYA	3.4	3	3/0/7	1.9	2	2/1/7	2.5	3	4/3/3
MVO	3.7	4	1/1/8	4.4	4	6/0/4	4.6	5	9/0/1
MSCA	5.3	6	5/0/5	7.0	7	10/0/0	7.3	8	10/0/0
HHO	6.5	8	6/0/4	7.1	8	9/0/1	6.5	6	10/0/0
IGWO	5.2	5	1/0/9	6.0	6	10/0/0	6.9	7	10/0/0

Furthermore, we chose to showcase the segmentation results of BC08 at 6 threshold levels for comparison. Figure 21 shows that in the segmentation process at low threshold levels, the previously blurry areas surrounding the original images are distinctly separated with vibrant colors. Upon meticulous observation, the results from PLO segmentation retain more local features of the image, displaying even brighter and more vivid colors. Analyzing the results of the low-threshold image segmentation experiments above reveals that the proposed PLO excels in low-threshold image segmentation within this model, outperforming other algorithms.

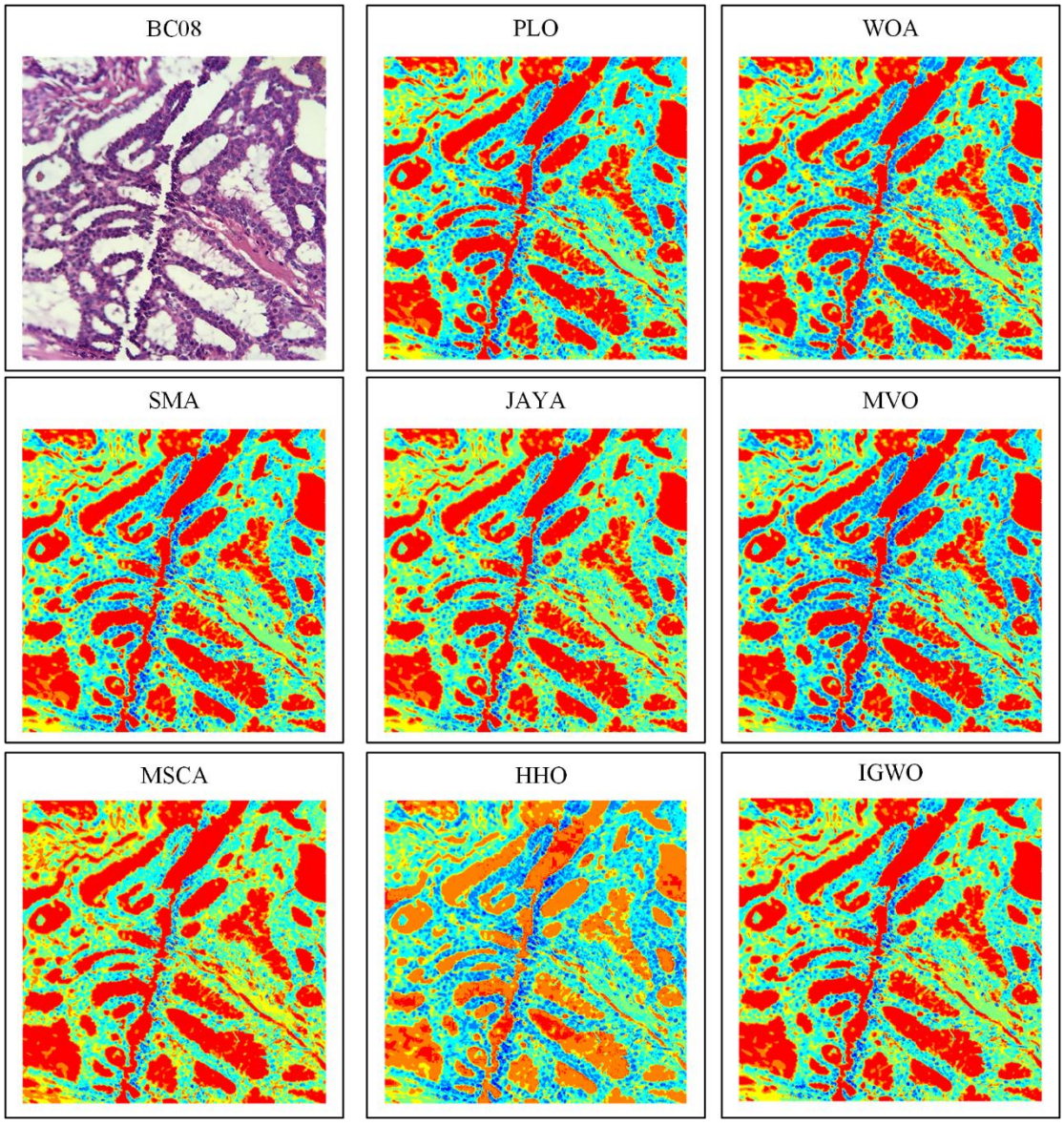

Figure 21. Comparison of segmentation results for BC08 at 6 threshold levels

6.2.2 Experimental at high threshold levels

This section increases segmentation precision by elevating the thresholds. Simultaneously grouping 16, 20, and 24 threshold levels, PLO competes again with the above 7 algorithms to segment the same set of 10 images. Tables A.6 to A.8 in the appendix present the averages and standard deviations of the three metrics after segmentation by PLO and the other 7 algorithms. In most images, PLO outperforms others at high

threshold levels with superior averages and more stability in standard deviations. Additionally, Tables 22, 23, and 24 summarize the statistical results of these metrics using WSRT and FT. Statistical analysis reveals that when confronted with the demand for higher segmentation accuracy, the proposed PLO method continues to surpass other algorithms.

Table 22. The FSIM results at 16, 20 and 24 threshold level

Thresholds	16			20			24		
	Mean	Rank	+/-/=	Mean	Rank	+/-/=	Mean	Rank	+/-/=
PLO	1.6	1	~	1.7	1	~	1.1	1	
WOA	3.0	2	3/1/6	2.5	2	4/1/5	3.1	2	2/0/8
SMA	5.2	5	5/0/5	4.1	4	6/0/4	3.4	3	2/0/8
JAYA	4.0	4	5/0/5	4.7	5	8/0/2	3.9	4	7/0/3
MVO	3.9	3	4/0/3	3.3	3	6/0/4	5.5	6	9/0/1
MSCA	6.5	8	8/0/2	6.4	6	9/0/1	6.9	7	9/0/1
HHO	5.9	6	6/0/4	6.4	6	8/0/2	5.1	5	8/0/2
IGWO	5.9	7	9/0/1	6.9	8	8/0/2	7.0	8	10/0/0

Table 23. The PSNR results at 16, 20 and 24 threshold level

Thresholds	16			20			24		
	Mean	Rank	+/-/=	Mean	Rank	+/-/=	Mean	Rank	+/-/=
PLO	1.6	1	~	1.5	1	~	1.3	1	~
WOA	2.1	2	2/1/7	1.9	2	4/2/4	1.9	2	3/0/7
SMA	3.3	3	5/0/5	2.9	3	6/0/4	2.9	3	6/0/4
JAYA	3.8	4	7/0/3	4.4	4	10/0/0	3.9	4	10/0/0
MVO	4.6	5	8/0/2	4.9	5	8/0/2	6.1	6	10/0/0
MSCA	7.1	7	10/0/0	6.1	6	10/0/0	6.5	7	10/0/0
HHO	6.1	6	7/0/3	6.4	7	8/0/2	5.7	5	10/0/0
IGWO	7.4	8	10/0/0	7.9	8	10/0/0	7.7	8	10/0/0

Table 24. The SSIM results at 16, 20 and 24 threshold level

Thresholds	16			20			24		
	Mean	Rank	+/-/=	Mean	Rank	+/-/=	Mean	Rank	+/-/=
PLO	1.5	1	~	1.5	1	~	1.4	1	~
WOA	2.6	3	3/1/6	2.0	2	2/2/6	2	2	2/0/8
SMA	2.3	2	2/1/7	2.5	3	3/1/6	2.6	3	2/0/8
JAYA	3.7	4	9/0/1	4.4	4	10/0/0	4	4	10/0/0
MVO	5.1	5	10/0/0	5	5	10/0/0	6.3	7	10/0/0
MSCA	6.4	6	10/0/0	5.8	6	10/0/0	5.9	5	10/0/0
HHO	6.9	7	10/0/0	6.8	7	10/0/0	6.1	6	10/0/0
IGWO	7.5	8	10/0/0	8	8	10/0/0	7.7	8	10/0/0

In a comparative analysis, we present the segmentation results of BC04 at the 24-threshold level in the Figure 22. With increasing thresholds, images are segmented into more regions, achieving greater accuracy, particularly for images with multiple objects, textures, or intricate structures. Examination of the original images reveals complex and dense structures in central regions and blurriness in edge areas due to noise interference. Post-segmentation, these areas are distinctly separated. Upon close observation, the results from PLO segmentation exhibit vividly colored and well-defined features in central regions, and even the previously blurry edge regions are precisely segmented. This level of precision is unmatched by other

algorithms. Analysis of these segmentation experiment results indicates that the proposed PLO method outperforms other algorithms in this image segmentation model, especially in achieving accurate segmentation at high threshold levels.

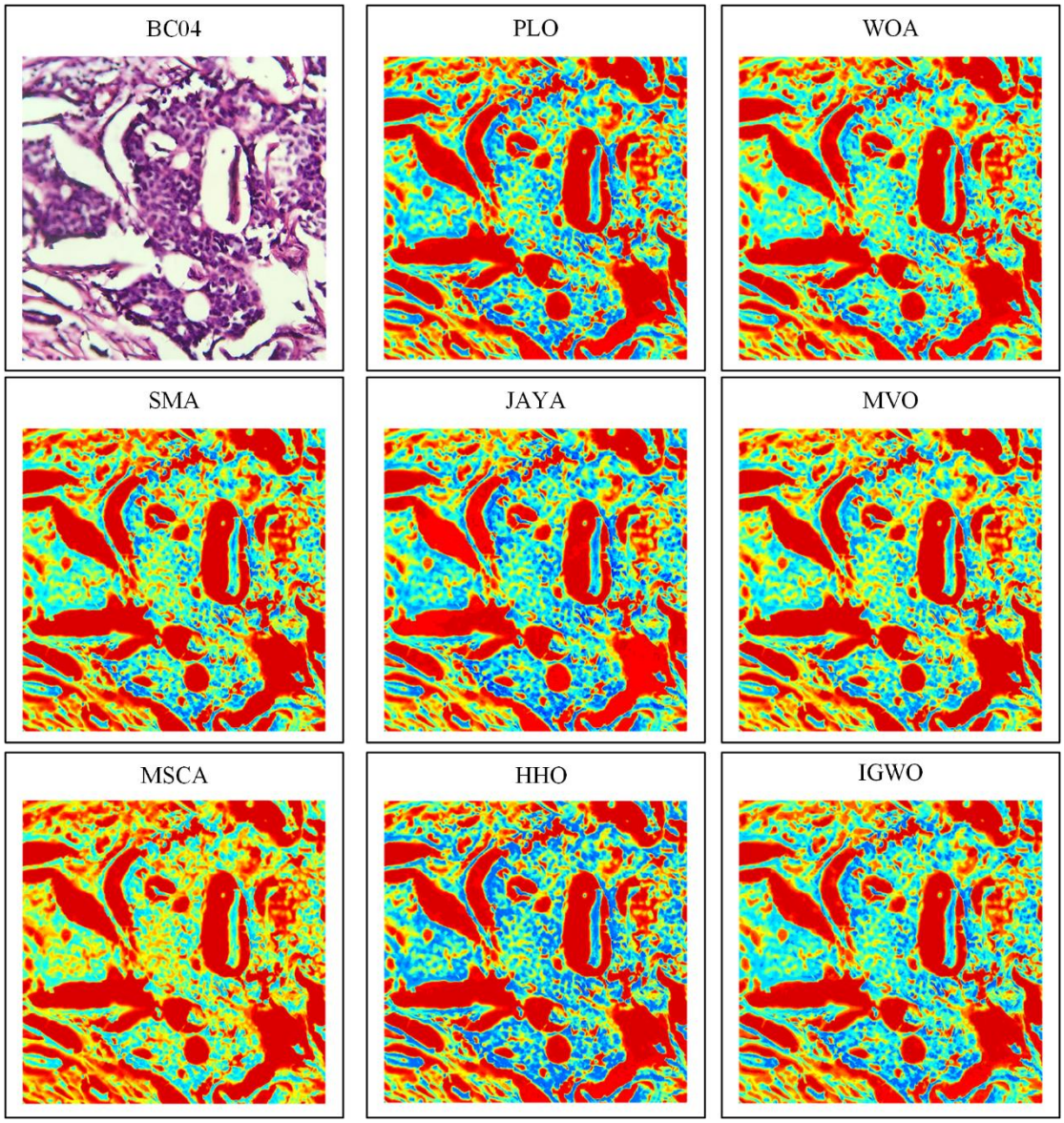

Figure 22. Comparison of segmentation results for BC04 at 24 threshold levels

6.3 Feature selection experiments

6.3.1 Dataset and experimental setup

In this section, the performance of our proposed Feature Selection (FS) model is assessed across eight medical datasets. Four of these datasets are sourced from the well-known UCI Machine Learning Repository, while the remaining four are collected from patients recruited from a single center between May 5th and May 31st, 2020 (Outpatient HD Unit, the First Affiliated Hospital, Wenzhou Medical University).

The application of the FS model to these datasets aimed to assess its effectiveness under various

conditions and validate its suitability for classifying medical data. Using publicly available datasets ensured transparency, and the incorporation of authentic medical data from reliable sources guaranteed the accuracy of the study. Table 25 provides a concise overview of these datasets, along with detailed information about their key parameters.

Table 25. The 8 Medical datasets.

Source	Dataset	Samples	Features	Classes
University of California Irvine datasets (UCI) (https://archive.ics.uci.edu/ml/datasets.php)	Breast cancer	699	10	2
	Breast	569	30	2
	Parkinson	195	22	2
	Heart	270	13	2
Outpatient HD unit of First Affiliated Hospital of Wenzhou Medical University	PH (Pulmonary Hypertension) [95]	90	25	2
	DH1 (Hemodialysis) [96]	1940	19	2
	DH2 (Hemodialysis) [97]	1940	15	2
	DH3 (Hemodialysis) [98]	1239	42	2

In the realm of pattern recognition, a confusion matrix serves as a schematic representation of classification predictions. The confusion matrix illustrates the association between the actual class attributes of sample data and the predicted categories, constituting a crucial metric for evaluating classification model performance. Evaluation metrics like accuracy, specificity, and sensitivity can be derived from the confusion matrix. In binary classification scenarios, samples are categorized as positive or negative. The confusion matrix includes True Positives (TP), False Positives (FP), True Negatives (TN) and False Negatives (FN).

Among them, accuracy (ACC) is the most well-known classification evaluation metric, which measures the ability of the classifier to recognize correct samples. The ACC lies in $[0,1]$, and the closer the ACC is to 1, the better the classification performance.

$$ACC = \frac{TP + TN}{TP + TN + FP + FN} \tag{43}$$

Precision (PRE) quantifies the ratio of correctly classified positive cases to the total instances classified as positive. A higher PRE value, closer to 1, signifies superior classifier performance. The PRE is computed using the following formula:

$$Precision = \frac{TP}{TP + FP} \tag{44}$$

Sensitivity (SEN), also known as recall or true positive rate, denotes the likelihood that a patient with a disease is correctly identified as positive by the classifier. It gauges the classifier's capacity to detect positive cases. A SEN value closer to 1 indicates a higher ability to correctly identify individuals with the condition. Sensitivity is computed using the following formula:

$$Sensitivity = \frac{TP}{TP + FN} \tag{45}$$

Specificity (SPE) represents the probability that an individual without the disease will be correctly identified as disease-free by the classifier. It evaluates the classifier's capability to recognize negative cases, reflecting its aptitude in identifying individuals without the condition. A specificity value closer to 1 indicates a higher ability to correctly identify disease-free individuals. SPE is calculated using the following formula:

$$Specificity = \frac{TN}{TN + FN} \tag{46}$$

The Matthews Correlation Coefficient (MCC) quantifies the correlation between the predicted and actual classifications. In balanced datasets, elevated values of both ACC and MCC indicate superior

prediction quality. However, in unbalanced datasets, MCC offers a more accurate assessment of the predictor's predictive quality compared to ACC. The MCC is calculated using the following formula:

$$MCC = \frac{TP \times TN - FP \times FN}{\sqrt{(TP + FP) \times (TP + FN) \times (TN + FP) \times (TN + FN)}} \quad (47)$$

Furthermore, as part of this experiment, several discrete algorithms are included for comparison, as detailed in Table 26. Moreover, the feature selection experiment employs a population size of 20, and the validity of the experimental results is confirmed through the classical tenfold cross-validation method.

Table 26. Participants and their parameter settings

Algorithms	Parameter(s)
Binary moth-flame optimization algorithm (bMFO)[64]	$b = 1$
Binary grey wolf optimization (bGWO) [99]	~
Binary particle swarm optimization (bPSO) [100]	$c_1 = 2;\ c_2 = 2;\ V_{max} = 6$
Binary ant lion optimization (bPLO) [101]	~
Binary bat algorithm (bBA) [102]	$A = 0.5; r = 0.5; r_0 = 0.5; \alpha = 0.9;$ $\lambda = 0.9; Q_{min} = 0; Q_{max} = 2$
Binary salp swarm algorithm (bSSA) [103]	~
Binary whale optimization algorithm (bWOA) [65]	$a_1 = [2,0]; a_2 = [-2,-1]; b = 1$
Binary polar lights optimization (bPLO)	$m = 100;\ \alpha = [1,1.5]$

6.3.2 Medical datasets experiments

In this subsection, we arrange bPLO and the other 8 algorithms for feature selection on the target dataset respectively. The results are analyzed based on 5 kinds of metrics.

Table 27 illustrates the accuracy results of eight algorithms on the UCI dataset. The method based on bPLO outperforms others with the best average results over 10 independent experiments. The average accuracy of the bPLO-based approach across the eight datasets stands at 98.57%, 98.77%, 92.83%, 94.44%, 97.78%, 95.97%, 92.78%, and 92.01%, showcasing its remarkable consistency across different datasets. Based on this analysis, the bPLO-based method excels in both predictive accuracy and stability, surpassing all other methods.

Table 28 presents the specificity results for these 8 algorithms. Visible in the table, the bPLO-based method consistently ranks first in most datasets. The average specificity achieved by bPLO ranges from 90.83% to 98.35% across various datasets, indicating the robustness of its predictions.

Table 29 displays the average accuracy results and standard deviations. The bPLO-based method exhibits superior and more consistent accuracy outcomes across eight datasets, achieving average results of 99.14%, 97.90%, 91.40%, 93.26%, 95.48%, 95.70%, 93.12%, and 93.66%. When compared to other prediction methods, bPLO stands out in accurately predicting positive instances.

Table 30 presents the average values and standard deviations of MCC. The proposed method consistently performs well with MCC average results of 0.9690, 0.9741, 0.8490, 0.8895, 0.9598, 0.8937, 0.8561, 0.8422, showcasing its superior performance and stability.

Table 31 shows the mean and standard deviation of the F-measure. F-measure obtained by PLO are higher in most of the datasets. Analysis of the experimental data leads to the conclusion that the proposed bPLO method is a more effective classification approach.

From the accuracy, specificity, precision, MCC, and f-measure experimental results, it is evident that bPLO meets our expectations, demonstrating reliable and robust predictive performance."

Table 27. Accuracy values on medical datasets

	Breast cancer		Breast EW		DH1		Heart	
	AVG	STD	AVG	STD	AVG	STD	AVG	STD
bMFO	98.15%	0.0201	98.42%	0.0162	92.37%	0.0203	92.22%	0.0395
bGWO	98.42%	**0.0106**	98.60%	0.0148	92.68%	0.0186	93.33%	**0.0344**
bPSO	98.14%	0.0118	98.59%	0.0163	92.37%	0.0166	94.07%	0.0538
bALO	98.28%	0.0113	98.60%	**0.0144**	92.47%	0.0248	93.33%	0.0437
bBA	95.57%	0.0305	94.02%	0.0242	84.07%	0.0650	84.07%	0.0532
bSSA	98.43%	0.0142	98.77%	0.0180	92.22%	**0.0133**	92.96%	0.0367
bWOA	98.28%	0.0132	98.25%	0.0176	91.55%	0.0190	93.33%	0.0555
bPLO	**98.57%**	0.0135	**98.77%**	0.0198	**92.83%**	0.0210	**94.44%**	0.0462
	PH		Parkinson		DH2		DH3	
	AVG	STD	AVG	STD	AVG	STD	AVG	STD
bMFO	93.33%	0.0777	94.90%	0.0478	92.17%	0.0191	91.69%	0.0208
bGWO	96.67%	**0.0537**	94.84%	0.0490	92.32%	0.0227	**92.17%**	0.0194
bPSO	95.56%	0.0574	93.89%	0.0392	92.37%	**0.0094**	91.69%	0.0287
bALO	96.67%	**0.0537**	94.34%	0.0375	92.11%	0.0183	91.69%	**0.0131**
bBA	77.78%	0.1960	83.94%	0.0924	82.10%	0.1355	87.97%	0.0372
bSSA	96.67%	0.0703	95.42%	0.0378	91.81%	0.0271	91.53%	0.0232
bWOA	94.44%	0.0586	93.79%	0.0411	91.70%	0.0195	91.77%	0.0284
bPLO	**97.78%**	0.0750	**95.97%**	**0.0317**	**92.78%**	0.0152	92.01%	0.0326

Table 28. Specificity values on medical datasets

	Breast cancer		Breast EW		DH1		Heart	
	AVG	STD	AVG	STD	AVG	STD	AVG	STD
bMFO	98.33%	0.0215	95.76%	0.0231	93.94%	0.0181	87.50%	0.1128
bGWO	97.92%	0.0295	96.23%	**0.0209**	94.28%	0.0197	88.33%	**0.0703**
bPSO	97.08%	0.0343	96.19%	0.0243	93.95%	0.0296	90.00%	0.1097
bALO	97.10%	0.0342	96.23%	0.0221	94.36%	0.0273	**90.83%**	0.0730
bBA	93.77%	0.0659	85.26%	0.0664	89.82%	0.0238	78.33%	0.1192
bSSA	97.92%	0.0220	96.71%	0.0254	94.28%	**0.0176**	89.17%	0.0966
bWOA	97.08%	0.0395	95.28%	0.0277	93.78%	0.0207	90.00%	0.0946
bPLO	**98.35%**	**0.0213**	**96.73%**	0.0295	**94.62%**	0.0203	**90.83%**	0.0829
	PH		Parkinson		DH2		DH3	
	AVG	STD	AVG	STD	AVG	STD	AVG	STD
bMFO	87.50%	0.1768	91.50%	0.1765	93.03%	0.0244	93.23%	**0.0253**
bGWO	**92.50%**	**0.1208**	89.00%	0.2025	92.62%	0.0234	93.99%	0.0285
bPSO	**92.50%**	**0.1208**	89.50%	**0.1343**	93.13%	0.0206	93.38%	0.0316
bALO	**92.50%**	**0.1208**	89.00%	0.1647	93.02%	0.0241	94.31%	0.0271
bBA	77.50%	0.2189	67.50%	0.2781	82.48%	0.1654	90.29%	0.0285
bSSA	95.00%	0.1581	94.00%	0.1578	91.71%	0.0415	94.30%	0.0333
bWOA	90.00%	0.1291	90.50%	0.1674	91.81%	0.0275	93.53%	0.0330
bPLO	**92.50%**	**0.1208**	**96.00%**	0.1350	**93.43%**	**0.0174**	**94.29%**	0.0396

Table 29. Precision values on medical datasets

	Breast cancer	Breast EW	DH1	Heart

	AVG	STD	AVG	STD	AVG	STD	AVG	STD
bMFO	99.13%	0.0113	97.60%	0.0231	90.41%	0.0270	91.26%	0.0726
bGWO	98.94%	0.0149	97.85%	**0.0209**	90.93%	0.0294	91.47%	**0.0491**
bPSO	98.52%	0.0172	97.86%	0.0243	90.57%	0.0429	92.94%	0.0743
bALO	98.51%	0.0173	98.11%	0.0221	91.08%	0.0401	93.16%	0.0523
bBA	96.81%	0.0330	92.46%	0.0664	81.72%	0.0591	84.06%	0.0801
bSSA	98.92%	0.0114	**98.12%**	0.0254	90.83%	**0.0257**	92.25%	0.0658
bWOA	98.52%	0.0196	97.37%	0.0277	89.99%	0.0318	92.62%	0.0627
bPLO	**99.14%**	**0.0111**	97.90%	0.0295	**91.40%**	0.0313	**93.26%**	0.0583
	PH		Parkinson		DH2		DH3	
	AVG	STD	AVG	STD	AVG	STD	AVG	STD
bMFO	92.14%	0.1071	94.45%	0.0496	92.70%	0.0231	92.41%	**0.0262**
bGWO	95.00%	0.0805	93.90%	0.0573	92.32%	0.0236	93.30%	0.0273
bPSO	95.00%	0.0805	93.70%	**0.0406**	92.83%	0.0191	92.55%	0.0331
bALO	95.00%	0.0805	93.86%	0.0491	92.68%	0.0236	93.54%	0.0284
bBA	81.48%	0.1871	85.25%	0.0742	82.65%	**0.1480**	88.88%	0.0311
bSSA	97.14%	0.0904	95.07%	0.0481	91.58%	0.0391	93.49%	0.0371
bWOA	93.33%	**0.0861**	94.28%	0.0453	91.54%	0.0273	92.72%	0.0356
bPLO	**95.48%**	0.0994	**95.70%**	**0.0406**	**93.12%**	0.0169	**93.66%**	0.0411

Table 30. MCC values on medical datasets

	Breast cancer		Breast EW		DH1		Heart	
	AVG	STD	AVG	STD	AVG	STD	AVG	STD
bMFO	0.9604	0.0419	0.9667	0.0325	0.8395	0.0436	0.8490	0.0848
bGWO	0.9660	**0.0226**	0.9704	**0.0293**	0.8459	0.0391	0.8680	0.0774
bPSO	0.9597	0.0255	0.9702	0.0342	0.8401	0.0340	0.8840	0.1036
bALO	0.9627	0.0244	0.9741	0.0303	0.8421	0.0527	0.8699	0.0892
bBA	0.9027	0.0684	0.8747	0.1145	0.6596	0.1443	0.6799	0.1569
bSSA	0.9657	0.0309	0.9706	0.0351	0.8359	**0.0280**	0.8620	**0.0722**
bWOA	0.9623	0.0289	0.9631	0.0389	0.8216	0.0402	0.8684	0.1182
bPLO	**0.9690**	0.0292	**0.9741**	0.0417	**0.8490**	0.0445	**0.8895**	0.0940
	PH		Parkinson		DH2		DH3	
	AVG	STD	AVG	STD	AVG	STD	AVG	STD
bMFO	0.8769	0.1422	0.8607	0.1319	0.8440	0.0379	0.8341	0.0415
bGWO	0.9372	**0.1012**	0.8573	0.1378	0.8468	0.0455	0.8447	**0.0376**
bPSO	0.9172	0.1070	0.8350	0.1115	0.8481	**0.0190**	0.8341	0.0571
bALO	0.9372	**0.1012**	0.8467	0.1012	0.8429	0.0364	0.8351	0.0262
bBA	0.5511	0.4242	0.4868	0.3489	0.6434	0.2695	0.7599	0.0727
bSSA	0.9388	0.1273	0.8796	**0.1008**	0.8374	0.0542	0.8315	0.0473
bWOA	0.8962	0.1094	0.8301	0.1161	0.8343	0.0391	0.8356	0.0568
bPLO	**0.9598**	0.1368	**0.8937**	0.0853	**0.8561**	0.0303	**0.8422**	0.0628

Table 31. F-measure values medical datasets

	Breast cancer		Breast EW		DH1		Heart	
	AVG	STD	AVG	STD	AVG	STD	AVG	STD
bMFO	98.56%	0.0159	98.77%	0.0118	90.09%	0.0280	93.30%	0.0353

bGWO	98.79%	**0.0082**	98.90%	0.0107	90.51%	0.0238	94.23%	0.0322
bPSO	98.58%	0.0090	98.90%	0.0126	90.16%	0.0193	94.93%	0.0442
bALO	98.69%	0.0086	99.03%	0.0113	90.17%	0.0341	94.03%	0.0427
bBA	96.63%	0.0227	95.56%	0.0385	77.81%	0.1096	86.15%	0.0648
bSSA	98.80%	0.0109	98.92%	0.0131	89.84%	**0.0176**	93.90%	**0.0301**
bWOA	98.70%	0.0098	98.65%	0.0142	88.97%	0.0245	94.13%	0.0525
bPLO	**98.91%**	0.0104	**99.04%**	0.0152	**90.66%**	0.0279	**95.18%**	0.0402
	PH		Parkinson		DH2		DH3	
	AVG	STD	AVG	STD	AVG	STD	AVG	STD
bMFO	94.50%	0.0620	96.74%	0.0300	91.94%	0.0202	91.14%	0.0226
bGWO	97.27%	**0.0439**	96.77%	0.0305	92.14%	0.0236	**91.61%**	0.0222
bPSO	96.16%	0.0499	96.06%	0.0250	92.16%	**0.0101**	91.13%	0.0308
bALO	97.27%	**0.0439**	96.40%	0.0235	91.89%	0.0192	91.04%	**1.51%**
bBA	78.35%	0.2025	90.10%	0.0555	82.07%	0.1290	87.03%	0.0443
bSSA	98.33%	0.0527	97.05%	0.0240	91.66%	0.0275	90.87%	0.0246
bWOA	95.25%	0.0504	95.99%	0.0265	91.55%	0.0197	91.23%	0.0302
bPLO	**97.42%**	0.0572	**97.39%**	**0.0202**	**92.59%**	0.0162	91.36%	0.0370

7. Conclusions and future works

This paper proposes a novel physical-based algorithm called Polar Lights Optimization. The PLO involves novel search strategies based mainly on the motion trajectories of energetic particles in the solar wind.

Within PLO, an equation governing the temporal evolution of the velocity of high-energy charged particles was derived through the analysis of their spiral motion along magnetic field lines, integrating the laws of Lorentz and Newtonian mechanics. Additionally, to account for the trajectory deviation caused by collisions of charged particles with air molecules in the auroral phenomenon, a damping factor was introduced into the velocity-time equation, thereby revising it and proposing a gyration strategy. Inspired by the transient pause of charged particles in the atmosphere and the elliptical luminous bands observed in the sky, a strategy termed the aurora oval walk is formulated by incorporating Levy flight random walks. Finally, the phenomenon of particle collisions during flight inspired the development of the particle collision strategy.

In the subsequent experimental section, the paper firstly designs experiments to analyze the optimization process of PLO, and its adaptation to dimension scaling. Then, PLO is compared with 9 classical algorithms as well as 8 high-performance improved algorithms in the IEEE CEC2014 classical test set and further compared using the IEEE CEC2022 latest test set, and the results prove that PLO is highly competitive. The results are also evaluated by the WSRT to rate the results, to separate the advantages and disadvantages among the algorithms, and to rank the algorithms in terms of their overall ability by the FT. In the analysis of the results, it can be understood that PLO can better coordinate exploration and exploitation and has higher search efficiency, which is mainly attributed to the proposed unique exploration and exploitation strategy:

1) Based on the laws of physics, a unique mathematical model is proposed in gyration motion to help energetic particles to carefully search for the optimal solution in the local utilization stage and gradually improve the convergence accuracy throughout the algorithm iterations.

2) In the auroral oval walk, high-energy particles can search the entire space in dynamic steps, while using the center of mass of the high-energy particles as a guide to ensure the direction of convergence of the entire particle population.

3) Particle collision strategy, in the whole flight process of high-energy particles, the collision behavior between particles throughout. Simulating the chaotic and disorderly collisions between particles provides the algorithm with a better ability to jump out of the local optimum. Moreover, the PLO does not require predefined additional parameters, which gives it an advantage over similar algorithms and makes it easier to apply to other complex problems.

Then, our study involves two key issues: multi-threshold image segmentation and feature selection. In MTIS, we harnessed the capabilities of the PLO algorithm to address challenging image segmentation problems. We integrated it with an MTIS technique, enabling the calculation of optimal threshold sets. The performance of the PLO algorithm was evaluated using ten images from the IDC medical dataset, showcasing its adaptability in real-world optimization challenges.

In FS, this paper has developed a binary version of PLO to tackle challenging feature selection problems. Leveraging its underlying structure, we devised a wrapper feature selection (FS) method to select pertinent features. We use medical datasets to assess the PLO, demonstrating its proficiency in real-world optimization problems. Experimental validation confirmed the efficacy of the PLO, underscoring its robust capabilities in tackling practical applications, particularly in the field of medicine. These outcomes affirm the emergence of PLO as a potent optimization tool poised to address diverse real-world problems.

In future endeavors, PLO is poised for expansion into a dynamic optimizer, with applications spanning complex problems in engineering design, resource allocation, supply chain management, and beyond. Additionally, further research into adapting the algorithm to more adaptable scenarios is warranted, with the potential to apply PLO to more optimization scenarios such as emission dispatch problem, intrusion detection, medical diagnostics, and bankruptcy prediction.

Acknowledgement

This work was supported in part by the Natural Science Foundation of Zhejiang Province (LZ22F020005), National Natural Science Foundation of China (62076185, 62301367), Natural Science Foundation of Jilin Province (YDZJ202201ZYTS567). We acknowledge the comments of the reviewers.

Declaration of AI and AI-assisted technologies in the writing process

During the revision stage of this work the author(s) used ChatGPT as a grammar checker in order to double check and proofread the English grammar of the paper. After using this tool/service, the author(s) reviewed and edited the content as needed and take(s) full responsibility for the content of the publication.

Appendix

Table A.1 IEEE CEC2014 function list

Class	Function	Describe	Range	$Fi* = Fi(x*)$
Unimodal Functions	F1	Rotated High Conditioned Elliptic Function	$[-100,100]$	100

	F2	Rotated Bent Cigar Function	$[-100,100]$	200
	F3	Rotated Discus Function	$[-100,100]$	300
Simple Multimodal Functions	F4	Shifted and Rotated Rosen brock's Function	$[-100,100]$	400
	F5	Shifted and Rotated Ackley's Function	$[-100,100]$	500
	F6	Shifted and Rotated Weierstrass Function	$[-100,100]$	600
	F7	Shifted and Rotated Griewank's Function	$[-100,100]$	700
	F8	Shifted Rastrigin's Function	$[-100,100]$	800
	F9	Shifted and Rotated Rastrigin's Function	$[-100,100]$	900
	F10	Shifted Schwefel's Function	$[-100,100]$	1000
	F11	Shifted and Rotated Schwefel's Function	$[-100,100]$	1100
	F12	Shifted and Rotated Katsuura Function	$[-100,100]$	1200
	F13	Shifted and Rotated HappyCat Function	$[-100,100]$	1300
	F14	Shifted and Rotated HGBat Function	$[-100,100]$	1400
	F15	Shifted and Rotated Expanded Griewank's plus Rosen brock's Function	$[-100,100]$	1500
	F16	Shifted and Rotated Expanded Schaffer's F6 Function	$[-100,100]$	1600
Hybrid Functions	F17	Hybrid Function 1 (N=3)	$[-100,100]$	1700
	F18	Hybrid Function 2 (N=3)	$[-100,100]$	1800
	F19	Hybrid Function 3 (N=4)	$[-100,100]$	1900
	F20	Hybrid Function 4 (N=4)	$[-100,100]$	2000
	F21	Hybrid Function 5 (N=5)	$[-100,100]$	2100
	F22	Hybrid Function 6 (N=5)	$[-100,100]$	2200
Composition Functions	F23	Composition Function 1 (N=5)	$[-100,100]$	2300
	F24	Composition Function 2 (N=3)	$[-100,100]$	2400
	F25	Composition Function 3 (N=3)	$[-100,100]$	2500
	F26	Composition Function 4 (N=5)	$[-100,100]$	2600
	F27	Composition Function 5 (N=5)	$[-100,100]$	2700
	F28	Composition Function 6 (N=5)	$[-100,100]$	2800
	F29	Composition Function 7 (N=3)	$[-100,100]$	2900
	F30	Composition Function 8 (N=3)	$[-100,100]$	3000

Table A.2 IEEE CEC2022 function list

Class	**Functions**	**Describe**	f_i
Unimodal Functions	F1	Shifted and full Rotated Zakharov Function	300

Multimodal Functions	F2	Shifted and full Rotated Rosenbrock's Function	400
	F3	Shifted and full Rotated Expanded Schaffer's f6 Function	600
	F4	Shifted and full Rotated Non-Continuous Rastrigin's Function	800
	F5	Shifted and full Rotated Levy Function	900
Hybrid Functions	F6	Hybrid Function 1 (N = 3)	1800
	F7	Hybrid Function 2 (N = 6)	2000
	F8	Hybrid Function 3 (N = 5)	2200
Composition Functions	F9	Composition Function 1 (N = 5)	2300
	F10	Composition Function 2 (N = 4)	2400
	F11	Composition Function 3 (N = 5)	2600
	F12	Composition Function 4 (N = 6)	2700

Table A.3 FSIM evaluation results at a low threshold

		2 thresholds		4 thresholds		6 thresholds	
Image	Method	AVG	STD	AVG	STD	AVG	STD
BC01	PLO	0.9155	0.0115	**0.9517**	0.0095	**0.9621**	0.0135
	WOA	0.9002	0.0198	0.9365	0.0161	0.9565	0.0170
	SMA	**0.9165**	**0.0089**	0.9410	0.0029	0.9430	0.0078
	JAYA	0.9068	0.0185	0.9409	**0.0026**	0.9409	**0.0055**
	MVO	0.8997	0.0273	0.9387	0.0113	0.9455	0.0256
	MSCA	0.8888	0.0425	0.9265	0.0360	0.9473	0.0291
	HHO	0.8910	0.0288	0.9455	0.0216	0.9567	0.0180
	IGWO	0.9106	0.0219	0.9372	0.0136	0.9497	0.0176
BC02	PLO	0.9483	0.0132	**0.9721**	0.0045	**0.9721**	0.0057
	WOA	0.9304	0.0347	0.9669	0.0093	0.9668	0.0028
	SMA	**0.9502**	**0.0000**	0.9682	0.0025	0.9660	0.0042
	JAYA	0.9437	0.0190	0.9681	**0.0012**	0.9654	**0.0008**
	MVO	0.9381	0.0174	0.9663	0.0087	0.9687	0.0089
	MSCA	0.9369	0.0261	0.9635	0.0143	0.9682	0.0123
	HHO	0.9329	0.0227	0.9686	0.0090	0.9716	0.0090
	IGWO	0.9445	0.0235	0.9675	0.0088	0.9689	0.0076
BC03	PLO	**0.9001**	0.0329	**0.9591**	0.0053	**0.9638**	0.0091
	WOA	0.8986	0.0354	0.9429	0.0275	0.9624	0.0110
	SMA	0.8885	0.0304	0.9561	0.0018	0.9581	**0.0085**
	JAYA	0.8780	**0.0278**	0.9565	**0.0010**	0.9567	0.0087
	MVO	0.8808	0.0287	0.9456	0.0302	0.9570	0.0119
	MSCA	0.8799	0.0323	0.9351	0.0284	0.9528	0.0172
	HHO	0.8818	0.0431	0.9395	0.0177	0.9591	0.0138
	IGWO	0.8864	0.0315	0.9442	0.0323	0.9470	0.0219
BC04	PLO	0.8192	0.0204	0.9277	0.0066	0.9606	0.0079
	WOA	0.7987	0.0331	0.9142	0.0250	0.9546	0.0111
	SMA	0.8140	0.0113	0.9334	0.0062	**0.9681**	**0.0032**

	JAYA	0.8125	**0.0105**	**0.9367**	**0.0017**	0.9673	0.0041
	MVO	**0.8273**	0.0214	0.9236	0.0137	0.9431	0.0271
	MSCA	0.8086	0.0477	0.9054	0.0209	0.9371	0.0185
	HHO	0.7751	0.0678	0.8994	0.0315	0.9365	0.0227
	IGWO	0.8254	0.0249	0.9125	0.0201	0.9383	0.0171
BC05	PLO	**0.9228**	0.0110	**0.9476**	0.0075	0.9592	0.0182
	WOA	0.9113	0.0208	0.9437	0.0171	**0.9642**	**0.0167**
	SMA	0.9176	**0.0000**	0.9415	0.0046	0.9542	0.0200
	JAYA	0.9177	0.0009	0.9411	**0.0007**	0.9457	0.0194
	MVO	0.9144	0.0212	0.9464	0.0143	0.9510	0.0178
	MSCA	0.9197	0.0199	0.9438	0.0345	0.9476	0.0335
	HHO	0.9002	0.0273	0.9453	0.0170	0.9632	0.0147
	IGWO	0.9147	0.0205	0.9430	0.0135	0.9529	0.0192
BC06	PLO	**0.9292**	**0.0091**	**0.9616**	0.0087	**0.9590**	0.0096
	WOA	0.9028	0.0335	0.9499	0.0169	0.9584	0.0090
	SMA	0.9232	0.0282	0.9552	0.0096	0.9578	0.0053
	JAYA	0.9186	0.0290	0.9559	**0.0021**	0.9563	**0.0045**
	MVO	0.8824	0.0644	0.9448	0.0188	0.9518	0.0161
	MSCA	0.8695	0.0851	0.9253	0.0414	0.9320	0.0381
	HHO	0.8814	0.0596	0.9400	0.0268	0.9579	0.0162
	IGWO	0.9208	0.0122	0.9428	0.0174	0.9425	0.0277
BC07	PLO	**0.8313**	0.0225	0.9168	0.0166	**0.9444**	0.0141
	WOA	0.7935	0.1004	0.8902	0.0479	0.9377	0.0176
	SMA	0.8275	**0.0120**	**0.9207**	**0.0071**	0.9326	**0.0135**
	JAYA	0.8191	0.0305	0.9083	0.0195	0.9335	0.0171
	MVO	0.8240	0.0418	0.9063	0.0257	0.9270	0.0357
	MSCA	0.7808	0.0628	0.8801	0.0448	0.9084	0.0465
	HHO	0.7832	0.0913	0.8783	0.1149	0.9217	0.0378
	IGWO	0.8295	0.0247	0.8925	0.0488	0.9112	0.0479
BC08	PLO	**0.8355**	0.0249	0.9340	0.0111	0.9656	0.0071
	WOA	0.8182	0.0408	0.9191	0.0337	0.9548	0.0192
	SMA	0.8308	0.0056	**0.9393**	**0.0036**	**0.9705**	**0.0039**
	JAYA	0.8263	**0.0147**	0.9378	0.0076	0.9631	0.0070
	MVO	0.8288	0.0152	0.9356	0.0078	0.9618	0.0128
	MSCA	0.8141	0.0582	0.9173	0.0296	0.9485	0.0195
	HHO	0.7903	0.0491	0.9021	0.0302	0.9301	0.0339
	IGWO	0.8323	0.0219	0.9198	0.0266	0.9468	0.0185
BC09	PLO	0.8895	0.0134	**0.9349**	0.0082	**0.9532**	0.0097
	WOA	**0.8951**	0.0144	0.9282	0.0118	0.9406	0.0106
	SMA	0.8862	**0.0064**	0.9288	0.0086	0.9400	**0.0069**
	JAYA	0.8812	0.0166	0.9328	**0.0063**	0.9394	0.0070
	MVO	0.8784	0.0176	0.9284	0.0098	0.9466	0.0116
	MSCA	0.8687	0.0448	0.9072	0.0271	0.9248	0.0288
	HHO	0.8825	0.0323	0.9201	0.0195	0.9374	0.0233

	IGWO	0.8830	0.0212	0.9253	0.0174	0.9330	0.0284
BC10	PLO	**0.8129**	**0.0507**	**0.9252**	0.0210	0.9455	0.0196
	WOA	0.7836	0.0935	0.9130	0.0394	0.9246	0.0742
	SMA	0.7929	0.0669	0.9365	**0.0091**	**0.9580**	**0.0052**
	JAYA	0.7979	0.0539	0.9176	0.0322	0.9467	0.0119
	MVO	0.7885	0.0839	0.8896	0.0598	0.9398	0.0225
	MSCA	0.6988	0.1465	0.8663	0.0991	0.9068	0.0648
	HHO	0.7862	0.1060	0.9079	0.0545	0.9349	0.0293
	IGWO	0.7707	0.0809	0.8843	0.0523	0.9155	0.0345

Table A.4 PSNR evaluation results at a low threshold

		2 thresholds		4 thresholds		6 thresholds	
Image	Method	AVG	STD	AVG	STD	AVG	STD
BC01	PLO	13.7945	0.3813	**18.6307**	0.2558	**20.9763**	0.6354
	WOA	13.5065	0.9374	17.8400	0.9716	20.5842	0.8174
	SMA	**13.9288**	**0.1338**	18.5147	0.0809	20.3879	0.3341
	JAYA	13.6586	0.7961	18.5220	**0.0441**	20.3071	**0.2375**
	MVO	13.5068	0.9265	18.0276	0.6317	20.2326	0.9573
	MSCA	12.8862	1.2709	17.1507	1.1986	19.5098	1.5030
	HHO	13.6370	1.4604	17.8661	1.1510	20.2976	1.0256
	IGWO	13.3459	0.8718	17.5927	0.8416	19.7169	0.9999
BC02	PLO	12.8503	0.7135	**18.2490**	0.2643	**20.6511**	0.3789
	WOA	12.0622	1.6135	17.3513	1.0085	19.9385	0.5436
	SMA	**12.9319**	**0.0000**	18.0870	0.4589	20.3967	0.3326
	JAYA	12.6137	0.9144	18.1791	**0.1564**	20.4316	**0.0812**
	MVO	12.5221	0.9068	17.6768	0.6187	20.0797	0.5402
	MSCA	12.3907	1.0385	17.2854	0.8521	19.5763	1.0430
	HHO	12.9010	1.0003	17.3179	1.0634	19.8282	1.1351
	IGWO	12.6532	1.1004	17.2537	0.9880	19.6712	0.7961
BC03	PLO	**13.3466**	0.2652	18.3440	0.2087	**20.8629**	0.4121
	WOA	12.8323	0.7539	17.3220	1.0681	20.1226	0.8315
	SMA	13.3005	**0.0621**	18.3508	0.0944	20.6722	**0.3814**
	JAYA	13.2632	0.5085	**18.3770**	**0.0492**	20.6003	0.3836
	MVO	13.2020	0.4326	17.6495	0.8870	20.1859	0.6300
	MSCA	12.9482	0.6626	16.9149	0.9564	19.5499	0.9460
	HHO	12.6908	1.2284	16.6965	1.0225	19.5473	1.0065
	IGWO	13.2193	0.4843	17.6018	0.8765	19.3972	0.9829
BC04	PLO	12.6963	0.4454	18.3972	**0.3596**	21.2059	0.5591
	WOA	12.4149	0.3635	17.8581	0.9625	21.0344	0.6859
	SMA	12.6035	**0.1714**	18.5015	0.4444	21.6389	0.3712
	JAYA	12.5417	0.1979	**18.6480**	0.0816	**21.7971**	**0.3358**
	MVO	**12.7593**	0.4862	17.9551	0.7100	20.1629	1.4399
	MSCA	12.7116	0.6248	17.2471	0.9123	19.6821	0.9604
	HHO	11.9705	1.0030	17.4546	0.8794	20.0253	1.2659
	IGWO	12.7989	0.4217	17.6034	0.8006	19.9019	0.8352

BC05	PLO	**12.5785**	0.6333	**18.0806**	0.2548	**20.8771**	0.9286
	WOA	12.1831	1.0276	17.2596	1.2239	20.3387	0.9865
	SMA	12.2633	**0.0000**	17.8558	0.2199	20.4671	0.9290
	JAYA	12.2672	0.0499	17.9063	**0.0460**	20.1652	**0.9059**
	MVO	12.2664	0.9626	17.4682	1.0131	19.7981	1.1265
	MSCA	12.7819	0.9947	17.2630	1.2396	19.5220	1.3342
	HHO	11.9394	1.0920	16.9311	1.1192	19.8004	1.2337
	IGWO	12.2798	1.0686	17.0793	1.1116	19.3684	1.3064
BC06	PLO	13.4683	**0.3161**	18.4421	0.2558	20.5816	0.3504
	WOA	12.6554	1.0017	17.7756	0.5578	20.0179	0.6391
	SMA	**13.5175**	0.2235	18.3638	0.3881	20.5307	0.4229
	JAYA	13.3610	0.3909	**18.4629**	**0.0686**	**20.7890**	**0.1824**
	MVO	13.1583	0.4983	17.6916	0.7226	19.7324	1.2846
	MSCA	12.5082	1.1457	16.5788	1.2291	18.3887	1.2588
	HHO	12.0741	1.5161	16.9816	1.1648	19.5183	1.3180
	IGWO	13.2685	0.3860	17.3569	0.6495	19.0124	1.2196
BC07	PLO	13.3515	0.7923	18.5427	0.4938	**21.3822**	**0.5660**
	WOA	12.4348	1.7378	17.4838	1.8334	20.5409	1.0473
	SMA	13.2490	0.3491	**19.0094**	**0.1787**	20.9041	0.7312
	JAYA	12.9867	1.0228	18.4249	0.7360	20.9504	0.6803
	MVO	**13.4715**	1.0334	18.2426	1.2421	20.3865	1.7742
	MSCA	11.9162	2.0521	16.7327	2.0497	19.1263	1.6847
	HHO	11.9979	2.0736	17.1918	2.5061	19.7298	1.7380
	IGWO	13.3947	**0.7006**	17.4359	1.6784	19.2679	1.9845
BC08	PLO	12.6446	0.7893	18.6294	0.4191	21.8556	0.4305
	WOA	12.1866	0.9090	18.1572	1.2196	21.2898	1.1072
	SMA	12.1712	**0.0578**	**18.9296**	**0.2268**	**22.0803**	**0.3824**
	JAYA	12.2258	0.3233	18.8110	0.3421	21.7777	0.4902
	MVO	12.2396	0.3511	18.6172	0.4160	21.5323	0.8380
	MSCA	**12.9613**	0.9322	18.0053	0.9843	20.5074	1.1978
	HHO	11.9936	1.1131	17.5901	1.0890	20.0256	1.5179
	IGWO	12.4005	0.6527	17.9634	1.0834	20.6733	1.0657
BC09	PLO	13.1711	0.3091	**18.1870**	0.1462	**21.0653**	0.3861
	WOA	13.2423	0.3283	17.9969	0.3277	20.6214	0.3600
	SMA	13.1288	**0.0789**	18.0992	0.1412	20.6657	0.2995
	JAYA	13.2316	0.2453	18.1611	**0.1087**	20.7573	**0.2348**
	MVO	**13.2586**	0.2251	17.8403	0.5542	20.2432	0.9109
	MSCA	12.9987	0.6222	16.7890	1.1621	18.8398	1.2941
	HHO	12.9334	0.8002	17.2555	0.9211	19.7801	0.9140
	IGWO	13.0036	0.5365	17.4435	0.8114	19.3483	1.2177
BC10	PLO	**13.5978**	**1.9801**	19.2055	0.8970	21.7485	1.3911
	WOA	12.8448	2.5564	18.6602	1.9073	20.5413	3.3908
	SMA	12.7336	2.7202	**19.6210**	**0.6244**	**23.0377**	**0.6255**
	JAYA	13.0072	2.0828	19.2575	1.5129	22.5158	1.2440

	MVO	13.0181	2.1122	17.9583	2.9372	21.8181	1.4738
	MSCA	11.5462	3.3214	17.0310	2.4278	20.1151	2.4957
	HHO	12.8496	2.8053	18.5916	2.5093	20.7009	1.8841
	IGWO	12.8220	2.1732	17.8097	2.3054	20.3736	2.0531

Table A.5 SSIM evaluation results at a low threshold

		2 thresholds		4 thresholds		6 thresholds	
Image	Method	AVG	STD	AVG	STD	AVG	STD
BC01	PLO	0.7230	0.0182	**0.8822**	0.0073	**0.9216**	0.0114
	WOA	0.7119	0.0423	0.8541	0.0352	0.9092	0.0128
	SMA	**0.7307**	**0.0070**	0.8799	0.0025	0.9107	0.0065
	JAYA	0.7201	0.0323	0.8802	**0.0014**	0.9085	**0.0054**
	MVO	0.7126	0.0416	0.8658	0.0200	0.9039	0.0276
	MSCA	0.6788	0.0635	0.8340	0.0466	0.8869	0.0428
	HHO	0.7161	0.0757	0.8523	0.0382	0.9056	0.0170
	IGWO	0.7030	0.0378	0.8513	0.0285	0.8934	0.0248
BC02	PLO	0.7250	0.0344	**0.9092**	**0.0071**	**0.9465**	0.0050
	WOA	0.6724	0.0923	0.8827	0.0305	0.9352	0.0117
	SMA	**0.7309**	**0.0000**	0.9067	0.0112	0.9438	0.0053
	JAYA	0.7132	0.0529	0.9089	0.0044	0.9447	**0.0016**
	MVO	0.7090	0.0485	0.8943	0.0167	0.9358	0.0092
	MSCA	0.6893	0.0586	0.8822	0.0253	0.9259	0.0246
	HHO	0.7260	0.0614	0.8794	0.0343	0.9282	0.0235
	IGWO	0.7087	0.0621	0.8789	0.0330	0.9273	0.0182
BC03	PLO	0.6887	0.0204	0.8783	0.0067	**0.9269**	0.0058
	WOA	0.6492	0.0501	0.8417	0.0390	0.9041	0.0223
	SMA	0.6907	**0.0177**	0.8787	0.0033	0.9265	**0.0045**
	JAYA	**0.6929**	0.0351	**0.8796**	**0.0018**	0.9247	0.0046
	MVO	0.6884	0.0312	0.8555	0.0265	0.9134	0.0119
	MSCA	0.6715	0.0461	0.8336	0.0366	0.8998	0.0232
	HHO	0.6465	0.0821	0.8080	0.0452	0.8873	0.0248
	IGWO	0.6878	0.0342	0.8565	0.0250	0.8955	0.0252
BC04	PLO	0.5374	0.0301	**0.7889**	0.0154	0.8751	0.0144
	WOA	0.5086	0.0208	0.7603	0.0362	0.8607	0.0172
	SMA	0.5197	0.0149	0.7852	0.0131	0.8802	0.0089
	JAYA	0.5186	**0.0142**	0.7867	**0.0022**	**0.8835**	**0.0076**
	MVO	0.5473	0.0340	0.7809	0.0252	0.8579	0.0242
	MSCA	**0.5499**	0.0431	0.7728	0.0244	0.8417	0.0276
	HHO	0.4961	0.0612	0.7546	0.0330	0.8292	0.0343
	IGWO	0.5431	0.0297	0.7731	0.0302	0.8394	0.0273
BC05	PLO	**0.6786**	0.0304	**0.8883**	0.0070	**0.9336**	**0.0086**
	WOA	0.6496	0.0567	0.8525	0.0376	0.9147	0.0171
	SMA	0.6650	**0.0000**	0.8825	0.0078	0.9277	0.0088
	JAYA	0.6652	0.0026	0.8850	**0.0015**	0.9247	0.0092
	MVO	0.6594	0.0581	0.8626	0.0346	0.9130	0.0252

	MSCA	0.6789	0.0506	0.8546	0.0417	0.9065	0.0294
	HHO	0.6299	0.0670	0.8348	0.0420	0.9027	0.0251
	IGWO	0.6571	0.0559	0.8510	0.0394	0.9003	0.0312
BC06	PLO	0.6955	0.0166	0.8764	0.0062	0.9196	0.0058
	WOA	0.6484	0.0601	0.8552	0.0192	0.9034	0.0163
	SMA	**0.7033**	**0.0101**	0.8769	0.0109	0.9209	0.0070
	JAYA	0.6956	0.0180	**0.8799**	**0.0027**	**0.9250**	**0.0034**
	MVO	0.6896	0.0210	0.8560	0.0243	0.8958	0.0409
	MSCA	0.6402	0.0786	0.8151	0.0482	0.8630	0.0406
	HHO	0.6138	0.0937	0.8184	0.0500	0.8814	0.0388
	IGWO	0.6860	0.0252	0.8431	0.0252	0.8793	0.0335
BC07	PLO	**0.6105**	0.0325	0.8041	0.0191	**0.8762**	0.0117
	WOA	0.5508	0.1048	0.7620	0.0729	0.8495	0.0274
	SMA	0.6105	**0.0206**	**0.8216**	**0.0054**	0.8707	0.0140
	JAYA	0.5964	0.0442	0.8012	0.0234	0.8666	0.0161
	MVO	0.6100	0.0558	0.7942	0.0404	0.8492	0.0551
	MSCA	0.5290	0.1039	0.7388	0.0830	0.8148	0.0591
	HHO	0.5338	0.1170	0.7423	0.1294	0.8249	0.0548
	IGWO	0.6076	0.0323	0.7623	0.0680	0.8162	**0.0679**
BC08	PLO	0.5374	0.0459	**0.7926**	0.0189	0.8731	0.0135
	WOA	0.5016	0.0423	0.7617	0.0448	0.8571	0.0264
	SMA	0.5101	**0.0094**	0.7875	**0.0076**	**0.8779**	**0.0112**
	JAYA	0.5037	0.0227	0.7897	0.0160	0.8678	0.0140
	MVO	0.5085	0.0222	0.7863	0.0180	0.8617	0.0267
	MSCA	**0.5420**	0.0559	0.7666	0.0414	0.8380	0.0371
	HHO	0.4835	0.0618	0.7434	0.0416	0.8148	0.0470
	IGWO	0.5196	0.0405	0.7668	0.0428	0.8434	0.0342
BC09	PLO	0.6152	0.0176	**0.8405**	0.0052	**0.9088**	0.0072
	WOA	0.6181	0.0163	0.8346	0.0109	0.9014	0.0065
	SMA	0.6135	**0.0088**	0.8385	0.0032	0.9054	**0.0047**
	JAYA	0.6251	0.0225	0.8385	**0.0020**	0.9047	0.0047
	MVO	**0.6287**	0.0233	0.8301	0.0221	0.8902	0.0251
	MSCA	0.6124	0.0330	0.8006	0.0528	0.8584	0.0365
	HHO	0.6010	0.0483	0.8070	0.0362	0.8733	0.0194
	IGWO	0.6064	0.0292	0.8144	0.0351	0.8637	0.0314
BC10	PLO	**0.5449**	**0.0812**	0.7759	0.0354	0.8494	0.0421
	WOA	0.5059	0.1152	0.7570	0.0759	0.7952	0.1355
	SMA	0.5114	0.1082	**0.7945**	**0.0236**	**0.8864**	**0.0149**
	JAYA	0.5226	0.0844	0.7849	0.0488	0.8688	0.0398
	MVO	0.5202	0.0939	0.7360	0.1116	0.8546	0.0415
	MSCA	0.4281	0.1609	0.6857	0.1187	0.7855	0.0973
	HHO	0.5144	0.1310	0.7535	0.0967	0.8119	0.0635
	IGWO	0.5074	0.1022	0.7228	0.0884	0.7990	0.0772

Table A.6 FSIM evaluation results at a high threshold

		16 thresholds		20 thresholds		24 thresholds	
Image	Method	AVG	STD	AVG	AVG	STD	AVG
BC01	PLO	**0.9933**	0.0038	0.9947	0.0035	**0.9971**	**0.0019**
	WOA	0.9920	0.0069	**0.9949**	0.0039	0.9967	0.0023
	SMA	0.9893	0.0098	0.9931	0.0065	0.9964	0.0029
	JAYA	0.9917	0.0038	0.9931	0.0049	0.9961	0.0020
	MVO	0.9918	**0.0060**	0.9937	**0.0032**	0.9929	0.0059
	MSCA	0.9870	0.0145	0.9926	0.0044	0.9939	0.0054
	HHO	0.9917	0.0059	0.9905	0.0108	0.9942	0.0045
	IGWO	0.9896	0.0051	0.9899	0.0080	0.9911	0.0081
BC02	PLO	**0.9940**	0.0045	**0.9965**	**0.0024**	**0.9971**	**0.0022**
	WOA	0.9907	0.0085	0.9944	0.0041	0.9956	0.0037
	SMA	0.9866	0.0104	0.9942	0.0040	0.9956	0.0043
	JAYA	0.9925	**0.0036**	0.9939	0.0052	0.9956	0.0034
	MVO	0.9905	0.0070	0.9946	0.0034	0.9955	0.0033
	MSCA	0.9874	0.0097	0.9923	0.0077	0.9954	0.0029
	HHO	0.9879	0.0113	0.9930	0.0043	0.9960	0.0027
	IGWO	0.9871	0.0098	0.9918	0.0049	0.9917	0.0081
BC03	PLO	0.9894	0.0105	**0.9952**	**0.0036**	**0.9964**	0.0017
	WOA	0.9862	0.0117	0.9927	0.0066	0.9962	**0.0016**
	SMA	0.9866	0.0100	0.9919	0.0071	0.9935	0.0111
	JAYA	**0.9896**	0.0088	0.9917	0.0045	0.9951	0.0022
	MVO	0.9876	0.0080	0.9929	0.0041	0.9926	0.0048
	MSCA	0.9829	0.0106	0.9891	0.0076	0.9916	0.0053
	HHO	0.9823	0.0119	0.9865	0.0124	0.9918	0.0065
	IGWO	0.9879	**0.0051**	0.9874	0.0059	0.9922	0.0063
BC04	PLO	**0.9892**	**0.0051**	**0.9920**	**0.0036**	**0.9927**	**0.0030**
	WOA	0.9848	0.0080	0.9869	0.0086	0.9920	0.0049
	SMA	0.9854	0.0077	0.9875	0.0073	0.9894	0.0052
	JAYA	0.9856	0.0077	0.9877	0.0063	0.9895	0.0048
	MVO	0.9795	0.0108	0.9837	0.0119	0.9872	0.0067
	MSCA	0.9786	0.0097	0.9845	0.0057	0.9871	0.0089
	HHO	0.9745	0.0162	0.9832	0.0080	0.9877	0.0071
	IGWO	0.9807	0.0084	0.9789	0.0137	0.9833	0.0098
BC05	PLO	0.9878	**0.0063**	**0.9928**	0.0057	**0.9950**	0.0037
	WOA	**0.9897**	0.0067	0.9891	0.0081	0.9945	0.0053
	SMA	0.9815	0.0087	0.9887	0.0087	0.9929	0.0072
	JAYA	0.9849	0.0092	0.9878	0.0091	0.9942	**0.0030**
	MVO	0.9841	0.0106	0.9922	**0.0033**	0.9919	0.0059
	MSCA	0.9841	0.0081	0.9852	0.0081	0.9901	0.0063
	HHO	0.9868	0.0106	0.9884	0.0073	0.9928	0.0049
	IGWO	0.9805	0.0134	0.9880	0.0087	0.9909	0.0059
BC06	PLO	0.9836	**0.0101**	0.9890	0.0148	**0.9936**	**0.0053**
	WOA	0.9755	0.0167	0.9893	0.0094	0.9892	0.0095

	SMA	0.9701	0.0148	0.9788	0.0137	0.9918	0.0079
	JAYA	0.9796	0.0176	0.9863	0.0106	0.9892	0.0136
	MVO	**0.9848**	0.0144	**0.9895**	**0.0094**	0.9910	0.0098
	MSCA	0.9793	0.0168	0.9779	0.0280	0.9912	0.0073
	HHO	0.9769	0.0191	0.9823	0.0172	0.9879	0.0120
	IGWO	0.9826	0.0108	0.9839	0.0203	0.9901	0.0067
BC07	PLO	0.9793	0.0108	0.9835	0.0078	**0.9910**	0.0053
	WOA	**0.9854**	**0.0050**	**0.9880**	**0.0045**	0.9906	0.0042
	SMA	0.9819	0.0076	0.9856	0.0075	0.9901	0.0049
	JAYA	0.9727	0.0089	0.9780	0.0107	0.9891	0.0056
	MVO	0.9769	0.0097	0.9844	0.0069	0.9852	0.0102
	MSCA	0.9652	0.0207	0.9796	0.0099	0.9858	0.0070
	HHO	0.9778	0.0130	0.9820	0.0100	0.9899	**0.0033**
	IGWO	0.9668	0.0136	0.9784	0.0094	0.9860	0.0048
BC08	PLO	**0.9856**	0.0065	**0.9892**	**0.0040**	**0.9919**	**0.0023**
	WOA	0.9845	**0.0054**	0.9883	0.0059	0.9904	0.0055
	SMA	0.9855	0.0065	0.9869	0.0083	0.9914	0.0033
	JAYA	0.9807	0.0095	0.9845	0.0077	0.9882	0.0070
	MVO	0.9818	0.0058	0.9856	0.0062	0.9872	0.0062
	MSCA	0.9776	0.0112	0.9838	0.0095	0.9832	0.0132
	HHO	0.9737	0.0205	0.9803	0.0169	0.9849	0.0099
	IGWO	0.9757	0.0107	0.9793	0.0154	0.9844	0.0074
BC09	PLO	0.9850	0.0142	**0.9932**	**0.0051**	**0.9951**	**0.0035**
	WOA	**0.9866**	0.0107	0.9854	0.0092	0.9890	0.0089
	SMA	0.9761	0.0136	0.9839	0.0095	0.9880	0.0102
	JAYA	0.9798	0.0123	0.9890	0.0065	0.9907	0.0070
	MVO	0.9848	**0.0094**	0.9876	0.0107	0.9909	0.0056
	MSCA	0.9778	0.0203	0.9845	0.0105	0.9876	0.0092
	HHO	0.9797	0.0107	0.9835	0.0123	0.9902	0.0073
	IGWO	0.9759	0.0166	0.9855	0.0102	0.9850	0.0146
BC10	PLO	**0.9885**	**0.0076**	0.9918	**0.0030**	0.9943	**0.0022**
	WOA	0.9882	0.0082	**0.9922**	0.0037	0.9921	0.0090
	SMA	0.9832	0.0138	0.9906	0.0101	**0.9946**	0.0023
	JAYA	0.9766	0.0161	0.9879	0.0076	0.9910	0.0049
	MVO	0.9814	0.0123	0.9843	0.0101	0.9895	0.0051
	MSCA	0.9770	0.0187	0.9861	0.0100	0.9870	0.0078
	HHO	0.9767	0.0182	0.9875	0.0080	0.9899	0.0076
	IGWO	0.9770	0.0189	0.9801	0.0116	0.9893	0.0048

Table A.7 PSNR evaluation results at high threshold

		16 thresholds		20 thresholds		24 thresholds	
Image	Method	AVG	STD	AVG	STD	AVG	STD
BC01	PLO	**28.5962**	**0.9945**	**30.2501**	1.0820	31.8132	**0.7975**
	WOA	28.4362	1.1837	30.2212	1.2076	**31.9243**	0.8350
	SMA	27.9305	1.3398	29.7037	1.6220	31.5984	1.1639

	JAYA	27.8967	1.1244	29.4154	**1.0377**	30.9584	0.9332
	MVO	27.7292	1.1833	28.9139	1.4970	29.5219	1.3880
	MSCA	27.0797	1.9681	29.0200	1.2241	30.0589	1.6131
	HHO	27.6716	1.5487	28.5481	1.8520	30.3710	1.3498
	IGWO	26.9873	1.1342	28.1485	1.3030	29.2566	1.5594
BC02	PLO	**28.0571**	**0.9677**	**30.0964**	**0.9511**	**31.5116**	**0.9372**
	WOA	27.4242	1.3917	29.4937	1.2717	31.0182	1.4142
	SMA	26.8724	1.7396	29.3646	1.3128	30.6909	1.3305
	JAYA	27.3685	0.9920	28.8898	1.3887	30.3119	1.2681
	MVO	26.5944	1.2766	28.5289	1.2490	29.7835	1.2011
	MSCA	25.9545	1.5788	27.9398	1.5558	29.8667	1.1463
	HHO	26.1307	1.9897	27.9008	1.4195	30.1592	1.1612
	IGWO	25.3835	1.2800	27.0613	1.3906	28.4955	1.9303
BC03	PLO	**27.8553**	1.4442	**30.3187**	**0.8889**	**31.9701**	**0.5648**
	WOA	26.9577	1.3925	29.3977	1.3802	31.4338	0.9533
	SMA	27.5502	1.3785	29.5913	1.4460	30.9577	1.9468
	JAYA	27.6363	1.1226	28.8827	1.0808	30.4237	0.8081
	MVO	27.2831	1.3023	28.9774	1.0319	29.4600	1.1584
	MSCA	26.2417	1.5133	28.0907	1.6437	29.5555	1.7595
	HHO	25.8680	1.7735	27.8121	2.0591	28.9181	1.7003
	IGWO	26.5236	**1.0999**	27.0054	1.3536	29.1069	1.2371
BC04	PLO	**28.9754**	**0.6088**	**30.6348**	**0.5840**	**32.0679**	**0.5309**
	WOA	28.4211	1.4943	29.4073	1.6934	31.6828	1.4978
	SMA	27.8844	1.4198	29.3440	1.4337	30.5654	1.3682
	JAYA	28.0089	0.6575	29.1586	1.2919	30.5812	1.0660
	MVO	26.9648	1.5755	28.3572	1.7098	29.6698	1.4405
	MSCA	26.1779	1.6080	28.4565	1.1867	29.7780	1.5383
	HHO	26.5426	2.0557	28.2625	1.4882	29.8118	2.0944
	IGWO	26.6143	1.0564	27.2711	1.8546	28.5553	1.4757
BC05	PLO	27.7543	**1.0944**	**30.1211**	**1.2510**	**31.6143**	**0.9802**
	WOA	**28.0959**	1.2464	29.2951	1.6142	31.3493	1.3739
	SMA	27.1735	1.2935	29.3172	1.6488	30.8668	1.4919
	JAYA	27.1470	1.3256	28.7349	1.4579	30.6203	1.0627
	MVO	26.9012	1.4975	28.7876	1.3177	29.9154	1.4538
	MSCA	26.6644	1.1859	27.9924	1.5131	29.6314	1.4077
	HHO	27.0625	1.7087	28.1957	1.5280	29.8468	1.5311
	IGWO	25.7641	1.8105	27.7816	1.4965	29.2748	1.1541
BC06	PLO	**27.1077**	**1.4377**	**29.3744**	2.0428	**31.4172**	**1.4359**
	WOA	26.1374	1.8472	29.3849	1.6887	30.4017	2.0404
	SMA	25.7053	1.4624	27.6608	1.8789	30.8662	1.8009
	JAYA	26.3766	1.6991	28.1703	**1.5903**	29.7832	1.9363
	MVO	26.4146	1.7841	28.5767	1.6065	29.6192	1.8391
	MSCA	25.4127	1.7376	26.7510	2.8923	29.6212	1.8857
	HHO	26.0563	2.3183	27.1587	2.5647	29.4965	2.6975

	IGWO	25.5765	1.4935	27.0558	2.1524	29.0569	1.3683
BC07	PLO	27.3853	1.3284	28.8577	1.4507	**31.1123**	1.5350
	WOA	**28.3590**	1.1873	**29.6671**	**1.1552**	30.8730	1.3153
	SMA	27.8894	**1.1023**	29.1440	1.4702	30.8619	**1.2717**
	JAYA	26.4927	1.2193	27.6982	1.7205	30.3730	1.3564
	MVO	26.6285	1.5658	28.3832	1.6440	29.2997	1.9989
	MSCA	25.0572	2.0278	27.7376	1.9622	29.0458	1.4920
	HHO	26.9064	1.9699	28.2382	1.7877	30.2720	1.4445
	IGWO	25.3391	1.7806	27.1370	1.6239	29.0979	1.5055
BC08	PLO	**28.8040**	**0.6800**	**30.3749**	**0.7978**	**31.8673**	**0.5492**
	WOA	28.3874	0.7013	30.0019	1.2844	31.3599	1.1196
	SMA	28.2781	0.8120	29.6024	1.0092	31.2152	0.8795
	JAYA	27.8283	1.3411	29.2542	1.1351	30.5367	1.2109
	MVO	27.3191	1.1790	28.8858	1.2375	29.6983	1.2816
	MSCA	26.9060	1.8299	28.7553	1.2896	29.5038	1.8620
	HHO	26.4427	2.1878	28.5323	2.1477	29.8591	1.8292
	IGWO	26.2674	1.4620	27.8616	1.5716	28.9444	1.4999
BC09	PLO	27.8789	1.3228	**30.1992**	**0.6843**	**31.5665**	**0.6355**
	WOA	**27.8951**	1.0671	29.3563	1.2144	30.6792	1.2732
	SMA	27.0087	1.3368	28.7353	1.2129	30.1612	1.3987
	JAYA	26.8698	**0.9840**	28.8507	0.9261	30.1529	1.1997
	MVO	26.9076	1.3619	28.1824	1.3905	29.4958	1.2516
	MSCA	26.2294	1.8668	27.7630	1.3199	28.9854	1.4363
	HHO	26.5466	1.3061	27.7096	1.9734	29.3832	1.4732
	IGWO	25.5883	1.5621	27.1439	1.5857	28.5538	1.6615
BC10	PLO	28.5586	**0.9106**	29.9186	**0.8825**	31.3629	1.1799
	WOA	**28.8058**	1.4184	**30.6366**	1.2192	**31.8088**	1.8961
	SMA	28.6158	1.5597	30.3778	1.2094	31.5133	**1.4372**
	JAYA	27.4750	1.3773	29.2359	1.4797	30.3068	1.6023
	MVO	27.4583	1.8844	28.0325	2.0134	29.8556	2.0144
	MSCA	27.3034	1.6869	28.7055	1.6376	29.2599	1.4856
	HHO	27.0232	2.2404	29.1915	1.9431	30.1783	1.7831
	IGWO	26.9413	2.2002	27.8555	1.8392	29.4878	1.4949

Table A.8 SSIM evaluation results at a high threshold

		16 thresholds		20 thresholds		24 thresholds	
Image	Method	AVG	STD	AVG	STD	AVG	STD
BC01	PLO	**0.9798**	**0.0044**	**0.9850**	**0.0038**	0.9888	0.0025
	WOA	0.9788	0.0071	0.9849	0.0046	**0.9890**	**0.0023**
	SMA	0.9773	0.0075	0.9832	0.0066	0.9884	0.0035
	JAYA	0.9753	0.0074	0.9802	0.0061	0.9858	0.0040
	MVO	0.9739	0.0085	0.9774	0.0097	0.9800	0.0068
	MSCA	0.9697	0.0156	0.9796	0.0068	0.9822	0.0070
	HHO	0.9733	0.0104	0.9763	0.0134	0.9837	0.0056
	IGWO	0.9696	0.0080	0.9751	0.0069	0.9786	0.0095

BC02	PLO	**0.9869**	**0.0031**	**0.9912**	**0.0017**	**0.9932**	**0.0014**
	WOA	0.9849	0.0057	0.9901	0.0027	0.9924	0.0022
	SMA	0.9831	0.0072	0.9900	0.0029	0.9916	0.0025
	JAYA	0.9843	0.0036	0.9877	0.0038	0.9906	0.0025
	MVO	0.9801	0.0060	0.9861	0.0045	0.9889	0.0035
	MSCA	0.9774	0.0082	0.9845	0.0065	0.9895	0.0027
	HHO	0.9771	0.0105	0.9841	0.0050	0.9898	0.0035
	IGWO	0.9744	0.0095	0.9810	0.0070	0.9855	0.0063
BC03	PLO	0.9761	0.0066	**0.9851**	**0.0030**	**0.9890**	**0.0021**
	WOA	0.9698	0.0088	0.9813	0.0054	0.9874	0.0033
	SMA	**0.9765**	**0.0046**	0.9839	0.0048	0.9861	0.0084
	JAYA	0.9741	0.0082	0.9788	0.0062	0.9843	0.0031
	MVO	0.9723	0.0076	0.9797	0.0043	0.9800	0.0067
	MSCA	0.9685	0.0103	0.9761	0.0073	0.9806	0.0097
	HHO	0.9610	0.0153	0.9726	0.0116	0.9776	0.0090
	IGWO	0.9688	0.0081	0.9699	0.0092	0.9788	0.0068
BC04	PLO	**0.9599**	0.0088	**0.9696**	**0.0064**	0.9738	0.0057
	WOA	0.9538	0.0114	0.9654	0.0075	**0.9746**	0.0047
	SMA	0.9558	**0.0082**	0.9651	0.0082	0.9711	**0.0046**
	JAYA	0.9517	0.0128	0.9621	0.0102	0.9671	0.0096
	MVO	0.9434	0.0135	0.9576	0.0130	0.9617	0.0131
	MSCA	0.9430	0.0178	0.9567	0.0086	0.9626	0.0127
	HHO	0.9313	0.0274	0.9519	0.0124	0.9626	0.0134
	IGWO	0.9405	0.0136	0.9453	0.0139	0.9545	0.0167
BC05	PLO	**0.9794**	0.0048	**0.9848**	0.0053	**0.9888**	**0.0024**
	WOA	0.9792	0.0049	0.9831	0.0050	0.9883	0.0032
	SMA	0.9785	**0.0037**	0.9842	**0.0045**	0.9877	0.0036
	JAYA	0.9762	0.0052	0.9811	0.0046	0.9860	0.0043
	MVO	0.9732	0.0083	0.9799	0.0070	0.9836	0.0055
	MSCA	0.9736	0.0056	0.9792	0.0053	0.9835	0.0043
	HHO	0.9724	0.0108	0.9777	0.0063	0.9829	0.0062
	IGWO	0.9659	0.0113	0.9758	0.0079	0.9822	0.0040
BC06	PLO	**0.9730**	**0.0062**	0.9794	0.0089	**0.9855**	**0.0035**
	WOA	0.9672	0.0087	**0.9799**	**0.0048**	0.9839	0.0049
	SMA	0.9682	0.0078	0.9757	0.0074	0.9848	0.0047
	JAYA	0.9677	0.0086	0.9741	0.0071	0.9788	0.0082
	MVO	0.9632	0.0147	0.9744	0.0108	0.9771	0.0096
	MSCA	0.9574	0.0132	0.9656	0.0204	0.9787	0.0082
	HHO	0.9602	0.0155	0.9650	0.0188	0.9773	0.0114
	IGWO	0.9575	0.0149	0.9649	0.0154	0.9758	0.0058
BC07	PLO	0.9518	0.0110	0.9620	0.0071	**0.9725**	0.0079
	WOA	0.9558	0.0108	**0.9656**	**0.0065**	0.9713	0.0064
	SMA	**0.9572**	**0.0066**	0.9639	0.0071	0.9722	**0.0056**
	JAYA	0.9437	0.0161	0.9517	0.0149	0.9680	0.0070

	MVO	0.9415	0.0172	0.9532	0.0155	0.9589	0.0151
	MSCA	0.9253	0.0265	0.9527	0.0137	0.9596	0.0101
	HHO	0.9388	0.0251	0.9514	0.0174	0.9649	0.0098
	IGWO	0.9244	0.0273	0.9430	0.0173	0.9584	0.0117
BC08	PLO	**0.9530**	**0.0095**	**0.9631**	**0.0072**	**0.9718**	**0.0045**
	WOA	0.9518	0.0098	0.9628	0.0117	0.9691	0.0082
	SMA	0.9513	0.0104	0.9600	0.0122	0.9697	0.0068
	JAYA	0.9436	0.0164	0.9551	0.0112	0.9635	0.0102
	MVO	0.9412	0.0123	0.9523	0.0133	0.9592	0.0116
	MSCA	0.9332	0.0234	0.9511	0.0164	0.9586	0.0121
	HHO	0.9255	0.0298	0.9486	0.0237	0.9554	0.0183
	IGWO	0.9293	0.0227	0.9386	0.0266	0.9502	0.0170
BC09	PLO	**0.9721**	0.0063	**0.9813**	**0.0024**	**0.9854**	**0.0020**
	WOA	0.9715	**0.0050**	0.9794	0.0036	0.9828	0.0043
	SMA	0.9691	0.0070	0.9765	0.0048	0.9810	0.0049
	JAYA	0.9657	0.0055	0.9747	0.0054	0.9796	0.0053
	MVO	0.9638	0.0109	0.9702	0.0092	0.9763	0.0070
	MSCA	0.9603	0.0156	0.9691	0.0079	0.9754	0.0074
	HHO	0.9607	0.0091	0.9655	0.0133	0.9751	0.0076
	IGWO	0.9505	0.0172	0.9617	0.0129	0.9713	0.0090
BC10	PLO	0.9521	**0.0119**	0.9627	**0.0078**	0.9717	**0.0096**
	WOA	0.9544	0.0154	0.9672	0.0107	**0.9731**	0.0119
	SMA	**0.9557**	0.0176	**0.9674**	0.0089	0.9728	0.0108
	JAYA	0.9392	0.0198	0.9541	0.0157	0.9611	0.0165
	MVO	0.9349	0.0315	0.9393	0.0285	0.9553	0.0236
	MSCA	0.9370	0.0271	0.9511	0.0179	0.9537	0.0164
	HHO	0.9270	0.0389	0.9517	0.0220	0.9601	0.0173
	IGWO	0.9254	0.0453	0.9381	0.0288	0.9554	0.0156

Reference

1. Zhao, T., et al., *A comprehensive review of process planning and trajectory optimization in arc-based directed energy deposition.* Journal of Manufacturing Processes, 2024. **119**: p. 235-254.
2. Lu, C., et al., *A Pareto-based hybrid iterated greedy algorithm for energy-efficient scheduling of distributed hybrid flowshop.* Expert Systems with Applications, 2022: p. 117555.
3. Desale, S., et al., *Heuristic and meta-heuristic algorithms and their relevance to the real world: a survey.* 2015. **351**(5): p. 2349-7084.
4. Sun, G., et al., *Low-latency and resource-efficient service function chaining orchestration in network function virtualization.* IEEE Internet of Things Journal, 2019. **7**(7): p. 5760-5772.
5. Lu, C., et al., *Human–Robot Collaborative Scheduling in Energy-Efficient Welding Shop.* IEEE Transactions on Industrial Informatics, 2024. **20**(1): p. 963-971.

6. Yu, F., et al., *A knowledge-guided bi-population evolutionary algorithm for energy-efficient scheduling of distributed flexible job shop problem.* Engineering Applications of Artificial Intelligence, 2024. **128**: p. 107458.
7. Cao, B., et al., *Applying graph-based differential grouping for multiobjective large-scale optimization.* Swarm and Evolutionary Computation, 2020. **53**: p. 100626.
8. Zeng, G.-Q., et al., *Adaptive population extremal optimization-based PID neural network for multivariable nonlinear control systems.* Swarm and Evolutionary Computation, 2019. **44**: p. 320-334.
9. Xu, X. and Z. Wei, *Dynamic pickup and delivery problem with transshipments and LIFO constraints.* Computers & Industrial Engineering, 2023. **175**: p. 108835.
10. Chen, H.L., et al., *A balanced whale optimization algorithm for constrained engineering design problems.* Applied Mathematical Modelling, 2019. **71**: p. 45-59.
11. Cao, B., et al., *Diversified personalized recommendation optimization based on mobile data.* IEEE Transactions on Intelligent Transportation Systems, 2020. **22**(4): p. 2133-2139.
12. Li, Q., S.Y. Liu, and X.S. Yang, *Influence of initialization on the performance of metaheuristic optimizers.* APPLIED SOFT COMPUTING, 2020. **91**.
13. Li, S., et al., *Slime mould algorithm: A new method for stochastic optimization.* Future Generation Computer Systems, 2020. **111**: p. 300-323.
14. Osher, S., et al., *Laplacian smoothing gradient descent.* RESEARCH IN THE MATHEMATICAL SCIENCES, 2022. **9**(3).
15. Cao, B., et al., *Multiobjective 3-D Topology Optimization of Next-Generation Wireless Data Center Network.* IEEE Transactions on Industrial Informatics, 2019. **16**(5): p. 3597-3605.
16. Boussaid, I., J. Lepagnot, and P. Siarry, *A survey on optimization metaheuristics.* Information Sciences, 2013. **237**: p. 82-117.
17. Kirkpatrick, S., C.D. Gelatt, and M.P. Vecchi, *Optimization by Simulated Annealing.* Science, 1983. **220**(4598): p. 671-680.
18. Hatamlou, A., *Black hole: A new heuristic optimization approach for data clustering.* Information Sciences, 2013. **222**: p. 175-184.
19. Faramarzi, A., et al., *Equilibrium optimizer: A novel optimization algorithm.* KNOWLEDGE-BASED SYSTEMS, 2020. **191**.
20. Mirjalili, S., S.M. Mirjalili, and A. Hatamlou, *Multi-Verse Optimizer: a nature-inspired algorithm for global optimization.* NEURAL COMPUTING & APPLICATIONS, 2016. **27**(2): p. 495-513.
21. Recioui, A., *Application of a Galaxy-Based Search Algorithm to MIMO System Capacity Optimization.* ARABIAN JOURNAL FOR SCIENCE AND ENGINEERING, 2016. **41**(9): p. 3407-3414.
22. Tzanetos, A. and G. Dounias, *A New Metaheuristic Method for Optimization: Sonar Inspired Optimization*, in *ENGINEERING APPLICATIONS OF NEURAL NETWORKS, EANN 2017*. 2017. p. 417-428.
23. Su, H., et al., *RIME: A physics-based optimization.* NEUROCOMPUTING, 2023. **532**: p. 183-214.
24. Rashedi, E., H. Nezamabadi-Pour, and S. Saryazdi, *GSA: A Gravitational Search Algorithm.* INFORMATION SCIENCES, 2009. **179**(13): p. 2232-2248.

25. Eskandar, H., et al., *Water cycle algorithm - A novel metaheuristic optimization method for solving constrained engineering optimization problems.* COMPUTERS & STRUCTURES, 2012. **110**: p. 151-166.
26. Formato, R.A., *Central Force Optimization: A New Nature Inspired Computational Framework for Multidimensional Search and Optimization*, in *NATURE INSPIRED COOPERATIVE STRATEGIES FOR OPTIMIZATION (NICSO 2007)*. 2008. p. 221-238.
27. Abedinpourshotorban, H., et al., *Electromagnetic field optimization: A physics-inspired metaheuristic optimization algorithm.* SWARM AND EVOLUTIONARY COMPUTATION, 2016. **26**: p. 8-22.
28. Cao, B., et al., *RFID reader anticollision based on distributed parallel particle swarm optimization.* IEEE Internet of Things Journal, 2020. **8**(5): p. 3099-3107.
29. Karaboga, D. and B. Basturk, *A powerful and efficient algorithm for numerical function optimization: artificial bee colony (ABC) algorithm.* Journal of Global Optimization, 2007. **39**(3): p. 459-471.
30. Yang, Y.T., et al., *Hunger games search: Visions, conception, implementation, deep analysis, perspectives, and towards performance shifts.* EXPERT SYSTEMS WITH APPLICATIONS, 2021. **177**.
31. Li, S.M., et al., *Slime mould algorithm: A new method for stochastic optimization.* FUTURE GENERATION COMPUTER SYSTEMS-THE INTERNATIONAL JOURNAL OF ESCIENCE, 2020. **111**: p. 300-323.
32. Heidari, A.A., et al., *Harris hawks optimization: Algorithm and applications.* Future Generation Computer Systems, 2019. **97**: p. 849-872.
33. Lian, J., et al., *Parrot optimizer: Algorithm and applications to medical problems.* Computers in Biology and Medicine, 2024: p. 108064.
34. Yang, X.S. and S. Deb, *Cuckoo Search via Levey Flights*, in *2009 WORLD CONGRESS ON NATURE & BIOLOGICALLY INSPIRED COMPUTING (NABIC 2009)*. 2009. p. 210-+.
35. Socha, K. and M. Dorigo, *Ant colony optimization for continuous domains.* European Journal of Operational Research, 2008. **185**(3): p. 1155-1173.
36. Yang, Y., et al., *Hunger games search: Visions, conception, implementation, deep analysis, perspectives, and towards performance shifts.* Expert Systems with Applications, 2021. **177**: p. 114864.
37. Ahmadianfar, I., et al., *RUN beyond the metaphor: An efficient optimization algorithm based on Runge Kutta method.* EXPERT SYSTEMS WITH APPLICATIONS, 2021. **181**.
38. Ahmadianfar, I., et al., *INFO: An Efficient Optimization Algorithm based on Weighted Mean of Vectors*. Expert Systems with Applications, 2022: p. 116516.
39. Tu, J., et al., *The Colony Predation Algorithm.* Journal of Bionic Engineering, 2021. **18**(3): p. 674-710.
40. Mirjalili, S., et al., *Grey Wolf Optimizer: Theory, Literature Review, and Application in Computational Fluid Dynamics Problems*, in *Nature-Inspired Optimizers: Theories, Literature Reviews and Applications*, S. Mirjalili, J. Song Dong, and A. Lewis, Editors. 2020, Springer International Publishing: Cham. p. 87-105.
41. Houssein, E.H., et al., *Liver Cancer Algorithm: A novel bio-inspired optimizer.* Computers in Biology and Medicine, 2023. **165**: p. 107389.
42. Arora, S. and P. Anand, *Chaotic grasshopper optimization algorithm for global*

optimization. NEURAL COMPUTING & APPLICATIONS, 2019. **31**(8): p. 4385-4405.
43. Sastry, K., D.E. Goldberg, and G. Kendall, *Genetic Algorithms*, in *Search Methodologies*. 2014. p. 93-117.
44. Hirsh, H., *Genetic programming*. IEEE INTELLIGENT SYSTEMS & THEIR APPLICATIONS, 2000. **15**(3): p. 74-74.
45. Storn, R. and K.J.J.o.G.O. Price, *Differential Evolution – A Simple and Efficient Heuristic for global Optimization over Continuous Spaces*. 1997. **11**(4): p. 341-359.
46. Mou, J., et al., *A machine learning approach for energy-efficient intelligent transportation scheduling problem in a real-world dynamic circumstances*. IEEE transactions on intelligent transportation systems, 2022. **24**(12): p. 15527-15539.
47. Pan, W.T., *A new Fruit Fly Optimization Algorithm: Taking the financial distress model as an example.* KNOWLEDGE-BASED SYSTEMS, 2012. **26**: p. 69-74.
48. Simon, D., *Biogeography-Based Optimization.* IEEE TRANSACTIONS ON EVOLUTIONARY COMPUTATION, 2008. **12**(6): p. 702-713.
49. Hayyolalam, V. and A.A. Pourhaji Kazem, *Black Widow Optimization Algorithm: A novel meta-heuristic approach for solving engineering optimization problems.* Engineering Applications of Artificial Intelligence, 2020. **87**.
50. Michalewicz, Z., et al., *Evolutionary algorithms for constrained engineering problems.* COMPUTERS & INDUSTRIAL ENGINEERING, 1996. **30**(4): p. 851-870.
51. David H. Wolpert and W.G. Macready, *No Free Lunch Theorems for Optimization.* IEEE Trans, 1997: p. 67–82.
52. Yin, L., et al., *Energy saving in flow-shop scheduling management: an improved multiobjective model based on grey wolf optimization algorithm.* Mathematical Problems in Engineering, 2020. **2020**: p. 1-14.
53. Teoh, C.K., A. Wibowo, and M.S. Ngadiman, *Review of state of the art for metaheuristic techniques in Academic Scheduling Problems*. Artificial Intelligence Review, 2013. **44**(1): p. 1-21.
54. Hussain, K., et al., *Metaheuristic research: a comprehensive survey.* Artificial Intelligence Review, 2018. **52**(4): p. 2191-2233.
55. Aresta, G., et al., *BACH: Grand challenge on breast cancer histology images*. MEDICAL IMAGE ANALYSIS, 2019. **56**: p. 122-139.
56. Meier, R.R., *THERMOSPHERIC AURORA AND AIRGLOW.* REVIEWS OF GEOPHYSICS, 1987. **25**(3): p. 471-477.
57. Akasofu, S.I., *ENERGY COUPLING BETWEEN THE SOLAR-WIND AND THE MAGNETOSPHERE*. SPACE SCIENCE REVIEWS, 1981. **28**(2): p. 121-190.
58. Wang, Q., H. Fang, and B. Li, *Automatic Identification of Aurora Fold Structure in All-Sky Images.* Universe, 2023. **9**(2).
59. Sigernes, F., et al., *MODULATION OF THE AURORAL PROTON SPECTRUM IN THE UPPER-ATMOSPHERE*. JOURNAL OF ATMOSPHERIC AND TERRESTRIAL PHYSICS, 1993. **55**(9): p. 1289-1294.
60. Akay, B., *A study on particle swarm optimization and artificial bee colony algorithms for multilevel thresholding*. APPLIED SOFT COMPUTING, 2013. **13**(6): p. 3066-3091.
61. Garcia, S., et al., *Advanced nonparametric tests for multiple comparisons in the design of experiments in computational intelligence and data mining: Experimental analysis of*

power. INFORMATION SCIENCES, 2010. **180**(10): p. 2044-2064.

62. Derrac, J., et al., *A practical tutorial on the use of nonparametric statistical tests as a methodology for comparing evolutionary and swarm intelligence algorithms.* SWARM AND EVOLUTIONARY COMPUTATION, 2011. **1**(1): p. 3-18.
63. Kennedy, J., R.C. Eberhart, and Ieee, *A discrete binary version of the particle swarm algorithm*, in *SMC '97 CONFERENCE PROCEEDINGS - 1997 IEEE INTERNATIONAL CONFERENCE ON SYSTEMS, MAN, AND CYBERNETICS, VOLS 1-5: CONFERENCE THEME: COMPUTATIONAL CYBERNETICS AND SIMULATION*. 1997. p. 4104-4108.
64. Mirjalili, S., *Moth-flame optimization algorithm: A novel nature-inspired heuristic paradigm.* Knowledge-based systems, 2015. **89**: p. 228-249.
65. Mirjalili, S. and A. Lewis, *The Whale Optimization Algorithm.* Advances in Engineering Software, 2016. **95**: p. 51-67.
66. Rawat, A., S. Singh, and J.C. Bansal, *Sine Cosine Algorithm: Introduction and Advances*, in *The Palgrave Handbook of Operations Research*, S. Salhi and J. Boylan, Editors. 2022, Springer International Publishing: Cham. p. 447-467.
67. Venkata Rao, R., *Jaya: A simple and new optimization algorithm for solving constrained and unconstrained optimization problems.* International Journal of Industrial Engineering Computations, 2016: p. 19-34.
68. Elhosseini, M.A., et al., *Biped robot stability based on an A–C parametric Whale Optimization Algorithm.* Journal of Computational Science, 2019. **31**: p. 17-32.
69. Chen, H., et al., *An efficient double adaptive random spare reinforced whale optimization algorithm.* Expert Systems with Applications, 2019.
70. Qais, M.H., H.M. Hasanien, and S. Alghuwainem, *Enhanced whale optimization algorithm for maximum power point tracking of variable-speed wind generators.* APPLIED SOFT COMPUTING, 2020. **86**.
71. Chen, H., et al., *Efficient multi-population outpost fruit fly-driven optimizers: Framework and advances in support vector machines.* Expert Systems with Applications, 2020. **142**(10.1016/j.eswa.2019.112999).
72. Qu, C., et al., *A Modified Sine-Cosine Algorithm Based on Neighborhood Search and Greedy Levy Mutation.* Computational intelligence and neuroscience, 2018. **2018**: p. 4231647-4231647.
73. Bao, X.L., H.M. Jia, and C.B. Lang, *A Novel Hybrid Harris Hawks Optimization for Color Image Multilevel Thresholding Segmentation.* IEEE ACCESS, 2019. **7**: p. 76529-76546.
74. Gupta, S. and K. Deep, *A novel Random Walk Grey Wolf Optimizer.* SWARM AND EVOLUTIONARY COMPUTATION, 2019. **44**: p. 101-112.
75. Heidari, A.A., R. Ali Abbaspour, and H. Chen, *Efficient boosted grey wolf optimizers for global search and kernel extreme learning machine training.* Applied Soft Computing, 2019. **81**: p. 105521.
76. Zhang, Y.Y. and Z.G. Jin, *Comprehensive learning Jaya algorithm for engineering design optimization problems.* JOURNAL OF INTELLIGENT MANUFACTURING, 2022. **33**(5): p. 1229-1253.
77. Tanabe, R. and A.S. Fukunaga. *Improving the search performance of SHADE using linear population size reduction*. in *2014 IEEE Congress on Evolutionary Computation (CEC)*. 2014.

78. Kumar, A., R.K. Misra, and D. Singh. *Improving the local search capability of Effective Butterfly Optimizer using Covariance Matrix Adapted Retreat Phase*. in *2017 IEEE Congress on Evolutionary Computation (CEC)*. 2017.
79. Zhu, B., et al., *Hilbert spectra and empirical mode decomposition: A multiscale event analysis method to detect the impact of economic crises on the European carbon market.* Computational Economics, 2018. **52**(1): p. 105-121.
80. Liu, L., et al., *Ant colony optimization with Cauchy and greedy Levy mutations for multilevel COVID 19 X-ray image segmentation.* Computers in biology and medicine, 2021. **136**: p. 104609.
81. Zhao, D., et al., *Ant colony optimization with horizontal and vertical crossover search: Fundamental visions for multi-threshold image segmentation.* Expert Systems with Applications, 2021. **167**: p. 114122.
82. Cai, J., et al., *Feature selection in machine learning: A new perspective.* Neurocomputing, 2018. **300**: p. 70-79.
83. Zhao, D., et al., *Multi-strategy ant colony optimization for multi-level image segmentation: Case study of melanoma.* Biomedical Signal Processing and Control, 2023. **83**: p. 104647.
84. Yang, X., et al., *Multi-threshold image segmentation for melanoma based on Kapur's entropy using enhanced ant colony optimization.* Frontiers in Neuroinformatics, 2022. **16**.
85. Abutaleb, A.S., *Automatic thresholding of gray-level pictures using two-dimensional entropy.* Computer Vision, Graphics, and Image Processing, 1989. **47**(1): p. 22-32.
86. Buades, A., B. Coll, and J.M. Morel, *A non-local algorithm for image denoising*, in *2005 IEEE COMPUTER SOCIETY CONFERENCE ON COMPUTER VISION AND PATTERN RECOGNITION, VOL 2, PROCEEDINGS*. 2005. p. 60-65.
87. Houssein, E.H., et al., *Enhanced Harris hawks optimization with genetic operators for selection chemical descriptors and compounds activities.* Neural Computing and Applications, 2021. **33**(20): p. 13601-13618.
88. Huang, H., et al., *A new fruit fly optimization algorithm enhanced support vector machine for diagnosis of breast cancer based on high-level features.* BMC bioinformatics, 2019. **20**(8): p. 1-14.
89. Oliva, D., et al., *Image segmentation by minimum cross entropy using evolutionary methods.* SOFT COMPUTING, 2019. **23**(2): p. 431-450.
90. Chen, H., M. Wang, and X. Zhao, *A multi-strategy enhanced sine cosine algorithm for global optimization and constrained practical engineering problems.* Applied Mathematics and Computation, 2020. **369**.
91. Cai, Z., et al., *Evolving an optimal kernel extreme learning machine by using an enhanced grey wolf optimization strategy.* Expert Systems with Applications, 2019. **138**.
92. Horé, A. and D. Ziou. *Image Quality Metrics: PSNR vs. SSIM*. in *2010 20th International Conference on Pattern Recognition*. 2010.
93. Wang, Z., et al., *Image quality assessment: From error visibility to structural similarity.* IEEE TRANSACTIONS ON IMAGE PROCESSING, 2004. **13**(4): p. 600-612.
94. Zhang, L., et al., *FSIM: A Feature Similarity Index for Image Quality Assessment.* IEEE TRANSACTIONS ON IMAGE PROCESSING, 2011. **20**(8): p. 2378-2386.
95. Li, Y., et al., *An optimized machine learning method for predicting wogonin therapy for the treatment of pulmonary hypertension.* Computers in Biology and Medicine, 2023. **164**:

p. 107293.
96. Yang, X., et al., *Boosted machine learning model for predicting intradialytic hypotension using serum biomarkers of nutrition.* Comput Biol Med, 2022. **147**: p. 105752.
97. Yang, X., et al., *An optimized machine learning framework for predicting intradialytic hypotension using indexes of chronic kidney disease-mineral and bone disorders.* Comput Biol Med, 2022. **145**: p. 105510.
98. Li, Y., et al., *Intradialytic hypotension prediction using covariance matrix-driven whale optimizer with orthogonal structure-assisted extreme learning machine.* 2022. **16**.
99. Emary, E., H.M. Zawbaa, and A.E. Hassanien, *Binary grey wolf optimization approaches for feature selection.* Neurocomputing, 2016. **172**: p. 371-381.
100. Mirjalili, S. and A. Lewis, *S-shaped versus V-shaped transfer functions for binary Particle Swarm Optimization.* Swarm and Evolutionary Computation, 2013. **9**: p. 1-14.
101. Emary, E., H.M. Zawbaa, and A.E. Hassanien, *Binary ant lion approaches for feature selection.* Neurocomputing, 2016. **213**: p. 54-65.
102. Yang, X.-S., *A new metaheuristic bat-inspired algorithm*, in *Nature inspired cooperative strategies for optimization (NICSO 2010)*. 2010, Springer. p. 65-74.
103. Mirjalili, S., et al., *Salp Swarm Algorithm: A bio-inspired optimizer for engineering design problems.* Advances in Engineering Software, 2017. **114**: p. 163-191.